THE TRANSDERMAL ROUTE AS AN ALTERNATIVE FOR THE DELIVERY OF DRUGS FOR NEURODEGENERATIVE DISEASES

By

DINA WADIE AMEEN

A dissertation submitted to the

School of Graduate Studies

Rutgers, The State University of New Jersey

In partial fulfillment of the requirements

For the degree of

Doctor of Philosophy

Graduate Program in Pharmaceutical Sciences

Written under the direction of

Professor Bozena Michniak-Kohn, Ph.D.

And approved by

_____

_____

_____

_____

New Brunswick, New Jersey

October, 2020

ABSTRACT OF THE DISSERTATION

THE TRANSDERMAL ROUTE AS ALTERNATIVE FOR THE DELIVERY OF DRUGS FOR NEURODEGENERATIVE DISEASES

By

DINA WADIE AMEEN

Dissertation Director:

Bozena Michniak-Kohn, Ph.D

The transdermal route is an attractive alternative for drug delivery with several advantages including avoidance of gastrointestinal side effects/metabolism and hepatic first-pass effect, constant drug plasma level, being non-invasive, acting as a visual reminder of drug administration, and improved adherence to treatment. The latter is important for the successful management of neurodegenerative diseases, due to their chronic progressive nature requiring prolonged treatment. Despite the advantages, skin is a tough barrier to drug absorption and not many drugs can passively diffuse through the skin into the blood in amounts sufficient to exert a therapeutic effect. The objective of this research was to explore the feasibility and develop transdermal drug delivery systems of drugs for Alzheimer's disease (AD) and multiple sclerosis (MS). In this work, we investigated the development of a transdermal drug delivery system containing galantamine, an oral drug for AD, in a drug-in-adhesive type of system. Different pressure sensitive adhesives, penetration enhancers, and drug loadings were tested to optimize the drug delivery system through permeation studies using Franz diffusion cells with human cadaver skin, and release and rheological studies. The optimized formulation had a flux enhancement ratio

of 2.7-fold and was predicted to achieve a therapeutic plasma level using a 20 cm^2 patch. The work also investigated the feasibility of transdermal delivery of dimethyl fumarate (DMF), an oral MS drug, by studying the effect of different penetration enhancers at varying concentrations on DMF permeation using vertical Franz diffusion cells and human cadaver skin. The most effective penetration enhancer was found to be 5% cineole with a 5.3-fold increase in enhancement ratio suggesting that DMF is a potential candidate for transdermal drug delivery. Additionally, the feasibility of transdermal co-delivery of DMF and nicotine as a potential treatment for AD was investigated through studying the effect of pH and nicotine form (free base vs. salt) on the permeability of both drugs using human cadaver skin and vertical Franz diffusion cells. The results suggested the possibility of interplay between pH, and ion-pair formation influencing the permeation of DMF if combined with an ionizable molecule (nicotine). Finally, the formulation of DMF in nanostructured lipid carriers (NLCs) was explored through investigating several methods of preparation and compositions and their effects on drug loading and entrapment efficiency. The study involved measuring particle size and distribution, NLCs morphology, drug release and permeation enhancement effect of NLC formulation. Microemulsion method was shown to be successful in producing DMF NLCs with acceptable characteristics and good penetration properties. In conclusion, chemical penetration enhancers and formulation optimization provide feasible approaches to develop transdermal drug delivery systems of the studied drugs for the treatment of AD and MS.

Dedications

To the dearest of all,

Hassanain, my husband and soulmate

Minatallah, my beautiful princess

Mohammed Ali, my smart boy

Sabah, the cutest boy ever

Mom and Dad for the unconditional love and support

Mother –in law, for the everlasting blessings and prayers

Acknowledgements

First and foremost, I would like to express my deepest gratitude to God, Allah almighty, for blessings and guidance through this endeavor and all my life. I am overwhelmed with blessings that I cannot be thankful enough for.

I would like to express my gratitude and deepest appreciation to my Advisor and Professor Bozena Michniak-Kohn for letting me join her wonderful group and learn and explore skin research. Her continuous support, mentorship, and encouragement throughout this entire journey helped me grow and thrive intellectually. Her leadership of the Center of Dermal Research CDR provided a great opportunity for me to be part of intradisciplinary research projects and industrial collaborations.

I would like to thank my thesis committee members, Dr. Tamara Minko, Dr. Leonid Kagan, and Dr. Allison Rush for their valuable time, comments, and guidance.

I would like to thank Department of Pharmaceutics at the Ernest Mario School of Pharmacy for giving me the opportunity to pursue my Ph.D. in Pharmaceutical Sciences, and for supporting me with a teaching assistantship part of my graduate study. I am very grateful to the administrative staff at the Department of Pharmaceutics, Hui Pung, Fei Han, and Sharana Taylor for your compassion and being always there when help is needed.

I would like to thank Rutgers, The State University of New Jersey, for preparing such state-of-the-art research platforms for graduate students to succeed and excel. Rutgers was a home away from home to me, where I had a great sense of security and pride. Special thanks to the School of Graduate Studies for their help and support, especially Mrs. Alexandra Bachmann (my RU Mom) for overwhelming love, and support.

Special thanks to the past members of the Laboratory for Drug Delivery LDD, especially to the late Dr. Pei-Chin Tsai, Dr. Mania Dorrani, Golshid Keyvan, and Dr. Tannaz Ramezanli for making our lab a wonderful place to work in and being there for me when I first joined the lab. Also, I must thank Dr. Sonia Trehan for creating a warm environment while managing the lab. I also extend my thanks to the current LDD members, especially those how I spent years sharing lab space, hopes and aspirations: Anika Alam, Vinam Puri, Julia Zhang, Jemima Shultz, Benjamin Goodyear, and others. It has been a long journey and I wish you the best of luck and success in your endeavors.

I want to take this opportunity to thank the past and current members at New Jersey Center for Biomaterials NJCBM who assisted me with my research for sharing their knowledge and experience.

I am also very grateful to Mr. Norman Richardson and Dr. Amy Ethier of BASF, and Dr. Inayat Ellis of Gattefosse´ for their generous supply of samples of their products.

Finally, nothing can express my love, gratitude, and appreciation to my family. I know you have been through a lot during this journey. Your support, unconditional love, and motivation helped me reach this point. Nothing in this world can match the love and care of parents. Although they are oceans away, they always have me in their minds and blessings, always advocating for my progress and growth. I still remember how you dedicated you time and care for me when I went to college to pursue my Pharmacy degree, during my master research, and through this journey. Nothing that I do can replaces a small portion of your giving.

TABLE OF CONTENTS

List of Tables

List of Figures

Chapter 1: Introduction and Specific Aims

1.1.Introduction

Neurodegenerative diseases comprise a group of chronic diseases affecting the central nervous system at an increasing prevalence associated with increased human life expectancy. Included under the definition are the following: Alzheimer's disease (AD), multiple sclerosis (MS), and Parkinson's disease (PD), among others (1, 2). These diseases are characterized by progressive loss of neurons with the consequent deterioration of cognitive and/or motor function. Although different proteins are involved, all types of the neurodegerative diseases have a common characteristic of accumulating proteins of abnormal structural properties within the brain that interfere with the normal function and nutrition of the neurons and lead to their death (3).

In this study we focused on developing transdermal drug delivery systems for two diseases, Alzheimer's disease (AD), and multiple sclerosis (MS). AD is characterized by accumulation of two proteinaceous materials, namely amyloid-β (Aβ) plaques in the brain interstitium and tau tangles within the neurons. This causes interference with the normal nutrition and function of the neurons leading eventually to their death. The exact mechanisms that lead to the development of AD are still unknown and there is no known cure for this condition. The disease symptoms include memory deterioration and reduced cognition, confusion, depression, hallucinations, and related psychoses. Eventually, the affected patients need institutional care (4, 5). MS, on the other hand, is an autoimmune disease of the central nervous system affecting younger adults. It is characterized by formation of lesions in the white matter of the brain that are composed of inflammatory

cells, cytokines, dead oligodendrocytes and this leads to the loss of myelin. These lesions interrupt normal neuronal function and nutrition leading to their death and consequent deterioration of cognitive or motor function relative to the affected area (6, 7). The cause of the disease is not fully known, however, it is suggested that in addition to the inflammatory reaction there is some genetic predisposition and environmental factors that increase the risk of developing the disease (8).

There is no known cure for these diseases as of now, and the drugs that modify the diseases are almost exclusively administered orally or parenterally. AD patients, in particular, rely on caregivers to receive their medication; this by itself is a huge burden for the caregivers given the clinical symptoms of the patients. Consequently, patient non-compliance is considered a major challenge in the treatment of AD. Therefore, developing medication that addresses this issue is an important step to overcome this problem.

The transdermal route presents a very appealing choice for the treatment of neurodegenerative diseases, as it possesses several advantages over other routes such as avoidance of first pass effect metabolism and gastrointestinal side effects and/or metabolism, improved efficacy, and decreased toxicity (9). Indeed, transdermal patches offer exceptional advantages for the AD patients by reducing the oral dosage form burden, thus improving compliance.

Nevertheless, transdermal delivery is impeded by the powerful barrier function imposed by the stratum corneum. Different strategies have been developed to overcome this barrier. One of the methods is to incorporate chemical penetration enhancers (CPE) into the formulation. These compounds act to increase the permeation of drugs by a combination

of mechanisms including disruption of the lipid bilayer, fluidization, and extraction of stratum corneum lipids (10). Other approaches are a) to optimize the drug delivery system to enhance the percutaneous absorption of drugs and b) to design formulations with nanocarriers (11).

The objective of this research was to develop a transdermal drug delivery system for AD and MS drugs. Three drugs were investigated for this purpose, galantamine (GAL), an orally administered drug for AD, dimethyl fumarate (DMF), a drug approved for the treatment of multiple sclerosis that may be potentially useful in AD treatment, and nicotine, which is being investigated for potential use in Alzheimer's disease and mild cognitive impairment (12, 13). The initial part of the studies was focused on the development and characterization of drug-in-adhesive transdermal patch of galantamine for AD. The patches were designed to be applied once daily to deliver the drug at therapeutic levels with minimum irritation. In the next stage, focus was shifted towards investigating the feasibility of the transdermal delivery of DMF alone, and then co-delivery of DMF and nicotine. Finally, a transdermal drug delivery of DMF was investigated using lipid nanoparticles.

Specific Aims

The goal of this research was to investigate the feasibility of delivering drugs for Alzheimer's disease and/or multiple sclerosis across the skin to reach the blood at therapeutic levels, and to develop transdermal drug delivery systems containing these drugs. Towards this goal, the research was divided into four specific aims**:**

Specific Aim 1: To design, prepare and characterize drug in adhesive type of patches for the transdermal delivery of galantamine.

Galantamine was formulated as a transdermal drug delivery system of the "drug in adhesive" design. The transdermal patches were prepared by thin film casting method, and evaluated by studying drug release, drug permeation through skin in vitro, drug content uniformity, microscopical examination of the patch to rule out crystallization, and rheological properties. The selected patch was optimized by studying the effect of different formulation factors on the performance and properties of the patch, including the type of the pressure sensitive adhesive (PSA) used, the drug loading, type of penetration enhancer included in the formulation, and the inclusion of a crystallization inhibitor.

Specific Aim 2: Investigation of the feasibility of transdermal delivery of dimethyl fumarate

In order to investigate the suitability of transdermal delivery of DMF, the permeability of DMF was initially tested across human cadaver skin in the presence of chemical penetration enhancers (CPE)s. Six penetration enhancers with different physicochemical properties and enhancement mechanisms were evaluated. Formulations of DMF containing a CPE were prepared at three different concentrations each, and the drug permeation from these formulations was tested using Franz diffusion cells. Then, the permeation rate of DMF was calculated along with the enhancement ratios.

Specific Aim 3: Investigation of the feasibility of transdermal delivery of DMF in combination with nicotine as a potential therapy for Alzheimer's disease.

Investigating the co-delivery of DMF and nicotine was achieved by studying the effect of adding either nicotine free base or hydrogen tartare salt, and changing the pH on the transdermal flux (the amount permeated per unit time and area) of both drugs across human cadaver skin using vertical Franz diffusion cells.

Specific Aim 4: Preparation and characterization of dimethyl fumarate nano-structured lipid carriers for transdermal delivery.

Dimethyl fumarate was formulated into nanostructured lipid carriers to deliver the drug transdermally in a safe and efficient way while ensuring the stability of the drug. For that purpose, several methods of NLC preparation, and different components were tested to produce nanoparticles of acceptable quality attributes. The next steps involved particle size determination, drug loading, drug release and permeation through human cadaver skin, and ex vivo skin irritation tests to verify any reduction in the irritation caused by application of the drug.

Chapter 2: Background and significance

2.1. Alzheimer's Disease:

Alzheimer's disease (AD) is a progressive degenerative disorder affecting the brain function in the elderly. However, people younger than 55 years of age can also suffer from early onset, or familial AD due to inherited genetic mutations (5).The disease symptoms include memory loss, confusion, depression, hallucination and related psychoses. AD is characterized by synaptotoxicity, neurotransmitter disturbances, and accumulation of two proteinaceous materials, namely amyloid-β (Aβ) plaques in the brain interstitium and tau tangles within the neurons. These events cause interference with the normal nutrition and function of the neurons leading eventually to their death and brain atrophy in later stages (14). AD represents a major public health problem in modern times. In 2020, it is estimated that there are about 5.8 million 65 years and older AD patients in the USA. By 2050 the number is expected to reach 13.8 million with the current situation of the lack of cure for this disease (15). It poses a huge socioeconomic burden due to the long duration of the disease and need for institutionalization or caregiving. In 2019, caregivers of AD patient provided an estimated 18.6 billion hours of unpaid assistance, a contribution to the nation valued at $244 billion (15, 16). AD has multifactorial complex etiopathologic mechanisms that are not fully elucidated. Different hypotheses have been proposed to explain the mechanism behind the disease initiation and progression, including Aβ hypothesis, Tau hypothesis, cholinergic neuronal loss hypothesis and oxidative stress and inflammation hypothesis, etc. To date, there is no cure for AD, however, continuous efforts have been focusing on discovering anti-AD drugs based on these hypotheses (17). Nevertheless, all the current approved drugs are based on the cholinergic hypothesis that proposes the

cognitive decline is due to the death of cholinergic neurons in the basal forebrain and loss of cholinergic neurotransmission in the cerebral cortex and other brain regions, therefore increasing the level of acetylcholine neurotransmitter in the CNS by the administering cholinesterase inhibitors would be beneficial for AD patients (18, 19). There are five FDA approved drugs for management of AD: rivastigmine, donepezil, and galantamine as cholinesterase inhibitors; memantine as a non-competitive N-methyl-D-aspartate (NMDA) receptor antagonist; and memantine with donepezil as a combination therapy. These therapeutics are mostly administered orally (20). Oral Anti-AD therapy are associated with GI side effects typical of cholinergic effects, which in addition to age and condition related factors e.g. other disease conditions, polypharmacy, dysphagia, etc. may predispose non adherence to treatment (21).

2.2. Multiple sclerosis

Multiple sclerosis is a chronic neuro-inflammatory disease affecting the young adult population with onset at an age of 20-40 years. Histopathologically, it is characterized by focal destruction of the myelin sheath in both gray and white matter with frequently concomitant cortical demyelination and may be followed by oligodendrocytes apoptosis (22). Axonal loss is a hallmark in MS pathogenesis and correlates very well to the irreversible neurological deficient in patients with the disease and is evident in all stages of the disease (6). Acute MS is also associated with immune cell infiltration. It has been hypothesized that MS is an autoimmune disease, where autoreactive T and B lymphocytes, directed at myelin mediate its destruction within the CNS (9). However, this hypothesis could not be proven yet, as there is not any evidence that could link any single antigen or

antibody to MS specific cell-mediated or humoral immunopathogenesis. This leads to the idea that inflammation is not the primary etiology of MS (23). Neurologists divide MS into 4 subtypes depending on the pattern of the disease: relapsing remitting MS, secondary progressive, primary progressive, and progressive relapsing. Relapsing remitting MS type is the most common type and is characterized by the swinging pattern with periods of flare ups and remissions, that may not be associated with complete recovery and would leave behind some permanent damage. The other subtypes represent the possible forms of the disease progression (8). MS symptoms vary greatly depending on the specific area affected and can include sensory disturbances, walking difficulties, vision problems, intestinal and urinary system dysfunction, and cognitive and emotional impairment (6). Like AD, MS has a multifactorial etiology with genetic predisposition and environmental factors being involved. With no cure yet, MS approved therapy is only palliative and does not stop the neurodegeneration (6). Currently, there are 10 FDA approved drugs for treatment of MS through immunomodulation. Most of these drugs are administered parentally and only few of them are available as oral tablets (24). Given the potentially incapacitating nature of the disease and the fact that it affects active young adults, it may be potentially beneficial to explore other routes of administration that are less invasive compared to injections, and not associated with GI side effects as opposed to oral route. Indeed, the transdermal route offers such advantages and would be an attractive alternative for administration of drugs for MS and would be worthy of investigation.

2.3. Skin

Skin, being the outermost organ, functions as a protective barrier of the body from the external environmental hazards including radiation, chemical, and microbiological. It also helps controlling and maintaining the body temperature and water content. Additionally, it has unique functions concerning physical appearance and sensory perception. Skin is the largest organ as well, weighing about 4.2 kg and having a surface area of about 1.2 m^2 (25). Structurally, the skin is divided into three layers, starting from the external surface to bottom: epidermis, dermis, and hypodermis as illustrated in Figure 2.1. The epidermis is the cellular part of the skin mostly composed of keratinocytes besides some other cells with specific functions, such as melanocytes, Langerhans cells, and Merkel cells, which are responsible for melanin production, immune reactions, and sensory reception, respectively.

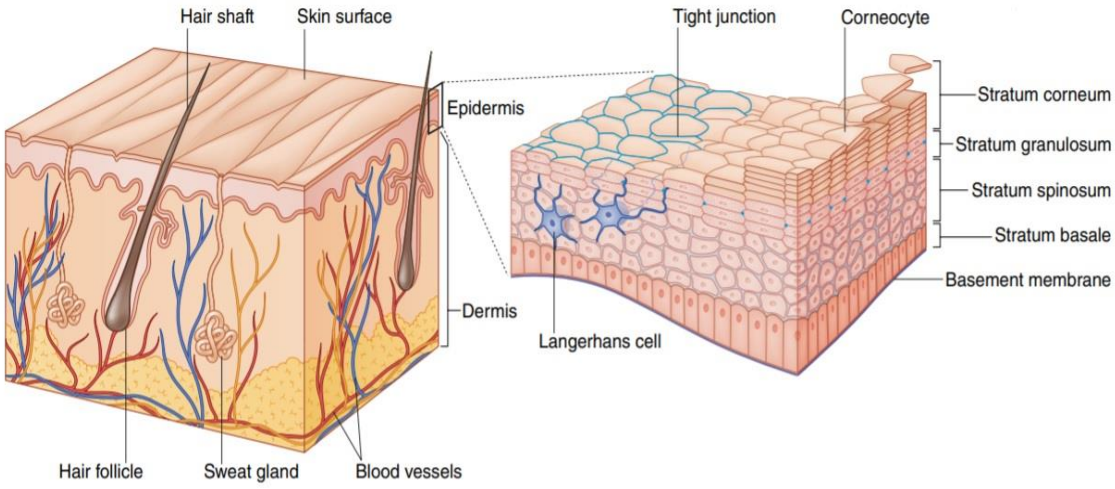

Figure 2.1. Human skin structure (26).

The epidermis (75-150 μm thick) starts as stratified columnar cells at the boundary right above the dermis anchoring to a specialized layer called basement membrane. As they divide, the keratinocytes move upward, stop proliferation, and start to differentiate until they flatten and die. Along their journey to the surface they form 4 distinct layers, stratum basale being the innermost, stratum spinosum, stratum granulosum, and the uppermost layer, the stratum corneum (SC) (27). Structurally, the SC is made of 10-25 layers of dead cornified cells, corneocytes, filled with keratin and embedded in a lamellar lipid matrix composed of ceramides, cholesterol, cholesteryl esters, and fatty acids in a brick and mortar type of structure (28). This unique organization imparts the barrier property to the skin. The dermis (0.6-3 mm thick) lies below the epidermis and is mainly composed of fibroelastic connective tissue with abundant collagen and elastin fibrils. It is also rich in blood capillaries with the main function of supporting and nourishing the epidermis. In addition, it contains the hair follicles, sweat glands, sebaceous glands, nerves, and sensory receptors. The hypodermis, is a layer of connective tissue mainly composed of adipose cells with the main function of thermal insulation, storing energy, and mechanical cushion by absorbing impact (29).

2.4. Skin as a route of drug delivery: Advantages and limitations

Being the largest and most accessible organ in the body, the skin presents an attractive route for drug delivery, whether intended for either a local (topical/dermal delivery) or a systemic action (transdermal delivery). There are 3 proposed pathways for drug absorption through the skin: across the corneocytes and lipid bilayers (transcellular), along the tortuous path between the cells (intercellular), through skin appendages (transappendageal), as shown in Figure 2.2. With the intercellular and transcellular

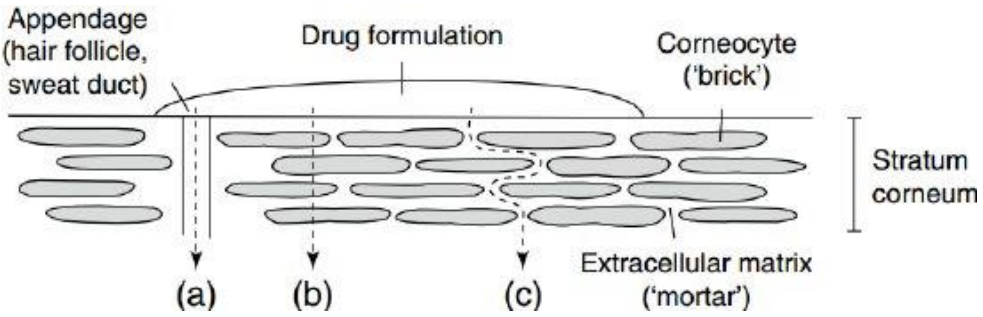

Figure 2.2. Drug permeation pathways in the skin (stratum corneum shown): (a) the transappendageal route, (b) the transcellular route, and (c) the intercellular route (30).

pathways, also known collectively as transepidermal routes, accounting for most of the drugs absorption. The drug permeation through skin involves alternating partition and diffusion processes through the different skin layers. Since transport is achieved mainly via passive diffusion, percutaneous absorption and can be described by Fick's first law of diffusion:

$$J = \frac{dm}{dt.S} = \frac{KD(C_0 - C_i)}{h}$$

Where *J* is the flux per unit area, dm is the amount of permeant passing through the membrane in time dt with a surface area of S, K is the partition coefficient of the permeant, D is the diffusion coefficient in the SC of path length h, C_o is concentration of permeant applied to the skin surface and C_i is the concentration of permeant inside skin. Assuming sink condition exists, $C_0 >> C_i$, then the above equation can be simplified into:

$$J = P.C$$

Where, $P = \frac{KD}{h}$ is the permeability constant of the penetrant

Indeed, drug delivery through the skin offers several advantages: a) targeting the organ itself and lowering the side effects associated with systemic drug delivery (local delivery), b) avoidance GI side effects/metabolism and hepatic first pass effect, c) non-invasive and to provide improved patient compliance, d) improve efficacy and reduce toxicity, etc. (31). Transdermal delivery offers an exceptionally ideal solution for ND therapeutics, as it may enhance the efficacy of the drugs, and improve the patient's compliance through reducing the oral treatment associated side effects. Patient compliance for such diseases is crucial in achieving a sustained therapeutic outcome (32). Non-compliance is a significant issue that is often underestimated. Besides being associated with poor disease control, drug adverse effects, hospitalizations, and mortality, non-compliance also represents a heavy burden to economy. In the USA, non-compliance causes about 33-69% of all medication-related hospital admissions, which is estimated to cost up to $100 billion per year (33).

2.5. Strategies to enhance skin permeability

Despite all the aforementioned advantages of transdermal delivery, only about 20 active drug molecules have been approved by the FDA for transdermal delivery due to the limitation of the skin permeability imparted by the powerful barrier function imposed by the stratum corneum (SC) (34). Currently, drugs with certain physicochemical characteristics, such as small molecular weight of <500 Da, ideal lipophilicity (logP 1-3.5), and low dose, have been formulated as transdermal drug delivery systems (31). Nevertheless, a significant amount of research has been done to investigate and develop different strategies to enhance the transdermal delivery of drugs, which fall generally into 2 main categories, shown in (Figure 2.3), those that utilize formulation optimization

approaches to enhance the penetration of actives. These approaches are also described as passive, as they rely on passive diffusion

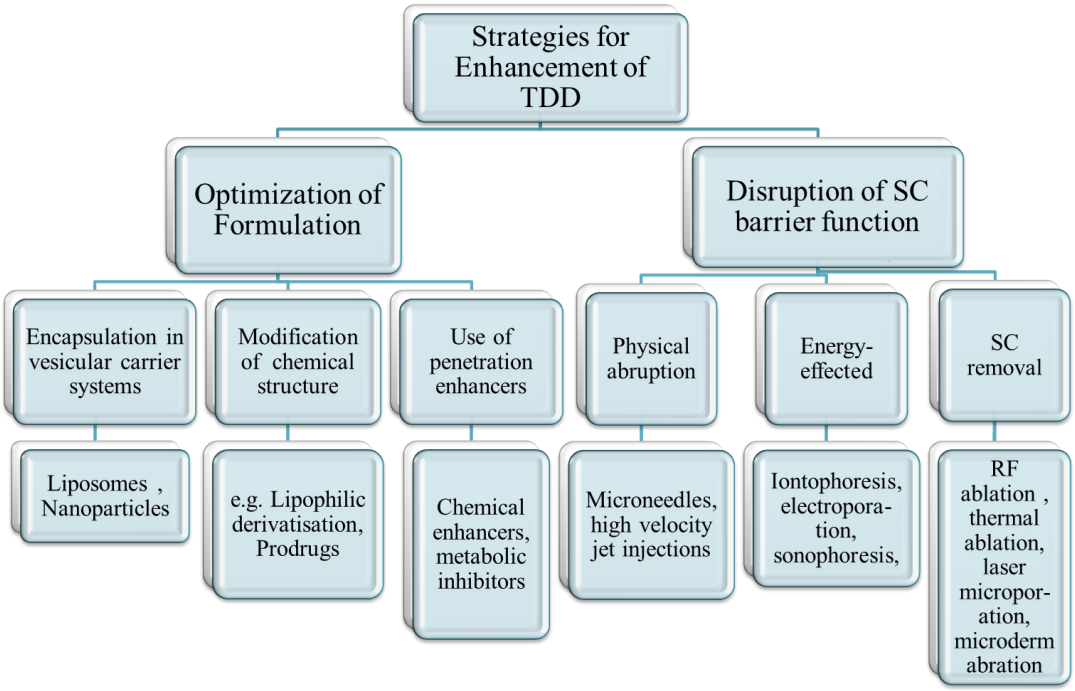

Figure 2.3. Different penertation enhancement strategies.

of the actives through the enhanced skin permeability, such as using more lipophilic prodrugs, or inclusion of chemical penetration enhancers, etc. Approaches that involve physically disrupting the SC comprise the other category and are also described as active methods because they involve applying a sort of a driving force to effect the permeation enhancement, for example, use of iontophoresis, microneedles, etc.(35). We will discuss the use of chemical penetration enhancers and lipid nanocarriers with nanostructure lipid

carriers (NLCs) in particular, as they constitute the main focus of the research in this dissertation.

2.5.1. Chemical penetration enhancers

The use of chemical penetration enhancers (CPEs) have been extensively studied. They include a broad range of materials that interact with the skin in certain ways causing a transient increase in its permeability (36). Although structurally variable, they need to have some common desirable characteristics, such as being nontoxic, nonirritant and nonallergenic; providing a rapid, reproducible, unidirectional, and reversible enhancement action; pharmacologically inactive; and compatible with the drug and other formulation excipients (37). The currently known CPEs have most of these criteria, but no ideal one has been discovered yet. They can be classified according to their chemical class as shown in table 2.1. Another classification is based on intended target, so CPEs can act as enhancers for dermal delivery, transdermal, or both (38). CPEs interact with the SC in different ways to alter its barrier function. Based on understanding the factors influencing the drug diffusion, Barry and co-workers proposed the lipid-protein partitioning theory (39), which postulate that the CPEs could enhance drug permeation through direct disruption of the SC lipid or protein structures, or by promoting the drug partitioning (40). Figure 2.4 illustrates the possible actions of CPEs on the SC lipids and protein structures and how they can modify them to promote the penetration of drug molecule. Disrupting the lipid packing plays a significant role in increasing the permeability of skin creating discontinuities and microcavities that facilitate movement of the drug molecule. CPEs can achieve this through interacting with polar headgroups of the lipid, or non-polar chains through H bonding

Table 2.1. Classification of chemical penetration enhancers according to their chemical class and some examples (41).

Chemical class Enhancer		Example
Alcohols	Short-chain alcohols	Ethanol, Isopropyl alcohol
	Long-chain alcohols	Decanol, Octanol
	Glycols	Propylene glycol (PG)
Amides	Cyclic amides	Azone® (1-dodecylazacycloheptan2-one or laurocapram)
Fatty acids		Lauric acid, Oleic acid, Linoleic acid
Esters Alkyl esters		Ethyl acetate, Butyl acetate, Methyl acetate
Fatty acid esters		Isopropyl myristate, Isopropyl palmitate
Ether alcohols		Transcutol® (diethylene glycol monoethyl ether)
Surfactants	Anionic surfactants	Sodium lauryl sulfate (SLS)
	Cationic surfactants	Benzalkonium chloride Cetylpyridinium chloride Cetyltrimethylammonium bromide
	Nonionic surfactants	Polysorbates (Tween® 20, Tween®80, etc.)
	Zwitterionic surfactants	Dodecyl betaine
Sulfoxides and analogues		Dimethyl sulfoxide (DMSO) Decylmethyl sulfoxide (DCMS)
Essential oils		Eucalyptus, Ylang ylang, Chenopodium
Terpenes and its derivatives		d-Limonene, l-Menthol, 1,8-Cineole
Pyrrolidones		*N*-methyl-1-2-pyrrolidone (NMP) 2-pyrrolidone (2P)

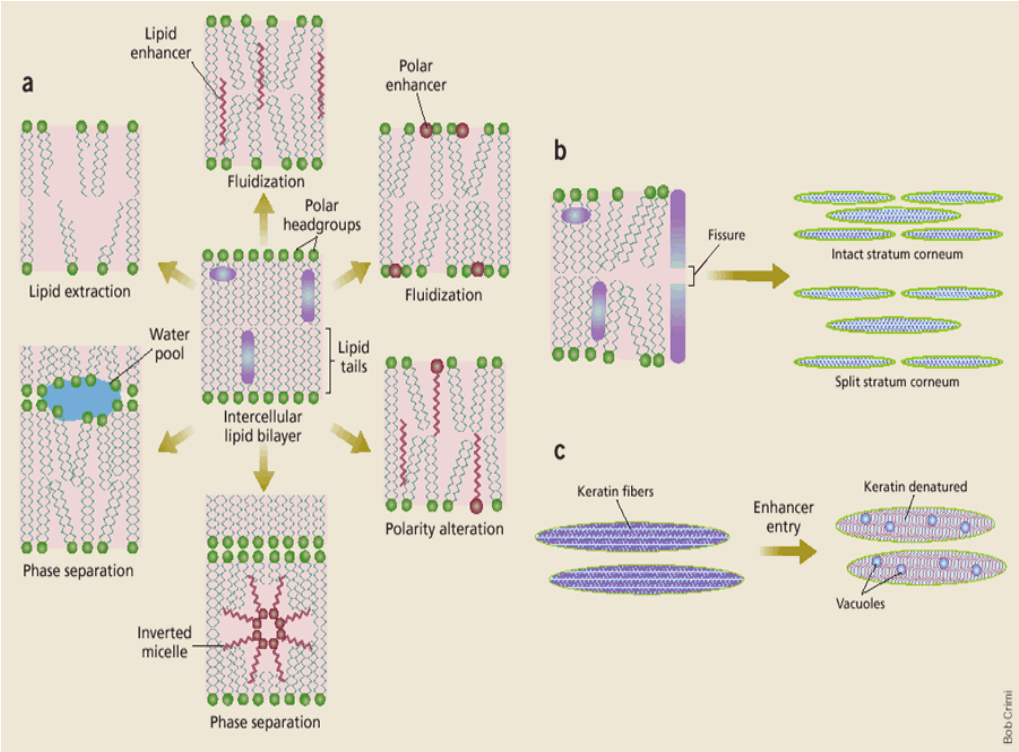

Figure 2.4. Representation of the sites of action of chemical penetration enhancers within the SC, a: action on the intercellular lipid; b: action on the desmosomes and protein structures; c: action on the corneocytes (42).

resulting in lipid fluidization. Solvents can extract lipids from the SC creating channels for drug diffusion. Additionally, some CPEs can cause heterogenous disruptions in lipid packing leading to phase separation and creating water filled pores (43, 44). Another mechanism of penetration enhancement involves the interaction of the CPE with the keratin filaments within the corneocyte causing their denaturation and changing their conformation, which decreases the diffusive resistance to the penetrant. On the other hand, solvents can act on the desmosome that maintain the integrity of the SC by binding the

corneocytes together resulting in fissuring and splitting of the squamae. Such effect is considered to be too harsh and may cause skin irritation (45). Finally, CPEs can increase the drug permeation through a partitioning effect, where it alters the chemical properties of the SC resulting in enhanced solubility of the drug within the SC leading to increase its partitioning (41). Further, CPEs may have an indirect effect on permeability through changing the solubility and thermodynamic activity of the drug in the vehicle promoting its penetration (36). CPEs can behave differently with different compounds, and their mixtures can act synergistically to provide more enhancement than when used alone (46). More details on CPEs will follow in the next two chapters.

Although some CPEs might be associated with skin irritation, and are not useful for delivery of large molecules, they still represent the most widely used enhancement method, as they can readily added to the formulation, do not require any instrumentation, cost-effective, and offer simple formulations that can be self-administered (46).

2.5.2. Nanostructured lipid carriers

Transdermal drug delivery using nano-carriers have been widely investigated due the advantages associated with the nanocarriers including increased surface area, improved drug solubility and stability, controlled drug release, reduced skin irritation, increased drug loading, and improved the skin permeability to drugs (47). Nano-carriers of interest in skin delivery can be broadly divided into polymeric-based and lipid-based, and nanocrystals. Lipid-based nanocarriers fall into two main groups, vesicular such as liposomes, ethosomes, etc., while solid lipid nanoparticles (SLN)s and nanostructured lipid carriers (NLC)s comprise the solid matrix nanocarriers (48). SLNs have a matrix made with a lipid

of a high melting point. NLCs on the other hand are made of a combination of both solid and liquid lipids mixed at different ratios, while maintaining the solid nature of the matrix. They are considered as the second generation of the SLN and were developed to overcome a major drawback associated with SLN is related to drug expulsion as a result of recrystallization of the lipid into a more ordered crystal form (40, 49, 50). NLCs have gained wide application in developing topical delivery systems, as they enhance the stability of otherwise loaded molecule, provide controlled release of the active, and hinder transepidermal water loss due to occlusion effect, therefore may result in enhancement of API efficacy and reduce toxicity (51). They can promote drug penetration physically by being small in size with larger surface area, they tend to adhere to the skin surface with the active molecules being attached to their surface presented to the skin surface close enough to promote interaction and penetration (52). Furthermore, this adhesion to the skin, further enhanced by the nature of the NLCs components, may create a continuous thin film on top of the skin resulting in an occlusion effect. Occlusion increases the skin hydration which in turn reduces the packing of the corneocytes and widens the gaps between them creating channels for the drug to diffuse through (49, 53). Additionally, NLCs lipid could potentially interact with the lipids of the SC, if they were miscible and had a lower melting point. Lipid chains of the NLC starts to diffuse into the SC lipid layers and ultimately integrating with them (40). Basically, NLCs are O/W nanoemulsion-derived particulate carriers having major ingredients, similar to any other emulsion, of lipid, water, and surfactant. The choice of the components of the lipid matrix plays a significant role in successfully producing NLCs. One governing factor is the solubility of the drug molecule in the lipid, as it influences the drug loading, and encapsulation pattern. Additionally, the

choice of the lipid mixture should ensure that the lipids are spatially different as much as possible. These differences create imperfections within the crystal lattice of the solid lipid and help both accommodating more drug molecules and reducing the chance of producing more uniform perfect crystals upon transitioning into a more stable lipid crystal modification. The most commonly used solid lipids in NLCs production include mono, di, and triglycerides e.g. glyceryl monostearate and glyceryl palmitostearate; fatty acids, such as stearic acid; and waxes. Liquid lipids can be fatty acids, such as oleic acid, or medium chain triglycerides. As for surfactants, they play an important role in dispersing the lipid droplets in the external aqueous phase and also help in stabilizing the nanoparticles against aggregation through steric hindrance (non-ionic surfactants), or through increasing the particles surface charge (ionic surfactants) (51, 54). There are several methods implemented to produce NLCs, some need high energy input such as high pressure homogenization, and ultrasonification method, high shear homogenization, low energy-based methods include microemulsion method and double emulsion method, and solvent-based methods; solvent emulsification-diffusion method and solvent-emulsification evaporation method (55). Both composition and method of production affect the structure of the NLCs and the drug loading pattern. More details on the methods of preparation of NLCs employed in this research are included in Chapter 6 of this dissertation.

2.6. Transdermal drug delivery systems

A transdermal drug delivery system (TDDS) is defined as a “flexible single-dose preparation intended to be applied to the unbroken skin to obtain a systemic delivery over an extended period of time” (56). Although the concept of transdermal drug delivery system is very old, the TDDSs, as we know them, have been introduced in the 70’s of the

last century. It started with scopolamine transdermal system as the first FDA approved patch in 1979 for the treatment of motion sickness, and followed with systems containing active pharmaceutical ingredients for pain management, hormonal replacement, contraception, angina, hypertension, smoking cessation and some CNS disorders (57). Table 2.2 list the currently FDA-approved TDDSs (58). In addition to the advantage of transdermal delivery discussed previously, TDDSs offer additional advantages such as, eliminating the frequent dosing, ease of termination, providing consistent drug levels and constant plasma levels, and reducing the possibility of over or under dose (59, 60). In addition, there is an advantage to being able to see the applied patch as opposed to remembering if the patient has or has not taken their oral medication especially in patients who have impaired memory functions (33)**.** Moreover, patches are associated with higher compliance due to ease of use and increased patient/caregiver satisfaction (61). A study involving 1059 AD patients' caregivers revealed that 70% of them preferred rivastigmine patch over capsules. The preference was based on the patch ease of application and less interference with everyday life (62). TDDSs fall primarily into 2 types, the reservoir type and matrix type, both have to have some common features including an impermeable backing membrane, an adhesive that adheres the patch to the skin, and a release liner protecting the adhesive layer, which is removed prior to application (Figure 2.5).

Table 2.2. Currently FDA approved TDDSs* (58)

Approval year	Drug/product name	Indication	Marketing company
1979	Scopolamine/TransdermScop	Motion sickness	Novartis Consumer Health (Parsippany, NJ, USA)
1984	Clonidine/Catapres-TTS®	Hypertension	Boehringer Ingelheim (Ridgefield,CT, USA)
1988	Nitroglycerin/Nitroglycerin	Angina pectoris	Fougera Pharmaceuticals Inc
1990	Fentanyl/Duragesic®	Chronic pain	Janssen Pharmaceutica (Titusville, NJ, USA)
1994	Estradiol/Climara®	Menopausal symptoms	Bayer Healthcare Pharmaceuticals Inc
1996	Nicotine/Nicoderm®	Smoking cessation	Sanofi Aventis US LLC
1998	Estradiol with norethidrone/ CombiPatch®	Menopausal symptoms	Noven Pharmaceuticals Inc
2003	Oxybutynin/Oxytrol®	Overactive bladder	Allergan Sales LLC
2003	Estradiol with levonorgestrel/ Climara Pro ™	Menopausal symptoms	Bayer Healthcare Pharmaceuticals (Wayne, NJ, USA)
2006	Selegiline/Emsam®	Major depressive disorder	Somerset Pharmaceuticals Inc
2006	Methylphenidate/Daytrana®	Attention deficit Hyperactivity disorder	Noven Pharmaceuticals Inc
2007	Rotigotine/Neupro®	Parkinson's disease	UCB Inc
2007	Rivastigmine/Exelon®	Dementia	Novartis Consumer Health (Parsippany, NJ, USA)
2008	Granisetron/Sancuso®	Chemo-induced emesis	Kyowa Kirin Inc
2010	Buprenorphine/BuTrans®	Chronic pain	Purdue Pharma L.P. (Stamford, CT, USA)
2011	Testosterone/Androderm®	Male hypogonadism	Allergan Sales LLC
2014	Ethinyl estradiol with norelgestromin/ Xulane®	Contraception	Mylan Technologies Inc
2019	Asenapine/Secuado®	Schizophrenia	Hisamitsu Pharmaceutical Co Inc

* Only the first approved brand of the active

What differentiates these transdermal drug delivery systems is the way in which the drug is incorporated into the system. In the reservoir type, the drug is dissolved or dispersed in a liquid or a gel form sealed in a compartment sandwiched between the backing layer and a rate-controlling membrane. Then the outer surface of the rate-controlling membrane is laminated with a thin layer of adhesive (63). Matrix patches, on the other hand can have any of the possible designs: drug dispersed or dissolved in a polymeric matrix fixed to a backing layer and has adhesive layer surrounding its periphery without covering the drug matrix, a second possibility is to have the adhesive coating cover the entire surface of the drug matrix. The other presentation of matrix patches involves dissolving the drug in the adhesive polymer, which provides a design with the least layers and is often referred to as drug in adhesive (DIA) (64). DIA types are preferred by patients as they are thin and offer flexibility and comfort (65). Of the FDA-approved TDDSs, DIA comprise 72% of patches, while drug-in-matrix type constitute 16% of them and drug-in-reservoir type has only 12% share (66).

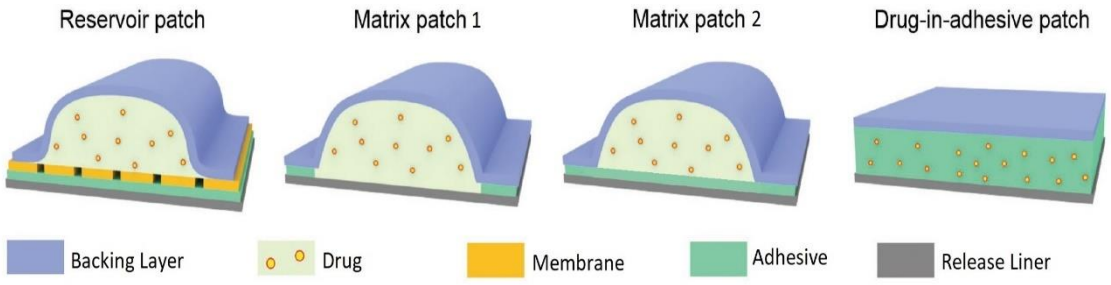

Figure 2.5. Schematic representation of the different patch designs (modified from (67)).

Patches regardless of design need polymers to formulate the drug reservoir/matrix, which can be selected from a wide range of polymers based on the nature of the desired design,

compatibility with active and excipients, drug release properties, and skin biocompatibility. The selections can include cellulosic polymers, non-adhesive acrylates and methacrylates (68). Adhesive polymers also known as pressure sensitive adhesives (PSA) because they are capable of sticking to surfaces with upon light pressure application (67). PSAs can serve as the adhesive layer of patches of reservoir and matrix types and can function as both adhesive and matrix at the same time for DIA patches. An ideal PSA should have the following behaviors, a) allows easy removal of the release liner of the patch prior to use; b) has a good adhesive property to human skin; c) stays in place on skin surface comfortably throughout the labelled application time without itching or irritation; (v) permits easy, non-traumatic, and clean removal of the patch at the end of use (69). All PSAs are viscoelastic materials, which means that they behave sometimes as liquids and others as solid depending on the frequency of applied stress at any temperature, a property essential for their function. The patch adhesion properties are described by the terms tack, shear adhesion, and peel adhesion. Tack is the initial bonding between the PSA and the substrate (skin surface) after a brief low-pressure contact. This initial bonding usually happens very fast and is governed by both the rheological properties of the PSA (acting as a viscous liquid) and the surface energies of both of the adhesive and the skin surface, where the surface energy of PSA is much lower than that of the skin. Shear adhesion is the resistance of the matrix to flow, which represents the cohesion of the PSA and is dependent upon the elastic property of the adhesive. PSA used in TDDS must exhibit high cohesiveness and resistance to flow upon shear stress, otherwise the matrix would creep and ooze from the edges of the patch applied to the skin. Peel adhesion the force required to peel away a patch for the skin surface. The higher the peel adhesion, the more painful

the peeling of the patch (70, 71). The viscoelastic moduli of PSAs determined by rheological analysis represent the best correlation to the adhesive's performance (tack and peel). These moduli are the elastic or storage modulus G′ and the viscous or loss modulus G″. The values of these two moduli can be used to describe the PSA behavior under stress. If G″ > G′, then the material behaves as a liquid. This occurs at low frequencies, as the material needs to act as a liquid to facilitate the bonding to the substrate. On the other hand, at high frequencies G′ should be greater, as the PSA starts to behave as a solid to facilitate the debonding from the skin surface without leaving residue. The ratio between the loss and storage moduli (G″/G′) represents the phase angle tangent (tan δ), which is ratio of the dissipated to stored energy (72).

There are different types of PSAs used for development of TDDSs that include polyisobutylenes, silicones, acrylates. Polyisobutylene adhesives are isobutylene homopolymers of a wide range of molecular weight and viscosities. Isobutylene PSAs for TDDS development are usually composed of a blend of high and low molecular weight polymers to adjust the tack and adhesion properties of the PSA. They have low permeability to air and water vapor, which may improve the drug flux. However, it could cause skin maceration upon prolong wearing (64, 71). Acrylates PSAs are copolymers of acrylic acid esters obtained by blending soft and hard monomers at different ratios to enhance the cohesiveness of the PSAs. Sometimes functional groups (-OH, or -COOH) can be incorporated into the backbone of the polymer that provide polar biding sites, and also for crosslinking (69). Acrylate adhesives are widely used due to their versatile physicochemical properties, high stability against oxidation, and transparency (73). Finally, Silicon based PSAs are mixtures of poly dimethyl siloxane (PDMS) and silicate

resin in different ratios. Silicon PSAs are known to be incompatible with amines due to the reaction between the latter and their silanol groups, which can be prevented by masking these terminal groups through methylation (71). The selection of the PSA is very critical for the development of a successful transdermal drug delivery system. Further, the physicochemical properties of the drug including chemical structure, solubility, molecular weight, etc.; type of and concentration of other excipients, such as penetration enhancers, solubilizers, and crystallization inhibitors are important factors affecting the choice of the PSA, as they have direct impact on the patch performance such as drug release and stability of the product (73). Zhao et al. found that addition of isopropyl myristate, a CPE, has increased the in vitro release of blonanserin from DURO-TAK® 87-2287 (polyacrylate) DIA patch, and that increasing the concentration of the CPE caused a reduction in both tack and shear-adhesion of the PSA. They attributed the results to CPE- induced plasticization of the PSA (72).

Chapter 3: Design and In vitro Evaluation of Pressure Sensitive Adhesive Patch for the Transdermal Delivery of Galantamine[1]

3.1. Introduction

Transdermal drug delivery systems (TDDS) present the active pharmaceutical ingredient (s) (API) to the systemic circulation through application of the device on the skin. In this case the APIs are expected to permeate across the skin usually by passive diffusion (some devices utilize non-passive approaches such as iontophoresis or ultrasound) to reach the microcirculation of the skin, and then the systemic circulation (74). TDDS offer several advantages over other routes of administration, such as avoidance of first pass metabolism and gastrointestinal side effects, non-invasiveness, self-application, controlled drug delivery, etc. (75). Indeed, passive transdermal patches, a type of TDDS, can reduce the number of doses taken by a patient per day, and some are specifically designed to continuously deliver certain APIs for up to a week (31). In general, TDD patches are of two types, the reservoir and the matrix type of patch. The latter involves dissolving or dispersing the API into an appropriate polymer solution, and then the patch is prepared by a solvent evaporation method, and this type of patch is also known as a drug-in-adhesive (DIA) patch(64). Acrylates, silicones, and polyisobutylene polymers are the most widely used polymers for the preparation of DIA patches. These polymers are also referred to as pressure sensitive adhesives since they provide strong bonding to surfaces

[1] A version of this chapter is published in the European journal of Pharmaceutics and Biopharmaceutics: Ameen D, Michniak-Kohn B, Euro J Pharm Biopharm, 2019;139: 262-271.

upon slight pressure and de-bond without leaving any residue (76). In addition to forming a matrix to load the API, PSA also provide adhesion to the skin, which is very important to ensure that the released drug is available for permeation. Furthermore, the choice of PSA plays a critical role in the overall patch performance (73). Transdermal patches have some superiority among other dosage forms when it comes to convenience of administration especially patients with neurological diseases, such as Alzheimer's disease (AD). AD, a major cause of senile dementia, is characterized by progressive neurodegeneration causing gradual neuronal and memory loss and cognition impairment (77). Indeed, adherence to treatment, especially in Alzheimer's disease is crucial for maximal clinical efficacy. Evidence showed that continuous galantamine treatment beyond 6 months was associated with reinforced therapeutic treatment and that discontinuation of treatment was associated with apparent cognitive impairment (78). However, research reveals that compliance to treatment is well below optimum, which can be attributed to several factors. The decline in memory and cognitive function of the patients and reliance on the caregiver to administer the medication are key factors in low adherence (79). Furthermore, elderly patients usually complain of chronic diseases requiring simultaneous drug therapies along with multiple daily dosing, drug-drug interactions and higher incidence of adverse reaction all predisposing to patient non-compliance (80). The effects of the aforementioned factors can be alleviated by using transdermal patches. Studies have shown that applying transdermal rivastigmine patches resulted in significantly higher caregiver preference and better patient compliance than the oral treatment (81). These results highlight the need to develop TDDS for other AD drugs in order to maximize their efficacy. Galantamine (GAL) is one of first-line treatments for mild-to-moderate AD with dual modes of action. It is both a selective

reversible acetylcholinesterase inhibitor as well as an allosteric nicotinic receptor modulator (82). GAL was shown to improve patient cognitive and global function, ability to perform activities of daily living and behavior compared to placebo and baseline, and also it reduced caregiver burden (83). However, it is associated with gastrointestinal side effects and induced weight loss that necessitates starting with lower dose then gradually increasing up to the desired level to improve tolerability (84). GAL, which chemical structure is depicted in Figure 3.1, is a tertiary alkaloid with a molecular weight of 287.35 g/mol and log p of 1.8 (PubChem CID: 9651). With such physicochemical properties, and therapeutic profile, it is considered as a good candidate for transdermal delivery.

The objective of this study was to develop a galantamine matrix transdermal patch based on PSA. The final formulation was optimized by selecting the best performing PSA, drug loading, penetration enhancer, and controlling crystallization. The optimized patch formulation was characterized, and the transdermal delivery of the drug was tested using human cadaver skin, which is the golden standard when it comes to testing transdermal flux in vitro. The flux of the drug was used to calculate the predicted steady state plasma levels and confirm attaining therapeutic concentrations in vivo.

3.2. Materials and Methods

3.2.1. Materials

Galantamine (GAL) was purchased from APExBio (Houston, TX, USA). Limonene (Lim), Terpineol (Terp), and Propandiol (Prop) were purchased from Sigma (St. Louis, MO, USA). Borneol (Bor) was purchased from Alfa Aesa evaporr (Tewksbury, MA, USA). Labrafac lipophile (Lab), Lauroglycol™ FCC (FCC), caproyl 90 (Cap) were

generous gifts from Gattefossé (Paramus, NJ). Oleic acid (OA) was a gift from Croda (Edison, NJ, USA). Oleyl alcohol (OAl), Decyl oleate (DO), and Octyldodecanol (OD) were gifts from BASF (Florham Park, NJ, USA). DURO-TAK 87-900A, DURO-TAK 87-2074, and GELVA GMS 788 were a gift from Henkel Corporation (Bridgewater, NJ). BIO-PSA 7-4202 silicone adhesive was a gift from Dow Corning (Midland, MI, USA). Backing film Scotchpak 9723 and 3M Scotchpak^{TM}1022 release liner were gifts from 3M Co. (St. Paul, MN, USA). High-performance liquid chromatography (HPLC) grade water, methanol and acetonitrile were purchased from BDH VWR Analytical (Radnor, PA, USA). Dermatomed human cadaver skin was obtained from New York Firefighter Skin Bank (NY, USA).

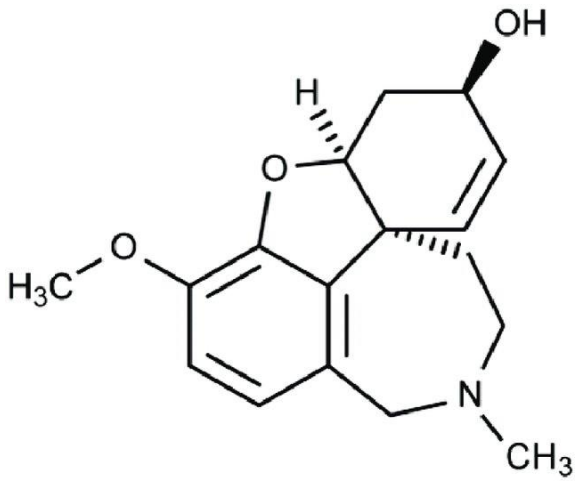

Figure 3.1. Chemical structure of galantamine.

3.2.2. Preparation and characterization of drug in adhesive patches

GAL patches were prepared by mechanically mixing the adhesive solution in ethyl acetate with a calculated amount of GAL as a solution in ethyl acetate to prepare 8, 10, 12,

and 15% GAL in dry polymer weight. The mixture then was applied onto the release liner using a micrometer adjustable wet film applicator (Zhengzhou TCH Instrument Co., Ltd, China) at a wet film with thickness of 500μm. Penetration enhancers at 5% of dry polymer weight each were added to the mixture of the polymer and GAL and mixed well and then casted as above. The wet patches were kept at room temperature for 15 min and then baked in a vacuum oven (Model 280A, Thermo Fisher, Waltham, MA, USA) at 80° C for 20 min. The dried patches were laminated with the backing layer and kept at ambient temperature until further testing. The final thickness of the patch was determined using a digital micrometer. Drug content was determined by punching 11mm disks at different locations of the patch and extracting each by sonication with an appropriate volume of 1:1 mixture of ethyl acetate and methanol for 1 hour. Then, the solution was filtered using 0.45μm syringe filter, diluted appropriately, and analyzed using a validated HPLC method described in the next section. All measurements were performed as triplicates.

3.2.3. HPLC Method of Quantification for GAL

3.2.3.1. Equipment and mobile phase

Galantamine was quantified using high pressure liquid chromatography (HPLC) with UV detection. The HPLC system included an Agilent 1100 Series Hewlett-Packard liquid chromatograph and the Agilent Chemstation software. The HPLC instrument was equipped with a UV detector (Agilent Dual Absorbance Detector G1315A), a pump (Agilent Quat pump G1311A), and an automatic injector (Agilent ALS G1313A Auto-samplers). A reversed-phase C18 column 5μm, 4.6x 150mm (Xterra, Waters) was used as

the stationary phase at a temperature of 25 ° C. The mobile phase composed of water for HPLC: Methanol (60:40 v/v) with 0.01% triethanolamine with pH adjusted to 5.2 using 85% *o*-phosphoric acid was pumped at a flow rate of 1.2 mL/min. The UV detector was set at a wavelength of 210 nm.

3.2.3.2. Standard solutions and calibration curve

A stock solution of GAL was prepared at concentrations of 0.2 mg/mL by dissolving 5mg of GAL in the mobile phase in 25 ml volumetric flask. Standard solutions were prepared by serial dilution of the stock solution with mobile phase. The standard solutions had a concentration range of 0.39-100µg/ml of GAL that covered the expected concentration range of GAL in the skin permeation samples.

3.2.3.3. Method validation

The HPLC method was validated by testing the linearity and precision through inter- and intra-day variability and determining the limit of quantification and limit of detection. The limit of quantification is defined as is the lowest concentration of the analyte that can be quantified with acceptable accuracy and precision and limit of detection value is the lowest concentration of the analyte that can be detected but not quantified. These values were calculated using the following equations :

$$LQ = \frac{10\sigma}{S}$$

$$LD = \frac{3.3\sigma}{S}$$

Where, LQ is the limit of quantification; σ is the standard deviation of the y-intercept of the regression lines of the calibration curves; S is the slope of the calibration curve; LD is limit of detection (85).

3.2.4. In vitro skin permeation

Frozen dermatomed human cadaver skin was obtained from New York Firefighters Skin Bank (New York, NY). The human cadaver skin pieces were harvested from the posterior torso of three different Caucasian donors (2 males and one female) with age range of 64-69 years. Upon receipt, the skin was kept frozen at -80 °C. On the day of study, the skin was thawed at room temperature, cut into pieces with an appropriate size to fit into the Franz diffusion cells, and hydrated in PBS pH 7.4 for 20 min. The permeation study was conducted using vertical Franz diffusion cells (Logan Instruments, Somerset, NJ). The skin pieces were sandwiched between the donor and receptor compartments with the stratum corneum facing upward toward the donor. Then, the whole assembly was clamped tightly. The skin barrier integrity was confirmed by measure TEWL using Vapometer. The receptor compartments were filled with 5.0 mL 5% ethanol in PBS (pH 7.4, 20mM) maintained at 37°C using a heating block and stirred continuously at 600 rpm. The diffusion cell area was 0.64 cm^2. The patches were punched to make 10 mm discs that were applied on top of the skin. At predetermined time points (2h, 4h, 6h, 10h, 11h, 22h and 24h), 0.3 ml of the receptor compartment was withdrawn and replaced immediately with an equal volume of fresh receptor medium. The withdrawn samples were analyzed using HPLC to determine GAL concentrations. All experiments were performed with 3-4 replicates.

3.2.5. Microscopic examination

Patches used for studying the crystallization of the drug were kept at room temperature in a closed container without lamination with a backing layer. The patches were visualized using Leica S8APO stereomicroscope equipped with an MC170 HD camera (Leica Microsystems, Inc., Chicago, IL, USA) at day 1, and every week for 4 weeks to investigate the potential of crystallization of GAL.

3.2.6. Galantamine release study

The release of GAL from selected patches was studied using vertical Franz diffusion cells (Logan Instruments, Somerset, NJ) mounted with a dialysis membrane with MWCO of 2K. Patches 10 mm in diameter were applied onto the dialysis membrane and the receptor medium was 5.0 mL 5% ethanol in PBS (pH 7.4, 20 mM) maintained at 37°C using a heating block and stirred continuously at 600 rpm. At 0.25, 0.5, 0.75, 1, 1.5, 2, 4, 6, 10, 20, 24 hours, 0.3 ml samples were withdrawn and replenished by an equal volume of fresh medium. The samples were analyzed using HPLC to quantify the amount of GAL released. The cumulative amount released per unit of surface area was plotted against time and fitted to several models including, Higuchi equation, first order, and zero order equations to obtain the best fit model (86, 87).

3.2.7. FT-IR Study

The FT-IR spectra of neat GAL, PEs, PSA, and patch formulations containing 10% GAL with or without PE were evaluated with Nicolet iS10 FT-IR Spectrometer (Thermo

Fisher, Waltham, MA, USA). The samples were tested by applying a drop of sample on top of the lens. The spectra were obtained at a resolution of 4 cm^{-1} from 4000 to 500 cm^{-1}.

3.2.8. Rheological study

Rheological measurements were performed with Kinexus rotational rheometer (Malvern instruments, Malvern, UK) using an 8 mm flat stainless steel plate. All tests were done at 32° C and a gap of 500 μm. The linear viscoelastic region (LVR), where the material usually behaves as an elastic solid, was determined at the strain range of 1-100% with a frequency of 1Hz. Frequency sweeps were done by oscillating the samples at angular velocity (ω) range of 0.1-100 rad/sec and a stress of 1000 pa within the LVR. Elastic and viscous moduli, G', and G'', as well as tan δ as a function of ω were recorded.

3.2.9. Data analysis

The individual permeation profile of each formulation was obtained by plotting the cumulative amounts of GAL permeated per unit skin area versus time. The cumulative amounts *(Qt)* is calculated using equation 1:

$$Q_t = (C_n \times V_s + \sum_{i-1}^{n-1} C_i \times V_r)/A \quad \ldots\ldots\ldots(1)$$

Where C_n is the drug concentration (μg/mL) in the receptor medium at sampling time *n*, C_i is the drug concentration (μg/mL) at time *i*, V_r (mL) is the volume of the receptor medium, V_s (mL) is the volume of the sample, and *A* represents the surface area of application (cm^2). The steady state flux (*J*) represents the slope of the linear portion of the plot. The lag time is equal to the x-axis intercept of the extrapolated linear portion of the permeation profile. The enhancement ratio (ER) was calculated according to equation 2:

$$ER = \frac{J\ with\ the\ \ enhancer}{J\ without\ enhancer} \ldots \text{Eq (2)}$$

All data are expressed as mean± standard deviation of four replicates. ANOVA and Student's t-test were used to test the level of significance. Results were considered statistically significant at p-value < 0.05.

3.3. Results and Discussion

3.3.1. HPLC method validation

Figures 3.2 depicts the chromatogram peak of GAL obtained with the HPLC method. The retention time for GAL was about 1.7 min, and the peak showed acceptable sharpness.

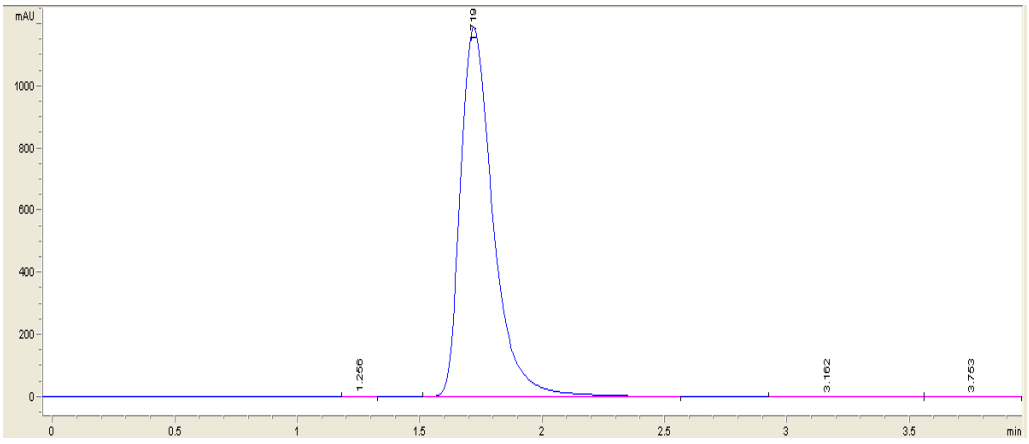

Figure 3.2. Chromatogram peak of galantamine at retention time of 1.7 min.

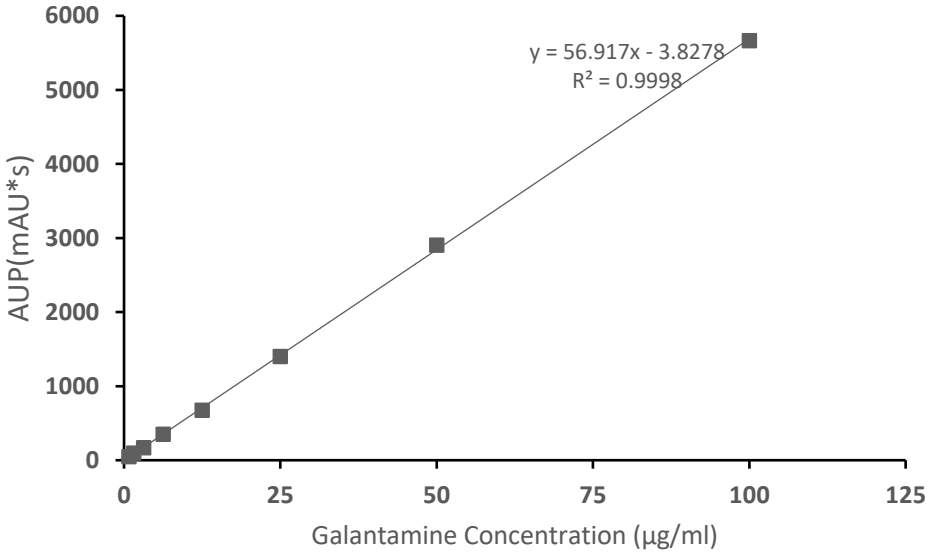

Figure 3.3. Galantamine standard calibration curve for HPLC assay method. Area under the peak (AUP) of the chromatogram against the concentration of galantamine. Values represent an average of 3 injections.

The calibration curve of GAL was constructed by analyzing standard solutions in the concentration range of 0.39-100 µg/ml using the HPLC method parameters for 3 injections and the average area under the peak was plotted against the concentration of the standard solution as shown in Figure 3.3. The method revealed a perfect linearity with R^2 of unity and LQ and LD of 0.27 and 0.09 µg/ml, respectively for GAL assay.

Table 3.1 shows the intra- and inter-day precision data for three different concentrations of GAL from 3 runs at different times on the same day or different days. All of the %RSD values fell below 2%, which indicted the repeatability and precision of the method.

Table. 3.1. Intra-Day and Inter-Day Precision Analyses of galantamine, n=3

GAL Concentration (µg/ml)	Intra-Day Analysis		Inter-Day Analysis	
	AUP (mAU*s) ±SD	%RSD	AUP (mAU*s) ±SD	%RSD
6.25	343.6±2.1	0.6	341.4±1.4	0.4
25	1381.6±8.8	0.6	1402.2±14.9	1.0
100	5637.2±58.7	1.0	5666.6±75.8	1.3

3.3.2. The effect of pressure sensitive adhesives on GAL permeation

Polymers selection plays a crucial role in designing matrix type transdermal patches. These polymers are integral not only to the performance, but also to the physicochemical stability of the transdermal patches (64, 73). Four different polymers were tested in this study to determine their compatibility with GAL, drug loading capacity and effects on the skin permeation of GAL. Table 3.2 lists the tested polymers along with their chemical composition and functional groups. The acrylate polymers tested had no functional group, a hydroxyl group, or a combination of -COOH and -OH.

Table 3.2. List of tested PSA with their chemical composition and in vitro skin permeation parameters of 8% GAL loading across human cadaver skin (n=3).

Adhesive	Chemical composition	Functional group	Flux (µg/cm²/h) ± SD	$R^{2\,a}$	$Q_{24}{}^{b}$ (µg/cm²) ± SD
DURO-TAK 87-900A	acrylates copolymer	None	2.25 ± 0.5	0.9893	55.56±1.7
DURO-TAK 87-2074	acrylates copolymer	-COOH / -OH	1.00 ± 0.8	0.9969	32.62±17
GELVA GMS 788	acrylates copolymer	-OH	6.00±0.9	0.9967	151.1±24
BIO-PSA 7-4202	Silicon adhesive	-	1.15 ± 0.4	0.9823	26.92±7.0

[a] R^2, linearity coefficient of the flux.

[b] Q_{24} is the amount of drug permeated after 24h.

On the other hand, the tested silicone polymer was specifically designed to be compatible with amine containing molecules. Initially, the suitability of the polymer was tested by studying the permeation of GAL from patches at a drug loading of 8% w/w of dry polymer. The results of the permeation study shown in Figure 3.4 demonstrate that the drug had higher permeation rate with the PSA containing –OH than other adhesives used. In addition, the acrylate PSAs were better than the silicone polymer for delivering GAL. Although the tested silicone adhesive was specifically designed to be compatible with amine compounds, it showed discoloration after oven drying, which was considered as a sign of incompatibility with GAL. PSAs with –COOH functional group are known to interact with amine containing compounds through hydrogen bonding between the –COOH and the amino group of APIs reducing their skin permeation (88, 89). GELVA GMS 788 exhibited the highest permeation of GAL among the tested polymers. Therefore, GELVA GMS 788 was selected as the polymer of choice for further experimentation.

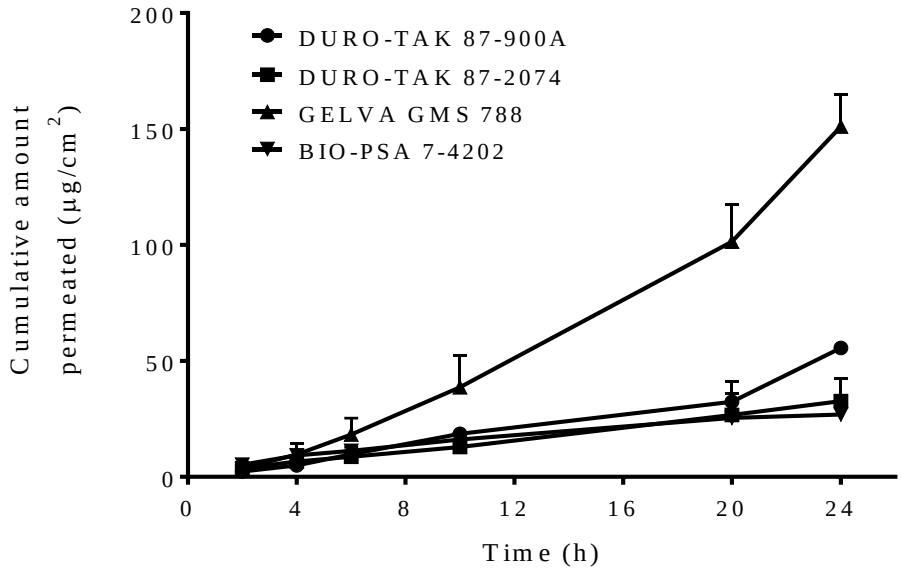

Figure 3.4. The effect of pressure sensitive adhesive type on the permeation of galantamine across human cadaver skin at 8% w/w drug concentration (mean±S.D., n=3).

3.3.3. The effect of galantamine loading on permeation

The effect of GAL loading on the skin permeability of the API was studied by preparing different GAL concentrations in GELVA GMS 788 (8, 10, 12, and 15% w/w of dry polymer weight). Figure 3.5 depicts the permeation profile of GAL from patches with different loadings. Data showed (Table 3.3) that 10% w/w had the highest cumulative amount permeated through human cadaver skin. It is anticipated that the flux would increase directly with the increase in sub-saturation drug loading. However, upon close examination, the patches with 15 and 12% w/w GAL loadings were found to have extensive crystallization.

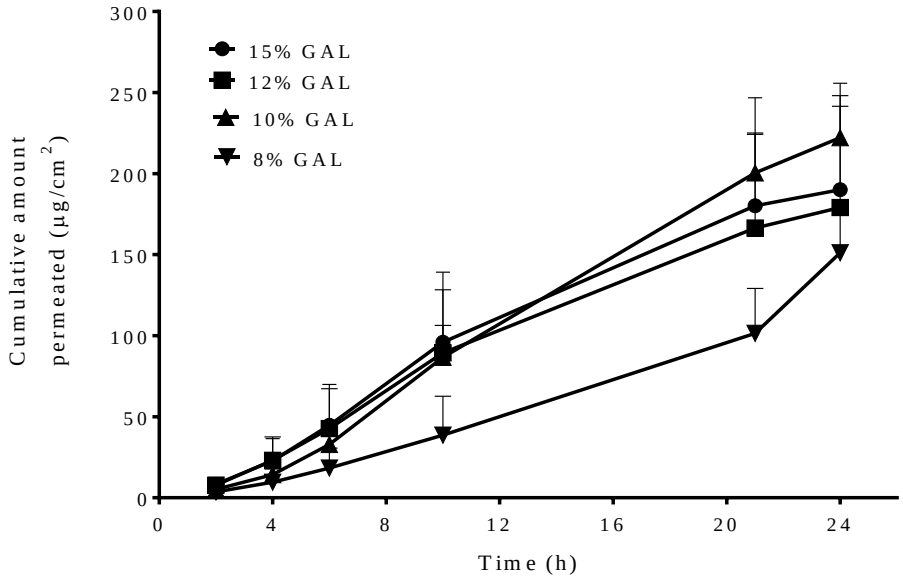

Figure 3.5. The effect of drug loading in GELVA GMS 788 on the permeation of galantamine across human cadaver skin (mean±S.D., n=3)

Table 3.3. In vitro skin permeation parameters of GAL from GELVA GMS 788 patches containing different drug loading amounts through human cadaver skin using (n=3-4).

Drug Loading %(w/w)	Flux (µg/cm²/h) ± SD	Q_{24}[a] (µg/cm²) ± SD	R^2[b]	Lag time (h) ±SD
8	6.00±0.9	151.0±19.4	0.9967	2.8±1.1
10	12.2±2.8	235.0±4.0	0.9976	3.0±0.1
12	11.1 ± 0.5	201.9±52	0.9847	2.0±1.0
15	13.9 ± 0.4	214.8±53	0.986	2.4±0.8

[b] Q_{24} is the amount of drug permeated after 24h.
[a] R^2, linearity coefficient of the flux.

Saturation of the drug in a vehicle is important to maximize the thermodynamic activity. On the contrary, crystallization of the drug within the PSA matrix reduces the thermodynamic activity causing a reduction in skin permeation (90, 91). Furuishi et al. demonstrated that the transdermal permeation of pentazocine from acrylate adhesive patches increased with drug loading to a maximum of 30% followed by a reduction at higher drug concentration. The results were attributed to the crystallization of pentazocine at higher loading levels (92). Our results were consistent with the previously published literature in that crystallization may be responsible for observed the reduction in GAL permeation. As a result, the saturation solubility of GAL in GELVA GMS 788 was considered to be around 10% w/w, and hence this drug loading was used for further optimization.

3.3.4. The effect of penetration enhancers on galantamine permeation

Several strategies have been developed to tackle the powerful barrier function imposed by the stratum corneum (SC). One of the methods is to include chemical penetration enhancers (CPEs) in the formulation. These enhancers increase the permeability of drugs by different mechanisms including disruption of the lipid bilayer, fluidization, extraction of stratum corneum lipids, etc. (10). The inclusion of CPEs into patches not only affects the permeation of the drug, but it might also influence its release (93). In order to further increase the permeability of GAL through the skin, ten CPEs were tested at 5% w/w of dry polymer weight, fixing GAL at 10% w/w loading. The CPEs tested belonged to different categories regarding their chemical properties and anticipated mechanism of action. Figure 3.6 depicts the permeation rates of GAL from matrices

containing different CPEs, and Table 3.4 shows the relevant permeation parameters. Among the tested CPEs, labrafac lipophile (Lab), lauroglycol™ FCC (FCC), and caproyl 90 (Cap) did not show a significant enhancement of GAL flux, while Propanediol (Prop) slightly reduced the permeation of GAL. On the other hand, limonene (Lim), terpineol (Terp), borneol (Bor), oleyl alcohol (OAl), octyldodecanol (OD), and decyl oleate (DO) showed a higher flux than that of the control (GAL patch without enhancer). Lim, Terp, and Bor belong to the family of terpenes, which are naturally occurring volatile oils widely used and tested as CPEs (44).

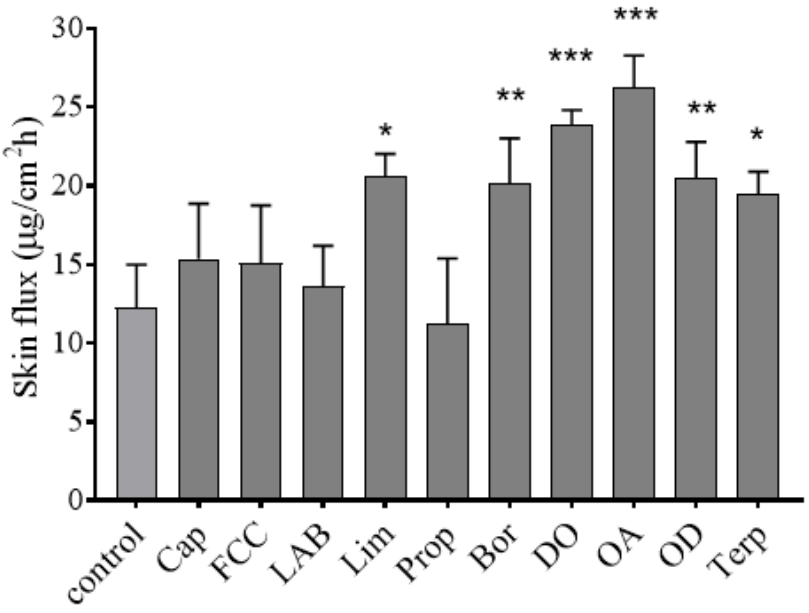

Figure 3.6. The flux of galantamine from GELVA GMS 788 patches containing different PEs through human cadaver skin (mean±S.D., n=3-4). * significant $p < 0.05$, ** at $P \leq 0.01$, *** at $P \leq 0.001$.

Table 3.4. In vitro skin permeation parameters of GAL from GELVA GMS 788 patches containing different PEs at 5% w/w through human cadaver skin using (n=3-4).

Formulation	Flux (µg/cm²/h) ± SD	Q_{24}[a] (µg/cm²) ± SD	R^{2}[b]	Lag time (h) ±SD	ER[c]
Control	12.2 ± 2.8	235.0 ± 4.2	0.9967	3.0 ± 0.1	--
Limonene *(Lim)*	20.6 ± 1.3	255.5 ± 55	0.9986	2.2 ± 0.3	1.7
Terpineol *(Terp)*	19.5 ± 0.5	281.0 ± 19	0.9603	3.4 ± 0.2	1.6
Borneol *(Bor)*	20.1 ± 1.2	288.0 ± 40	0.9909	2.5 ± 0.3	1.7
Oleyl alcohol *(OAl)*	26.3 ± 1.4	349.0 ± 25	0.999	2.1 ± 0.1	2.2
Labrafac lipophile *(Lab)*	13.6 ± 1.0	202.2 ± 30	0.9949	3.4 ± 0.2	1.1
Caproyl 90 *(Cap)*	15.4 ± 1.5	193.6 ± 33	0.9975	3.0 ± 0.5	1.3
Propanediol *(Prop)*	11.3 ± 2.0	157.5 ± 43	0.9994	2.1 ± 0.3	0.9
Lauroglycol FCC™ *(FCC)*	15.1 ± 1.7	190.0 ± 42	1.00	2.5 ± 0.3	1.2
Docyl oleate *(DO)*	24.0 ± 1.0	333.5 ± 7.4	0.9944	2.5 ± 0.2	2.0
Octyl dodecanol *(OD)*	20.5 ± 1.6	297.2 ± 27	0.9971	2.5 ± 0.5	1.7
Oleyl alcohol+Oleic acid *(OAl+OA)*	25.0 ± 0.7	344.4 ± 75	0.9991	1.8 ± 0.5	2.0
Limonene+Oleic acid *(Optimized Patch)*	32.4 ± 1.4	466.7 ± 56	0.9954	2.4 ± 0.2	2.7

[a] Q_{24} is the amount of drug permeated after 24h.
[b] R^2, linearity coefficient of the flux.
[c] ER, enhancement ratio.

Generally, terpenes competitively make hydrogen bonds with skin ceramides causing disruption of the lipid packing in the SC resulting in increased permeability of active molecules (94). The results showed that all tested terpenes significantly enhanced the permeation of GAL as compared to control patch without PE. Also, it was shown that Lim had significantly reduced the lag time more than did the other two terpenes. The reduction in the lag time indicated an increased diffusivity of the drug. This behavior of Lim may be attributed to its lipophilicity, which favors its fast permeation through the skin (37, 95). OAl and OD are unsaturated fatty alcohol and aliphatic fatty alcohol, respectively. These

long chain lipophilic molecules act as PE by fluidizing the SC lipids through interactions with the lipid layer boundary phospholipids and reducing the barrier integrity (96, 97). Our study showed that OAl resulted in the highest GAL flux amongst all other PEs tested. Agyralides et al. showed that the incorporation of 10% w/w OAl increased the permeation of furosemide from gels by 25-fold. OAl enhancement property was attributed to the presence of double bond causing a kink in its molecular structure that can disrupt the SC lipid packing (98). Whereas OD was shown to increase the flux of Formoterol Fumarate from ethylene vinyl acetate matrix patches by 6.3-fold across human skin. When incorporated into acrylate PSA patches, fatty alcohols act as plasticizers for the polymer. They enhance the polymer flexibility and drug molecules mobility facilitating the latter release from the polymer matrix. Hence, more drug molecules will be available for permeation (99). The best enhancers of the two PE groups were chosen for further investigations, namely Lim, and OAl.

3.3.5. Drug crystallization

Crystallization of the API represents a critical issue for the stability of matrix patches. It also adversely impacts the delivery of the drug (100).The prepared patches were examined under the microscope one day after preparation and every week until the end of 1 month or until signs of crystallization appeared, whichever came first. Patches containing FCC, Lim, Lab, and Prop did not show any signs of crystallization after 4 weeks of storage at room temperature. On the other hand, formulations containing DO, OD, Bor, Trep, and OAl showed signs of crystallization in less than a week after preparation as shown in Figure 3.7. The PE free GAL patch showed crystallization after 3 weeks (Figure 3.8 (c)),

suggesting that 10%w/w GAL was above saturation level. Weng et al. reported the increased crystallization of risperidone in acrylate PSA matrices upon the addition of various compounds as crystallization inhibitors.

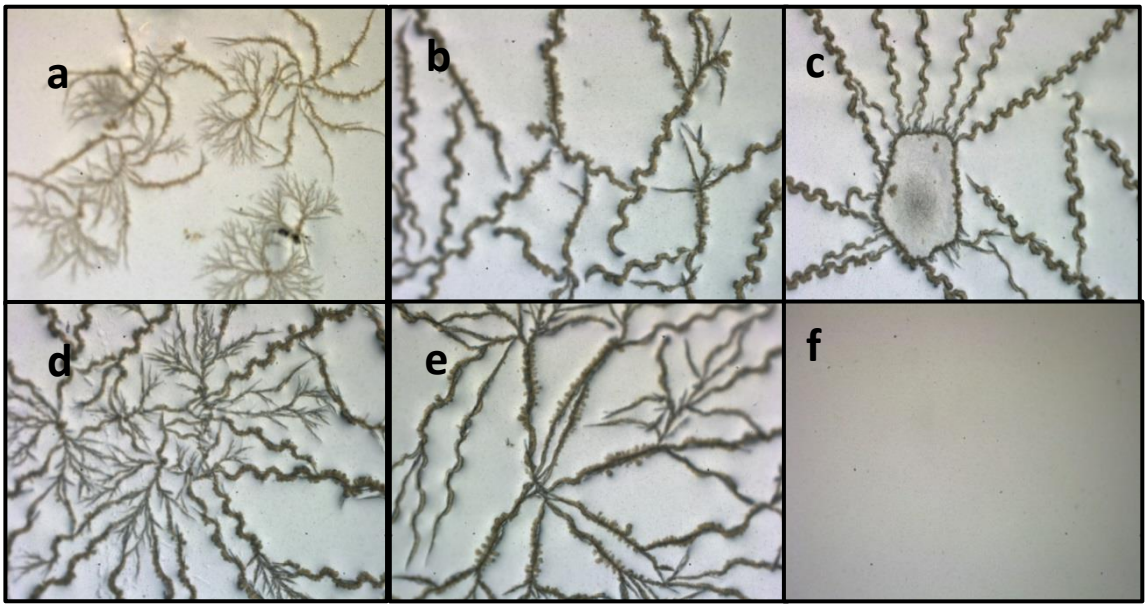

Figure 3.7. Galantamine crystallization study in Gelva PSA at 10% w/w drug loading after one week with (a) oleyl alcohol, (b) borneol, (c) decyl oleate, (d) Octyldodecanol, (e) terpineol, and (f) no additives.

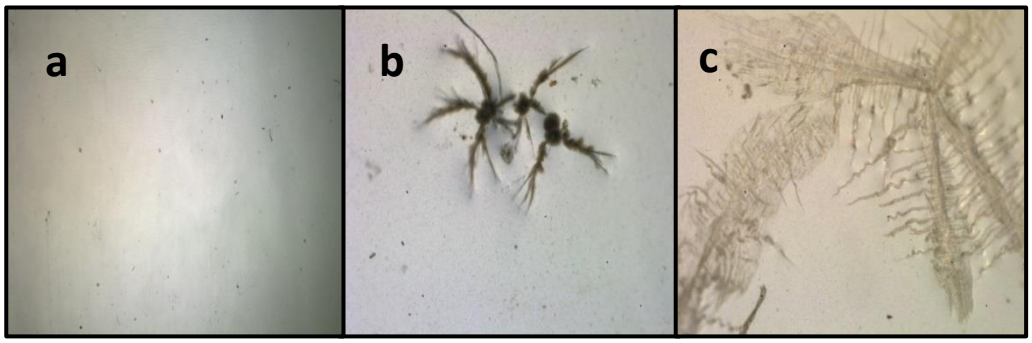

Figure 3.8. Galantamine crystallization study in Gelva PSA at 10% w/w drug loading with 5% w/w oleic acid as crystallization inhibitor after 3 weeks with (a)limonene, (b) oleyl alcohol, (c) no additives.

They suggested that compounds with OH group tend to reduce the lipophilicity of the PSA, which might reduce the solubility of the drug in the PSA matrix resulting in crystallization of the drug (91). Further, OAl was shown to enhance the induction of ibuprofen crystallization when included in the formulation of multiple polymer adhesive system as a surfactant (101). Crystallization is likely to initiate in supersaturated systems with the formation of a nucleation of drug molecules that is too big and thus hard to re-dissolve (102). However, it may take some time for the crystals to grow due to the high viscosity of the PSA matrices. As mentioned earlier, crystallization is a critical issue in transdermal patches formulation, as it adversely affects the amount of drug delivered through the skin, besides its negative impact on the quality of the product that will affect the patient's acceptability. Since patches with Lim produced high flux and were crystal free for 4 weeks, these presented a good candidate for further investigation. The permeation of GAL from the same batch of the Lim patches was tested again at 6 weeks to examine the effect of aging on the permeation profile of the drug and the results are shown in Figure 3.9.

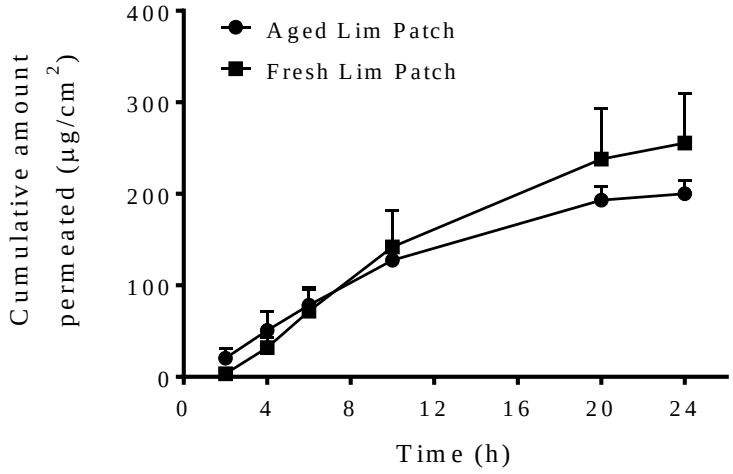

Figure 3.9. The effect of aging on the permeation profile of GAL galantamine from GELVA GMS 788 patches containing 5%w/w Limonene as a penetration enhancer. (mean±S.D., n=3-4)

Surprisingly, the permeation of GAL was reduced, although no signs of crystallization were found at 4 weeks. Moreover, the flux of GAL was significantly lower after 6 weeks than when fresh (12.72±0.93, and 20.6±1.28 µg/cm²/h, respectively). These results suggested that crystallization of the drug happened at a slower rate, and there is a need to include an excipient to inhibit crystallization. Excipients that inhibit the crystallization of drugs in PSA matrices are proposed to do so by several mechanisms: (i) increasing the solubility of the drug in the matrix, (ii) adsorption onto the drug crystals halting further nuclei growth, or (iii) formation of solid solution with the drug, i.e., amorphous co-precipitates (103). Oleic acid (OA) was tested for its ability to inhibit the crystallization of GAL. The patches with highest flux values were chosen for this purpose and OA was added at 5%w/w of dry polymer weight into formulations containing either Lim or OAl. Figure 3.10 shows the permeation profile of GAL from the freshly prepared patches containing OA as crystallization inhibitor.

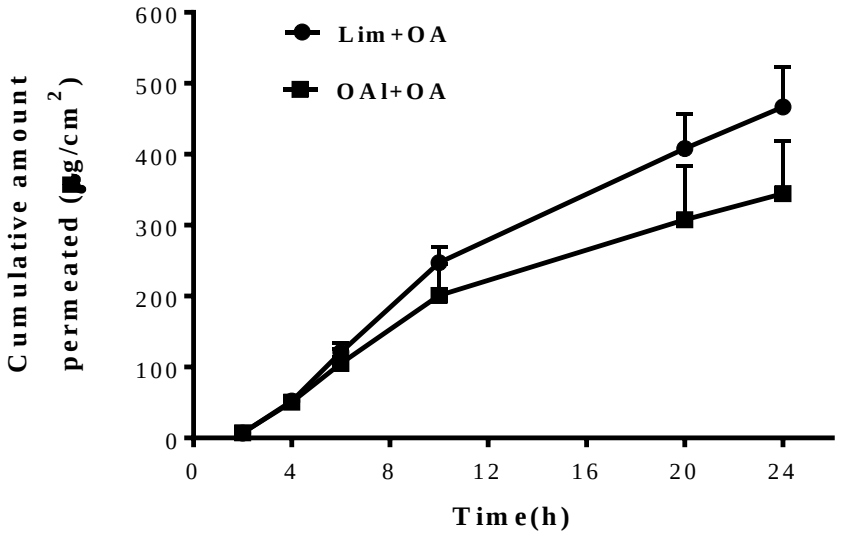

Figure3.10. The effect of 5% w/w oleic acid on the permeation rate of galantamine from GELVA GMS 788 patches containing 5% w/w of either Limonene or oleyl alcohol as penetration enhancers across human cadaver skin. (mean±S.D., n=4)

The addition of OA resulted in dramatic increase in the flux of GAL from Lim+OA patches. On the other hand, there was a small reduction in the flux with OAl+OA patches, although not statistically significant as shown in Table 3.4 Further, the microscopical examination revealed that OAl+OA patches showed crystallization after 3 weeks (Figure 3.8(b)), unlike Lim+OA, which did not show any signs of crystallization for more than 3 months. OA, a fatty acid, is an extensively studied PE, which could also function as a crystallization inhibitor in the PSA matrix patches (91). Additionally, OA acted synergistically with Lim to enhance the permeation of GAL besides being effective crystallization inhibitor. However, this OA behavior was not observed when combined with OAl. Such enhancement synergy was also observed with a combination of OA and terpenes for the transdermal delivery of zidovudine, and may be attributed to a combined effect of each enhancer's mechanism of interaction with the SC and/or enhanced solubilization of drug (46, 104). The crystallization inhibitory effect of OA may be attributed to interaction between its carboxyl group and the amine group of GAL that improved the solubility of the drug into the PSA matrix. However, it seems that the presence of Lim has a crucial role for the effective crystallization inhibition of OA. Therefore, a composition of 10% w/w GAL, 5% w/w of each of Lim and OA in GELVA GMS 788 represented a good candidate for further characterization.

3.3.6. Optimized TDDS characterization

The in vitro permeation parameters of the optimized formulation are listed in Table 3.4 The average patch thickness was found to be 154±2 μm (n=3). The drug content uniformity of the patch was 99.2±2.3% (n=3). Further, the permeation of GAL from the

optimized patch was repeated after 1 month to determine the effect of aging on drug permeation rate. The results showed that there was no significant difference in the flux of GAL from the same patches after a month of storage at room temperature (30.34 ± 1.99 μg/cm^2 h, n=4). The plasma steady state concentration (Css) of GAL can be predicted from its transdermal flux (J) and pharmacokinetic data with the following equation:

$$C_{ss} = \frac{A \times J}{Cl}$$

Where, A is the surface area of application, Cl is the clearance of the drug. Moreover, we can use the above equation to determine the surface area of the patch required to achieve therapeutic concentration. Based on pharmacokinetic parameters of GAL in healthy volunteers, where Cl and Css were found to be 20.16 l/h and 34.6 μg/l, respectively (105). We can predict that a patch of about 20 cm^2 would be sufficient to achieve and maintain the drug concentration within the therapeutic window during the time of application for 24 hours

3.3.7. Drug release

The release of GAL from the candidate formulation was tested and the release profile was depicted in Fig. 3.11, along with that of control patch. The dramatic increase in the release rate of GAL from the optimized patch can be attributed to changes in the mechanical properties of the matrix due to the inclusion of Lim and/or OA. A similar effect was seen with the release of blonanserin from acrylate PSA patches in the presence of CPE as compared to patches without CPE (72).

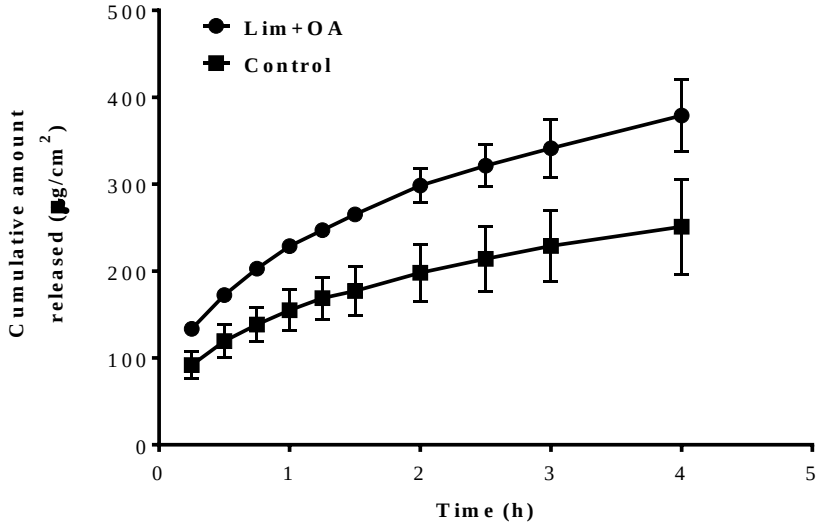

Figure 3.11. The release profile of galantamine of from GELVA GMS 788 patches with 5% w/w of limonene and oleic acid and control patch (without PE). (mean±S.D., n=3)

The release data of the optimized patch were fitted to different kinetic models and linear regression coefficient R^2 values were used to determine the goodness of fit of the respective models. The release parameters listed in Table. 3.5, showed that Fickian diffusion model (Higuchi) was best to describe the kinetics of GAL release from PSA matrix patches regardless of the inclusion of PE (Figure 3.12). Additionally, a mild burst effect was noticed in GAL release profile, an effect that could be caused by higher concentration of the drug at the surface of the patch due to its migration along with the solvent during drying phase (106).

Table 3.5 Different release kinetic models of galantamine from optimized patch (n=3).

Model	Equation [a]	K	R^2 [b]
Zero order	$Q_t = Q_0 + Kt$	62.85 µg/cm²/h*	0.939
First order	$logQ_t = logQ_0 + \frac{Kt}{2.303}$	0.25 /h*	0.8491
Higuchi	$Q_t = K_H\sqrt{t}$	164.0 µg/cm²/h^{½} *	0.995

[a] Q_t, amount released at time t; Q_0, amount at time 0; K, release rate constant; t, time.
[b] R^2, linearity coefficient.
* Statistically significant difference ($p < 0.05$) from the control patch.

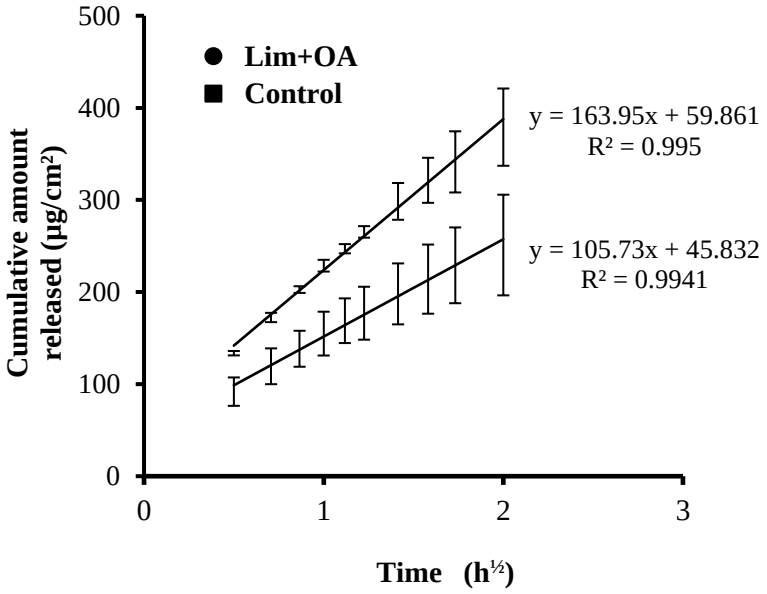

Figure 3.12 The release amount of galantamine of from GELVA GMS 788 patches with 5% w/w of limonene and oleic acid and control patch (without PE) plotted against the square root of time.

3.3.8. FT-IR study

FT-IR study was conducted to shed light on possible interactions between the PSA, drug, PE and crystallization inhibitor, if any. Figure 3.13 shows the spectra of pure GAL with the characteristic broad enolic –OH stretching vibrational peak at 3267 cm^{-1}, $–CH_2$ stretching vibrations at 2800- 3000cm^{-1}.

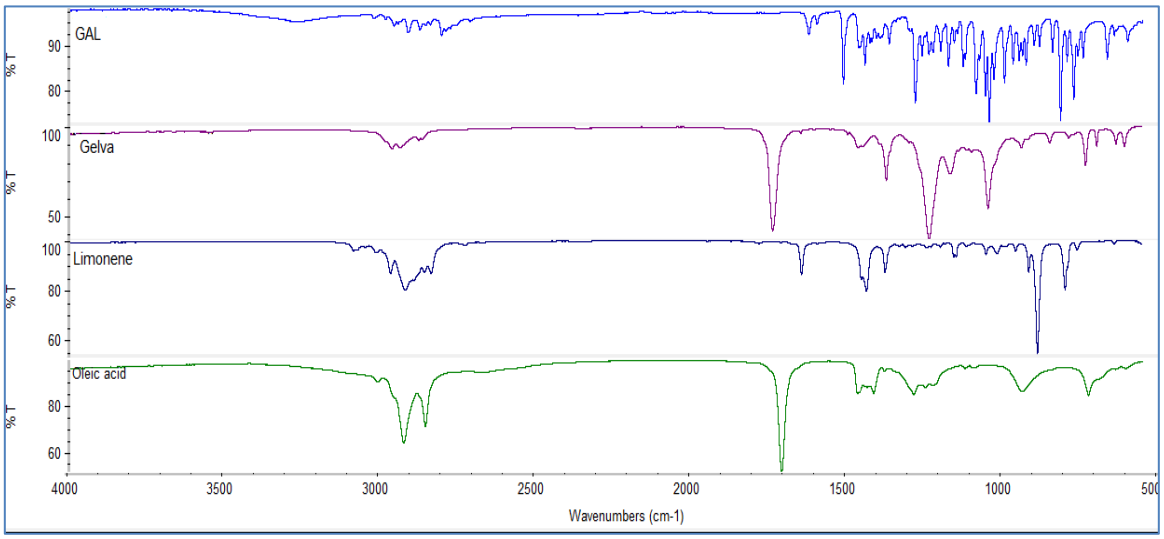

Figure 3.13. FT-IR spectra of neat galantamine, Gelva, limonene, and oleic acid.

Prominent neat GELVA GMS 788 peaks including C=O stretching vibrations are seen at 1737 cm^{-1} and C-H stretching peaks at 2860-2960 cm^{-1}. Limonene has an out of plane $=CH_2$ stretching peak at 885.67cm^{-1}, C=C stretching at 1645 cm^{-1}. Whereas OA has its typical peaks at 1707.88 and 1463.35 cm^{-1} C=O stretching, and out of plane O-H stretching, respectively. Upon mixing GAL with Gelva, the peaks of the former mostly disappeared and only the Gelva spectrum was predominantly detectable. The same observation was noticed with the optimized patch FT-IR spectrum. Figure 3.14 compares the FT-IR spectra of GAL, Gelva, and the formulation of their mixture, where it can be clearly seen that all

peaks in the region 2800-3400 cm^{-1} of GAL have disappeared including the enolic –OH stretching vibration, which could be attributed to the peaks of the lower fraction component (GAL) being masked by the larger fraction component (PSA) .

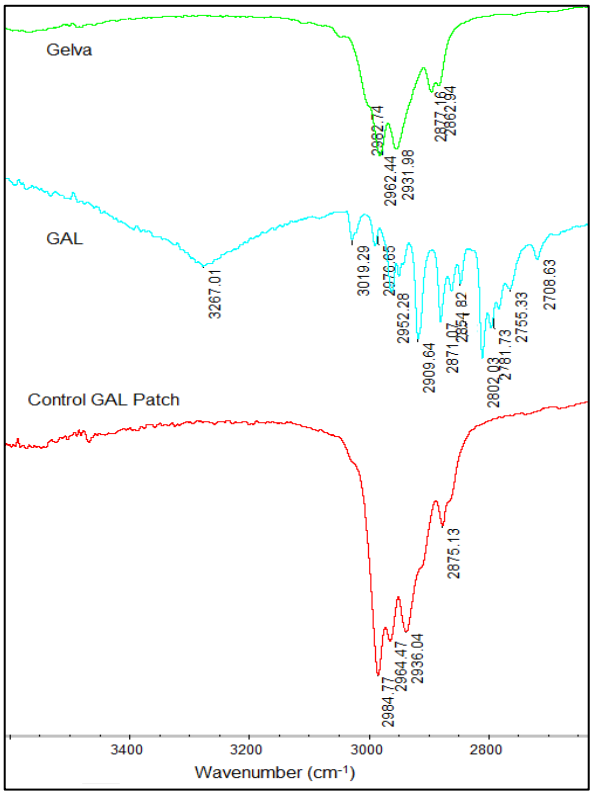

Figure 3.14. Comparison of FT-IR spectra of neat galantamine, Gelva, and control galantamine patch formulation.

Therefore, at the current setting it might be hard to confirm that any interactions were taking place with the PSA. On the other hand, Gelva maintained its –C-H stretching vibration peaks pattern. However, the peak at 2931.98 cm^{-1} showed a slight shift in the presence of GAL to 2936 cm^{-1}, which could be due to interactions between the drug and the PSA. Mufamadi et al. also reported the disappearance of GAL O-H stretching peak upon encapsulation into liposome, attributing it to interaction between the drug and the liposomes (107).

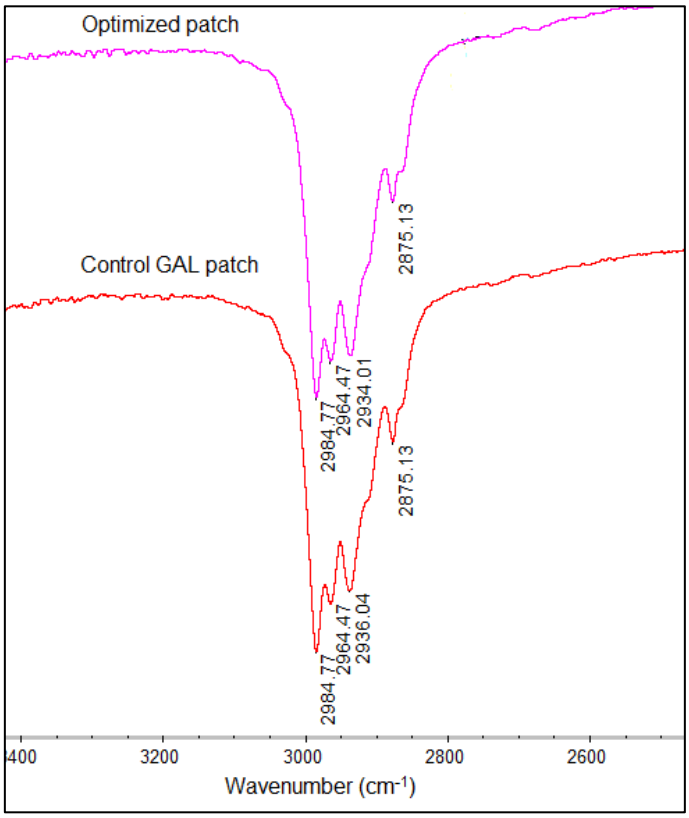

Figure 3.15. Comparison of FT-IR spectra of Control galantamine and optimized patch formulations.

In addition, Figure 3.15 shows the spectra for formulations containing GAL with and without Lim+OA, which does not show any difference from the GAL control except for a slight shift of C-H stretching peak from 2936 to 2934cm^{-1}, which is closer to the original peak of Gelva seen at 2931.98cm^{-1}. This might indicate some interactions taking place between Lim and/or OA and GAL that disrupted the interactions between the latter and Gelva. Such hypothetical interaction could be further supported by the crystallization inhibition, release improvement and enhanced permeation. These results were similar to the data reported by Weng et al., who demonstrated that excipients reduced the interactions

between risperidone and PSA as manifested by returning FT-IR peaks back to their original wave numbers after the addition of some fatty acids to the drug in PSA formulation (91).

3.3.9. Rheology

PSAs are viscoelastic materials, which means that they behave as either liquid or solid depending on the applied shear frequency at certain temperature. This property determines the PSA's skin adhesion (108). Rheological analysis of the mechanical properties of PSA was used to determine the viscoelastic parameters such as elastic modulus (G') and viscous modulus (G''). (G') corresponds to the solid-like behavior, while (G'') corresponds to the liquid-like behavior of the PSA (109). Ideally upon the application of the patch, the PSA should exhibit a liquid-like behavior so that it has enough flowability allowing close contact with the skin to bond. On the other hand, debonding requires the PSA to behave more like a solid and to demonstrate more cohesiveness. In other words, tack required for bonding occurs at lower frequencies, is associated with a larger (G''). On the contrary, the process of debonding (peel) occurs at higher frequencies and is associated with a larger (G'). Further, the study of the mechanical properties of the transdermal patches can highlight some of the interactions between the PSA polymer chain and the drug and/or additives (110). Indeed, the viscoelastic moduli would increase with increasing polymer chain stiffness and mechanical strength, whereas increased chain flexibility brought about by plasticization is associated with decreasing moduli values (72, 111).

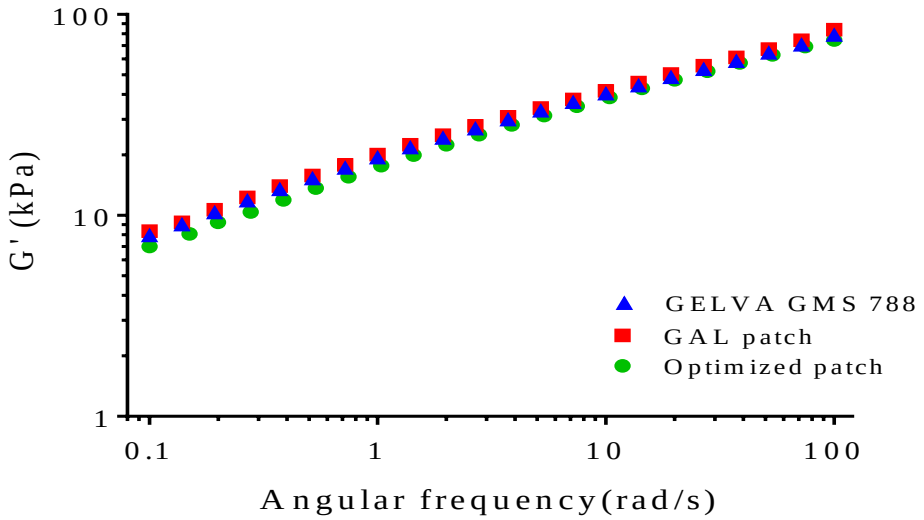

Figure 3.16. Oscillation frequency sweep data of blank PSA, 10% w/w galantamine containing PSA, and optimized patch. The elastic modulus plotted against angular frequency.

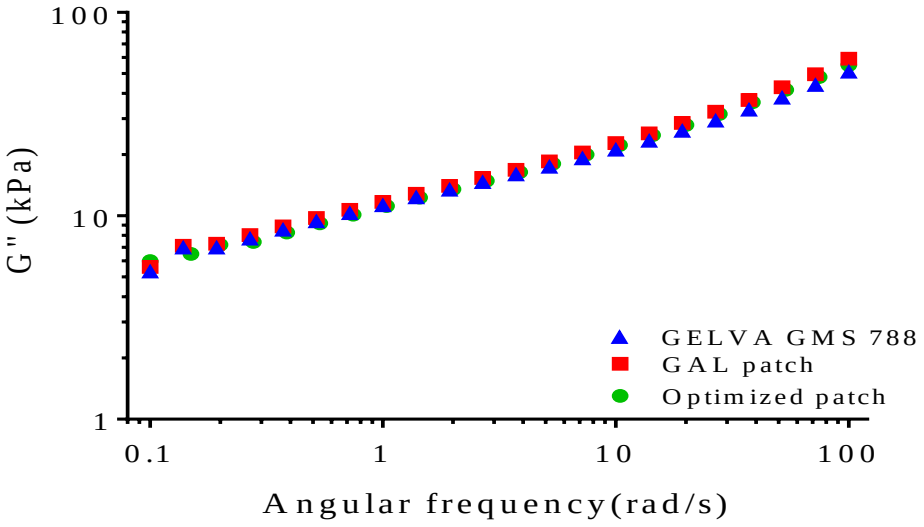

Figure 3.17. Oscillation frequency sweep data of blank PSA, 10% w/w galantamine containing PSA, and optimized patch. the viscous modulus plotted against angular frequency.

Phase angle (δ) is another parameter that is used to study rheological properties of PSA. δ describes the ratio of the lost to stored energy, hence it is expected to be high at both lower and higher frequencies. The larger the angle the more flexible the polymer (72). Oscillation frequency sweep results are depicted in Figure 3.16-3.18 and are consistent with acceptable behavior of PSA. Figure 3.16 shows a small reduction in G′ for the optimized patch relative to blank PSA. This reduction, although very small, might indicate some plasticization effect due to Lim and OA reducing chain stiffness and cohesion. The latter observation is backed by the increase in δ for the optimized patch compared to blank PSA and GAL containing patch (Figure 3.18). Similar rheological behavior was observed with other acrylate PSAs upon incorporation of olanzapine and the penetration enhancer (110).

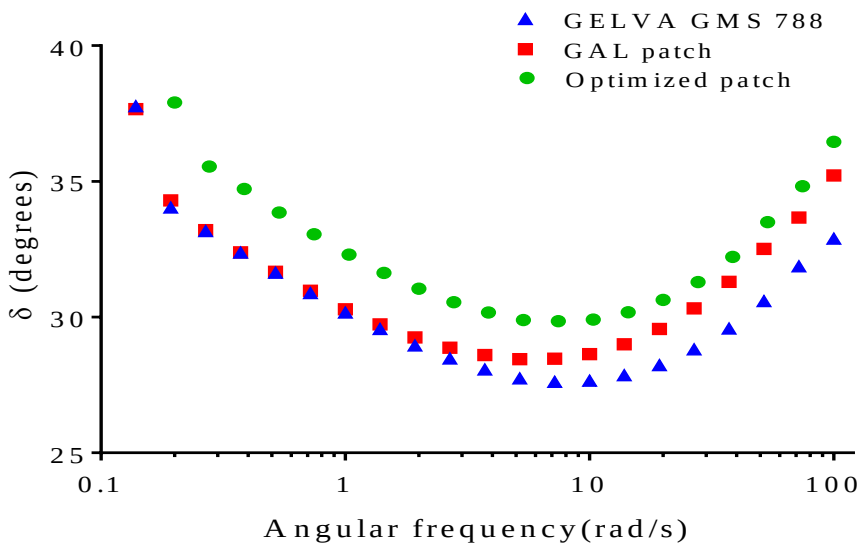

Figure 3.18. Oscillation frequency sweep data of blank PSA, 10% w/w galantamine containing PSA, and optimized patch. The phase angle plotted against angular frequency.

3.4. Conclusions

The results of the present study emphasize the importance of selecting a suitable combination of PSA, drug loading, PE, and crystallization inhibitor for the development of transdermal patches with optimum performance. The optimized patch was composed of 10% w/w GAL, 5%w/w Lim, 5% w/w OA, GELVA GMS 788 as PSA, and was casted on Scotchpak™1022 release liner and laminated with Scotchpak 9723 as a backing film. The selected excipients showed a synergistic enhancement of GAL permeation while successfully inhibiting the drug crystallization. Based on the in vitro permeation studies using human cadaver skin, the optimized patch produced a steady state flux of GAL that is predicted of achieving therapeutic plasma level with a patch size of about 20 cm^2 , which indicates that GAL transdermal patch was a promising drug delivery system for the treatment of Alzheimer's disease. Next step should be evaluating the skin toxicity and irritation potential of the system, investigate the skin-drug interaction/metabolism and finally proceeding to pharmacokinetic and in vivo studies to confirm efficacy.

Chapter 4: Transdermal Delivery of Dimethyl Fumarate for Neurodegenerative Diseases[2]

4.1. Introduction

Multiple Sclerosis (MS) and Alzheimer's disease (AD) are neurodegenerative diseases that affect different age populations. however, they share some common aspects related to pathogenesis, and lack of cure (3). The exact mechanisms that lead to the development of AD and MS are still unknown. However, oxidative stress (OS) and subsequent inflammation is thought to play a key role in their pathogeneses. Indeed, OS represents the first stage of the disease before the formation of Aβ plaques and tau tangles within the brain in AD (112, 113). Currently, the antioxidant cytoprotective pathways are increasingly thought to play an important role in new therapeutic approaches for the treatment of neurodegenerative diseases (22). The nuclear factor (erythroid-derived 2)-related factor 2 (Nrf2) pathway is one of the important mechanisms that are involved in cytoprotection that can be activated by potential anti AD drugs, such as DMF (114).

DMF was first indicated in 1950s for the treatment of psoriasis under the false assumption that psoriasis was associated with fumaric acid deficiency. Its effectiveness is attributed to a reduction in lesional T-cell infiltration and normalization of epidermal cell proliferation and keratinization (115). Now, in Germany, DMF accounts for more than 66% of all anti-psoriatic prescriptions (116). In 2013, the US Food and Drug Administration (FDA) and the European Medicines Agency (EMA) approved DMF under the brand name Tecfidera®

[2] A version of this chapter is published in the International Journal of Pharmaceutics: Ameen A, Michniak-Kohn B, Int J Pharm; 2017; 529(1-2): 465-473.

for the treatment of multiple sclerosis (117). DMF is the dimethyl ester of fumaric acid with molecular weight 144.12 g/mol, and log p of 0.7. Figure 4.1 depicts the chemical structure of DMF. It is rapidly converted to monomethyl ester, monomethyl fumarate (MMF), due to either pH, or esterase enzyme catalyzed hydrolysis (118). MMF has a molecular weight of 130.1 g/mol and log p of 1.1. Both DMF, and MMF enhanced cellular antioxidant response in treated astrocytes and neurons improving cell viability in a concentration dependent effect (119). DMF possess significant antioxidant activity through the activation of the Kelch-like ECH-associated protein (Keap1)-Nrf2 pathway, which induces the expression of multiple cytoprotective genes. These genes encode for cytoprotective antioxidant enzymes and proteins such as glutathione synthesizing enzymes, NADPH, etc. In addition, DMF was found to reduce pro-inflammatory cytokine production and activation of T-cells (120-122). Indeed, DMF has a great potential for the treatment of AD through tackling the underlying pathogenetic factors predisposing the disease.

The transdermal route presents a very promising alternative for the treatment of neurodegenerative disease, especially AD, as it possesses several advantages over other routes. Since it avoids the GIT, there will be no first pass effect metabolism and gastrointestinal side effects and/or metabolism. Ultimately, transdermally delivered drugs may exhibit improved efficacy, and decreased toxicity. Indeed, transdermal patches offer exceptional advantages for the AD patients by reducing the oral dosage form burden, thus improving compliance.

Nevertheless, transdermal delivery is impeded by the powerful barrier function imposed by the stratum corneum (SC). In order to overcome the SC, different strategies have been developed including the incorporation of chemical penetration enhancers (CPE) into the

formulation. These compounds act to enhance the percutaneous absorption of drugs by several mechanisms including disruption of the lipid bilayer, fluidization, and extraction of stratum corneum lipids, etc. (10).

This present work was conducted to investigate the feasibility of the transdermal delivery of DMF. With this goal in mind, in vitro transdermal permeation experiments were conducted to study the percutaneous absorption of DMF and test the effect of various CPE with different mechanisms of action on the ability of the DMF to be transported through the skin at a rate sufficient to achieve therapeutic plasma levels.

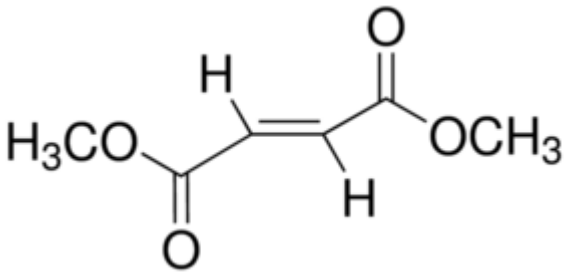

Figure 4.1. Chemical structure of dimethyl fumarate.

4.2. Materials and Methods

4.2.1. Materials

Dimethyl fumarate (DMF), monomethyl fumarate (MMF), cineole (Cin), and terpineol (Terp) and were purchased from Sigma Chemical Co. (St. Louis, MO, USA). N-methylpyrrolidone (NMP), laurocapram (Az), Polysorbate 80 (T80), and phosphate-buffered saline tablets (PBS, pH 7.4) was purchased from Thermo Fisher Scientific Co.

(Pittsburgh, PA, USA). Transcutol P (Tc) a generous gift from Gattefossé (Paramus, NJ) High-performance liquid chromatography (HPLC) grade water, methanol and acetonitrile were purchased from BDH VWR Analytical (Radnor, PA, USA). Dermatomed human cadaver skin was obtained from New York Firefighter Skin Bank (NY, USA). Strat-M® was a gift from EMD Millipore (Billerica, MA, USA).

4.2.1. HPLC Method of Quantification for DMF and MMF

4.2.1.1.Equipment and mobile phase

DMF and MMF were analyzed simultaneously using HPLC. The HPLC system consisted of an Agilent 1100 Series Hewlett-Packard liquid chromatograph and the Agilent Chemstation software. The HPLC machine was equipped with a UV detector (Agilent Dual Absorbance Detector G1315A), a pump (Agilent Quat pump G1311A), and an automatic injector (Agilent ALS G1313A Auto-samplers). A reversed-phase column (Luna C18, Phenomenex) was used as the stationary phase at ambient temperature. The mobile phase, 0.05M monobasic sodium phosphate at pH 3.2: acetonitrile (65:35, v/v), the pH was adjusted using 85% *O*-phosphoric acid. The mobile phase was pumped at a flow rate of 1.0 mL/min, and the UV detector was set at a wavelength of 230 nm.

4.2.1.2. Standard solutions and calibration curves

Stock solutions of DMF and MMF were prepared separately at concentrations of 0.1mg/mL each. Both stock solutions were prepared by dissolving 10mg of DMF, or MMF in mobile phase buffer in 100ml volumetric flask. Standard solutions of each compound

were prepared by serial dilution of the respective stock solution with 0.05M monobasic sodium phosphate, pH 3.2. the standard solutions had a concentration range of 1.56-100µg/ml for both DMF and MMF that covered the range of expected concentration in the skin permeation samples.

4.2.1.3. Method validation

The HPLC method was validated by testing the linearity and precision through inter- and intra-day variability and determining the limit of quantification and limit of detection as discussed before in chapter 3.

4.2.2. Determination of Solubility of DMF

Saturated solutions of DMF were prepared by adding excess amount of DMF to a fixed volume of vehicle, either PG alone or selected % (V/V) of penetration enhancers in PG as shown in Table 3.6. The mixtures were sonicated in a water bath/sonicator for 1h at 32°C and were then incubated in a shaking water bath for 48h at 32°C to reach equilibrium. The suspension was passed through a membrane filter (0.45µm pore size) and the concentration of DMF in the filtrate was determined using HPLC. The experiments were performed in triplicate.

4.2.3. Stability of DMF

The stability of DMF in PBS at pH 7.4, and 5.8 was studied by incubating a certain volume of each buffer spiked with a standard solution of DMF to produce a final concentration of 16 µg/ml. at 37°C for 24 hours. Samples were withdrawn at specified time

intervals and analyzed for the drug using HPLC. The results were expressed as percentage of DMF remaining with time. In addition, to confirm whether retained skin esterase activity could affect DMF hydrolysis a permeation experiment was conducted using Franz diffusion cells mounted with human cadaver skin and Strat-M® as an artificial "skin equivalent" using PBS at pH 5.8 as a receptor medium. More details are provided in the section below. All experiments were performed in triplicate.

4.2.4. In vitro skin permeation study of DMF

Frozen dermatomed human cadaver skin of posterior torso of Caucasian male donors was obtained from New York Firefighters Skin Bank (New York, NY). The human cadaver skin was kept in a freezer (-80°C). At the day of study, the skin was thawed at room temperature, cut into approximately 2 cm^2 pieces, and hydrated in PBS pH 7.4 for 30 min before the permeation study.

The in vitro permeation study was conducted using vertical Franz diffusion cells (Logan Instruments, Somerset, NJ) mounted with human cadaver skin kept at 32°C. Each skin piece was clamped between the donor and receptor compartments with the stratum corneum facing upward toward the donor. The donor compartment was filled with 0.6 mL of different DMF saturated solutions in PG with the various concentrations of each PE used. The receptor compartments were filled with 5.0 mL PBS (pH 7.4, 20mM) which used as the receptor medium, maintained at 37°C using a heating block and stirred continuously at 600 rpm. The diffusion cell area was 0.64 cm^2. At predetermined time points (1h, 3h, 5h, 7h, 11h, 15h and 24h), 0.3 ml of the receptor compartment was withdrawn and replaced immediately with an equal volume of PBS (pH 7.4, 20mM). Samples withdrawn were

analyzed using HPLC to determine DMF and MMF concentrations. All experiments were performed with five replicates. To study the effect of skin esterase activity on the hydrolysis of DMF, Franz diffusion cells mounted with human cadaver skin or Strat-M® were assembled in the heat block. The receptor compartments were filled with PBS at pH 5.8 to prevent the pH induced hydrolysis of DMF. Samples were withdrawn at specified time intervals over 12 hours and analyzed for MMF content.

4.2.5. Data Analysis

The amounts of DMF and MMF contained in the receptor samples were quantified in order to calculate the cumulative amount (Q) of DMF in the receptor compartment as a function of time. The total amount of DMF permeated was normalized to account for conversion to MMF (which is also active) and was termed DMF_{Total}. The individual permeation profile of each formulation was obtained by plotting the cumulative amounts of DMF permeated per unit skin area versus time. The steady-state flux (*J*) was determined from the slope of the linear portion of the plot. The lag time represents the x-axis intercept of the extrapolated linear portion of the permeation profile. Permeability coefficient P and enhancement ratio (ER) are calculated using equations 1, and 2 respectively:

$P = J/C$ ….Eq (1)

Where, C is the concentration of DMF in the donor.

$ER = J\ with\ the\ \ enhancer/J\ without\ enhancer$ …Eq (2)

The permeation parameters obtained for the different formulations were compared using ANOVA and Tukey's test. Differences among the treatments were assumed to be significant at $p < 0.05$.

4.3. Results and Discussion

4.3.1. HPLC method of determination of DMF and MMF

Figures 4.2 and 4.3 depicts the chromatogram peaks of DMF and MMF obtained with the HPLC method, respectively. The retention times for DMF was about 8.1 min, while that of MMF was about 3.0, min and both peaks showed acceptable sharpness and symmetry.

The calibration curve of DMF was constructed by analyzing standard solutions in the concentration range of 1.56-100 µg/ml using the HPLC method parameters for 3 injections and the average area under the peak was plotted against the concentration of the standard solution as shown in Figure 4.4. The method revealed a perfect linearity with R^2 of unity and LQ and LD of 0.2 and 0.07 µg/ml, respectively for DMF assay. Similarly, MMF calibration curve, depicted in Figure 4.5., was linear for the tested concentration range with

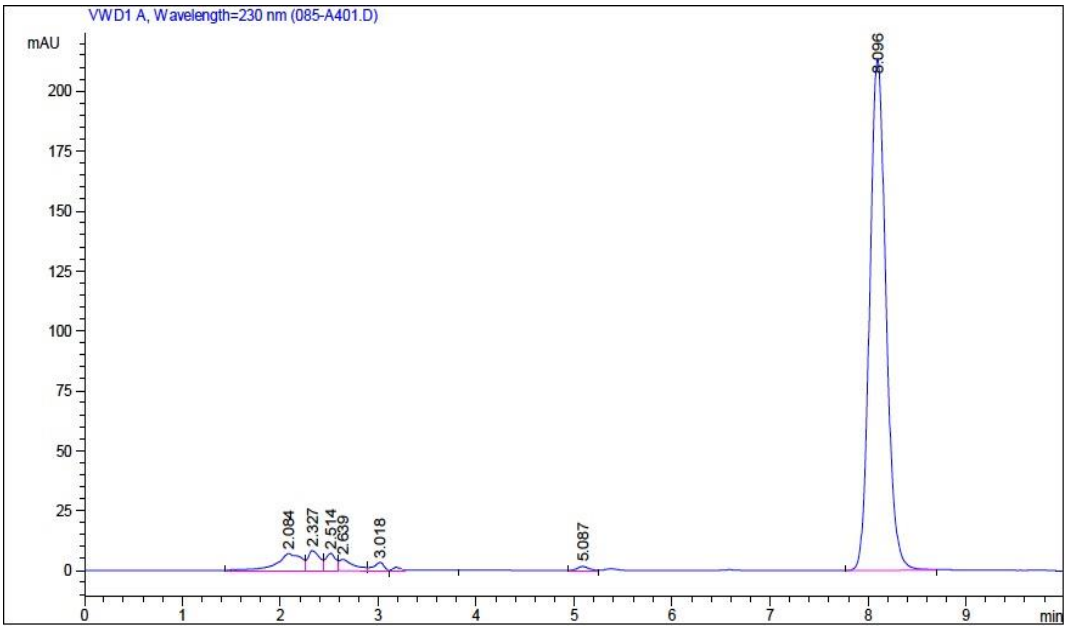

Figure 4.2. Chromatogram peak of dimethyl fumarate at retention time of 8.1 min.

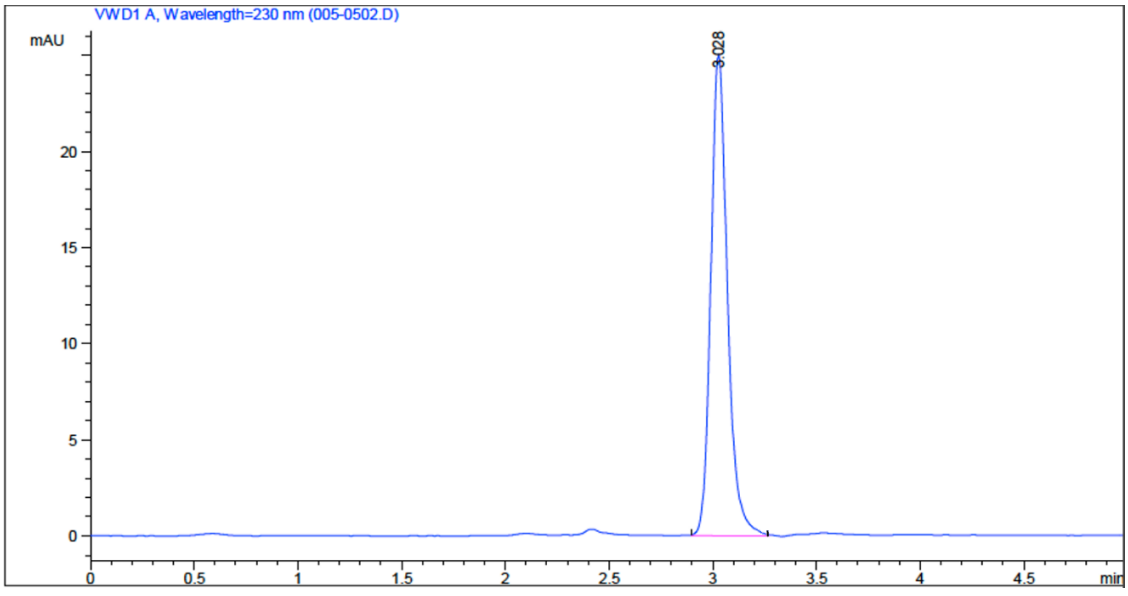

Figure 4.3. Chromatogram peak of monomethyl fumarate at retention time of 3.0 min.

R^2 of 0.999. The values of LQ and LD for MMF HPC method were 0.5 and 0.1 µg/ml, respectively.

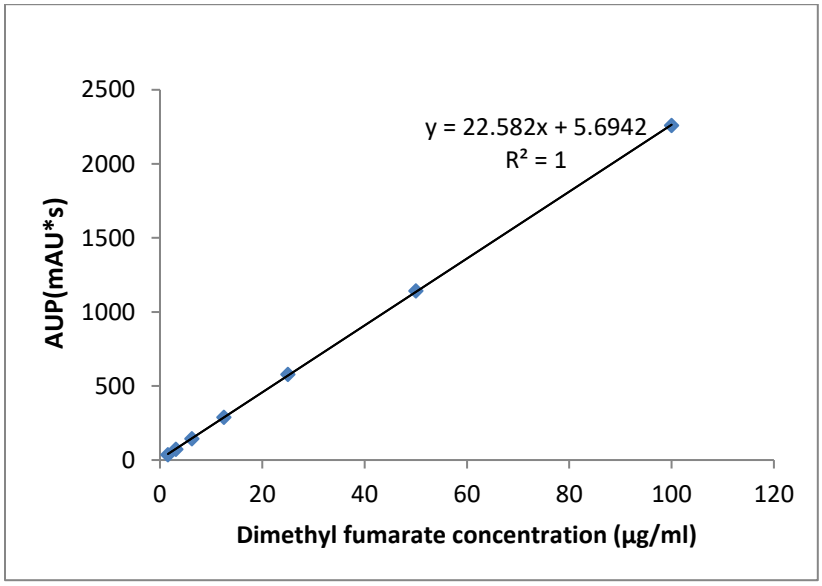

Figure 4.4. Dimethyl fumarate standard calibration curve for HPLC assay method. Area under the peak (AUP) of the chromatogram against the concentration of dimethyl fumarate. Values represent an average of 3 injections.

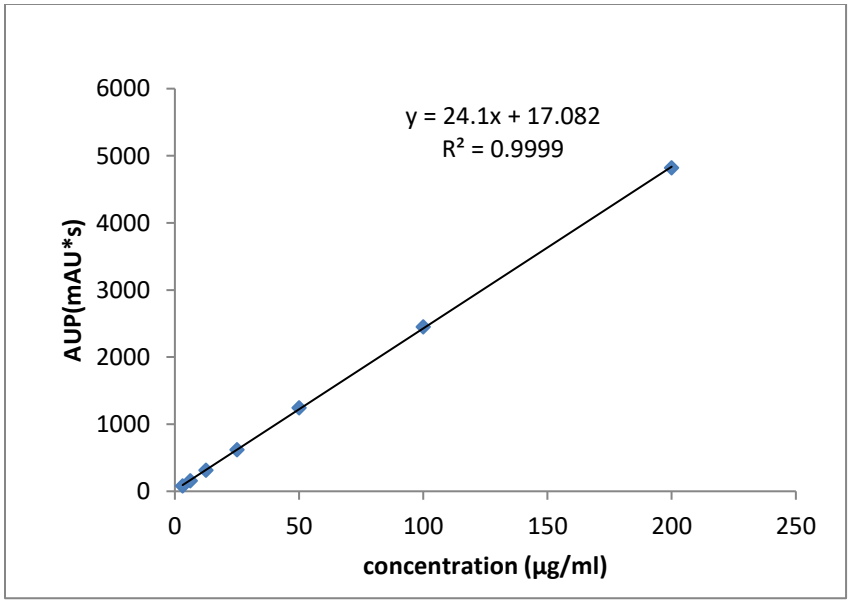

Figure 4.5. Monomethyl fumarate standard calibration curve for HPLC assay method. Area under the peak (AUP) of the chromatogram against the concentration of monomethyl fumarate. Values represent an average of 3 injections.

Method precision is measured through calculating the relative standard deviation %RSD of three levels and three readings, and the acceptable value is ≤ 2%.

Table. 4.1. Intra-Day and Inter-Day Precision Analyses of dimethyl fumarate, n=3.

DMF Concentration (µg/ml)	Intra-Day Analysis		Inter-Day Analysis	
	AUP (mAU*s) ±SD	%RSD	AUP (mAU*s) ±SD	%RSD
6.25	144.8±0.6	0.41	144.9±0.6	0.41
50	1138.2±9.2	0.81	1133.5±14.1	1.24
100	2251.4±12.7	0.56	2241.1±27.5	1.23

Tables 4.1 and 4.2 show the intra- and inter-day precision data for three different concentrations of DMF and MMF, respectively. All of the %RSD values fell below 2%, which indicted the repeatability and precision of the method.

Table. 4.2. Intra-Day and Inter-Day Precision Analyses of monomethyl fumarate, n=3.

MMF Concentration (µg/ml)	Intra-Day Analysis		Inter-Day Analysis	
	AUP (mAU*s) ±SD	%RSD	AUP (mAU*s) ±SD	%RSD
6.25	157.2±0.9	0.57	157.4±0.8	0.51
50	1243.8±5.0	0.4	1244.7±4.5	0.36
100	2450.2±14.6	0.6	2453.2±13.4	0.55

4.3.2. Determination of Solubility of DMF

The saturation solubility of DMF in all vehicles is shown in table 4.3. The results show that the addition of enhancers had different effects on the solubility of DMF.

Table 4.3. The effect of PE on the solubility of DMF at 32° C.

Penetration Enhancer	Concentration of Enhancer (%v/v)	Solubility (mg/ml) ±SD*	ER_{sol}
PG (Control)	-	6.1±0.66	1
Tween80	1%	8.4±1.9	1.38
Tween80	2.5%	9.9±0.8[a]	1.63
Tween80	5%	10.9±0.9[a]	1.8
NMP	5%	9.6±0.1[a]	1.58
NMP	10%	12.4±0.04[a]	2.05
NMP	20%	13.0±1.4[a]	2.14
Azone	1%	6.7±0.6	1.1
Azone	2.5%	7.6±0.2	1.25
Azone	5%	7.3±0.2	1.2
Terpineol	2.5%	4.9±0.1[b]	0.81
Terpineol	5%	4.9±0.1[b]	0.81
Terpineol	10%	4.9±0.03[b]	0.8
Cineole	1%	11.99 ± 1.2[a]	1.98
Cineole	2%	12.9 ± 2.21[a]	2.13
Cineole	5%	13.9 ± 0.8[a]	2.3
Transcutol P	5%	13.8 ± 0.1[a]	2.3
Transcutol P	10%	14.5 ± 0.2[a]	2.4
Transcutol P	20%	17.5 ± 1.5[a]	2.9

* n=3.

** ER_{sol}, enhancement ratio of DMF solubility.

[a] significant increase in DMF solubility ($p < 0.05$).

[b] significant reduction in DMF solubility ($p < 0.05$).

The penetration enhancers: Tc, Cin, T80, and NMP have significantly increased the solubility of DMF, while Azone had no effect on the solubility. On the hand, in the presence of Terp, DMF showed a dramatic reduction in solubility. The highest solubility (17.5

mg/ml±1.47) was obtained with 20% TC, which constitutes three-fold increase in solubility of DMF in PG.

4.3.3. Stability of DMF

The results of stability study of DMF are depicted in Figure4.6. It was shown that DMF was relatively stable at pH 5.8. On the other hand, DMF underwent rapid hydrolysis to monomethyl fumarate (MMF) in phosphate buffer, pH 7.4 confirmed by increasing concentration of MMF with time as shown in Figure 4.7. These results were consistent with previously published data (118).

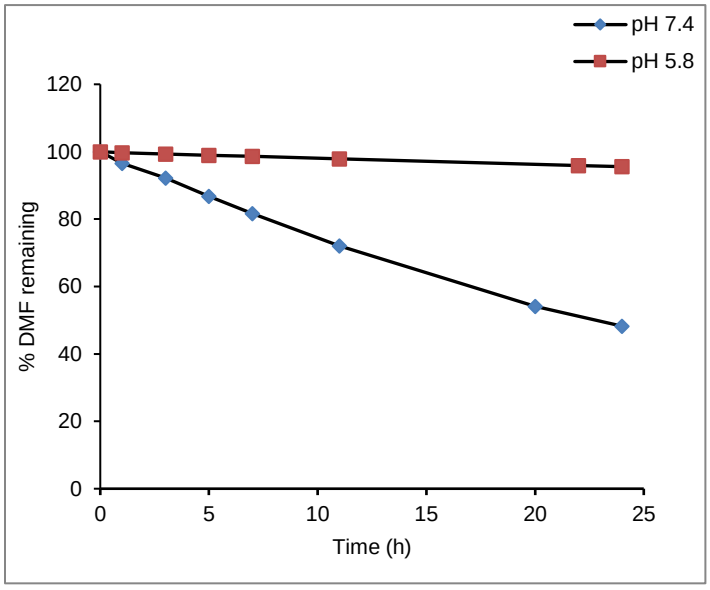

Figure 4.6. Stability of DMF in phosphate buffer at pH values 7.4, and 5.8. (Each point represents the mean±S.D. of three experiments).

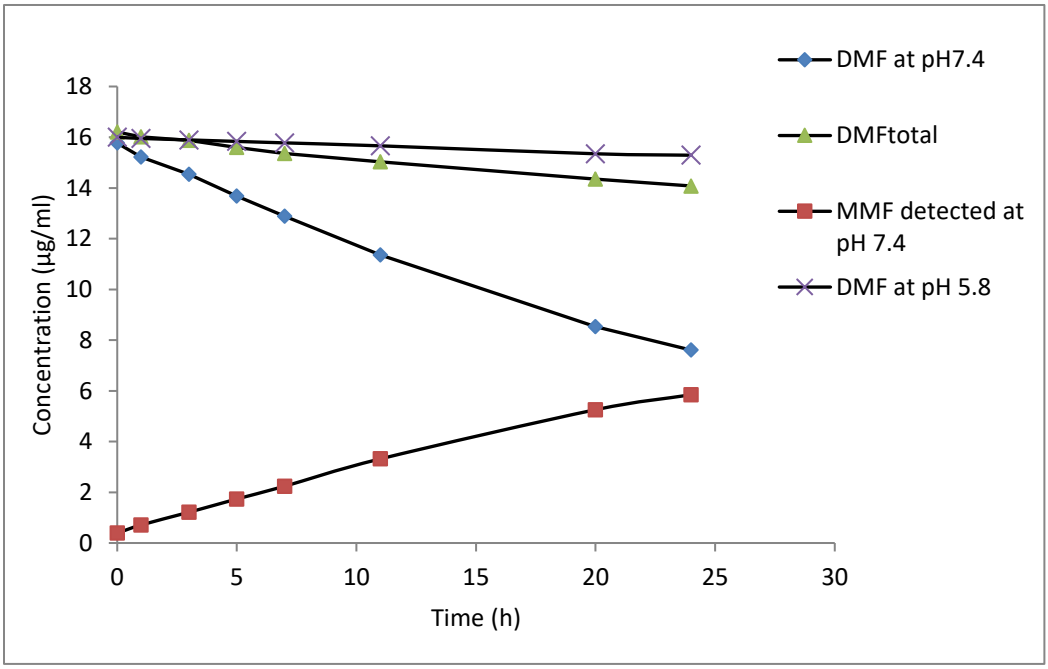

Figure 4.7. The concentration of DMF, MMF, and their combined concentrations (DMF_{total}) at pH 7.4, compared to DMF at pH 5.8 (Each point represents the mean±S.D. of three experiments).

Figure 4.7 shows the concentration of DMF and MMF in phosphate buffer pH 7.4, and pH 5.8 spiked with DMF to produce a concentration of 16µg/ml kept at for 24 hours. At pH 7.4, DMF underwent hydrolysis and the concentration declined fast coupled with increase in MMF concentration. By normalizing the DMF concentration through combining it with MMF after appropriate corrections, we had a theoretical line representing DMF_{total}. The concentration of DMF at each time point was compared between samples at pH 5.8 and the DMF_{total} using Student -t test, and there was no significant difference between each pair at $p < 0.05$. Therefore, this approach of calculating DMF_{total} could be justified and was used throughout the studies involving DMF to report the total amount of DMF.

Since DMF was more stable at pH 5.8, PBS at 5.8 was chosen as the receptor medium to conduct the skin permeation study using human cadaver skin and Strat-M®. Interestingly, the average concentration of MMF detected with human cadaver skin was almost three times higher than its concentration when Strat-M® was used MMF concentration was significantly higher with skin mounted cells compared to Strat-M® at each time point tested (Figure 4.8). This might be attributed to some retained activity of esterases within the skin samples. Hydrolysis products of ketorolac ester prodrugs, and dimorphone were also observed during permeation studies using human cadaver skin, and human premature neonatal cadaver skin, respectively. Those results were attributed to residual skin esterase activity (123, 124).

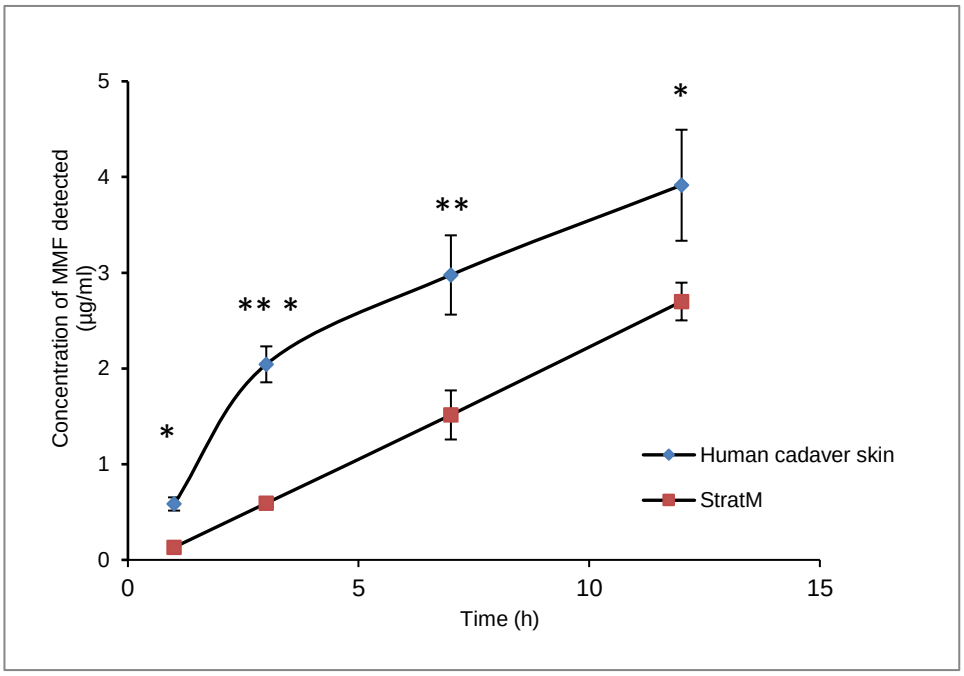

Figure 4.8. The concentration of MMF detected in the receptor medium using human cadaver skin, and StratM® (Each point represents the mean±S.D. of three experiments). Significance level: * at $P \leq 0.05$, ** at $P \leq 0.01$, *** at $P \leq 0.001$.

Table 4.4. The effect of penetration enhancers on the solubility and permeation parameters of DMF.

Penetration Enhancer	Flux (µg/cm²/h) ± SD	Q_{24}[a] (µg/cm²) ± SD	P x10^{-3} (cm/h)± SD	Lag time (h)± SD	ER[c]
PG	20.6±0.72		3.93±0.13	--	1.00
Tween80					
1%	41.9±1.88		4.33±0.19	1.05±0.16	2.03
2.5%	42.2±3.79		3.99±0.36	0.89±0.11	2.03
5%	55.7±5.4		5.1±0.49	0.72±0.22	2.58
NMP					
5%	39.8±3.47		3.13±0.36	0.07±0.02	1.93
10%	39.5±8.33		4.09±0.89	3.17±0.82	1.92
20%	51.5±1.82		5.35±0.19	2.7±0.49	2.5
Azone					
1%	39.5±3.62		6.34±0.58	0.69±0.21	1.92
2.5%	57.6±5.86		7.73±0.79	2.39±0.68	2.78
5%	86.4±14.37		11.6±1.93	3.64±0.83	4.19
Terpineol					
2.5%	52.7±6.66		10.8±1.38	1.14±0.38	2.34
5%	50.3±2.99		10.1±0.59	0.84±0.37	2.33
10%	60.0±4.85		12.3±0.99	2.77±1.35	3.33
Cineole					
1%	66.6±5.04		4.76±0.36	0.78±0.23	3.23
2%	77.2±12.9		6.4±1.08	1.78±0.34	3.75
5%	108.5±17.5		8.39±1.35	1.14±0.37	5.28
Transcutol P					
5%	42.1±4.81		3.04±0.31	3.74±0.32	2.04
10%	53.4±7.79		3.68±0.53	2.67±0.69	2.59
20%	68.3±7.63		3.69±0.41	2.91±0.67	3.32

* n=3.

[c] enhancement ratio is calculated based on flux value

4.3.4. Effect of Penetration Enhancers type

The permeation profiles of DMF using PG alone as a vehicle and PG containing T80, NMP, Az, Terp, Cin, and Tc through human cadaver skin are shown in Figures. 4.9-4.14, respectively. The flux (*J*), permeability coefficient (*p*), lag time (t_{lag}), and *ER* are shown in Table 4.4. The inclusion of CPEs has increased the rate of permeation of DMF across human cadaver skin compared to that of control (100% PG). The rank order of enhancement of the highest concentration of PE used: Cin>Az> TC>Terp>T80≥NMP. PG was chosen as a vehicle because it is widely included as a co-solvent in topical formulations and as a single vehicle to study the percutaneous absorption(125). PG was reported to exert some penetration enhancement activity and increased the permeation of ibuprofen through a partitioning effect, supposedly, by improving the solubility parameters of the stratum corneum (126).

4.3.4.1. The effect of terpenes

Terpenes act by disrupting the lipid bilayer through competitively hydrogen bonding with skin ceramides causing disruption of the lipid packing in the stratum corneum resulting in increased drug diffusivity (127). In a study of the effect of terpenes on the transdermal permeation of zidovudine, it was found that the energy of activation for the permeation of the drug was halved when 5% Cin was added to the vehicle. It was concluded that the lowering of the activation energy was due to the disruption of H bonds within the lipid bilayer (128). Although Cin and Terp are both terpenes, their effect on DMF permeation was different. Not all terpene enhancers behave similarly due to differences in the physicochemical properties governing their interaction with both drug molecules and

skin (129). Table 4.4 shows that the calculated P with Terp was almost doubled from that with Cin. This clearly indicates that they have a different mechanism of penetration enhancement of DMF. Terpenes are known to enhance both lipophilic and hydrophilic drugs (93), and Cin has a particularly good penetration enhancement with hydrophilic drugs (37). A linear correlation was postulated to occur between the lipophilicity of the permeant molecule and log P of the CPE, where a more lipophilic compound would require a CPE with a larger log P value for good penetration enhancement (130). Zhao et al, showed that the lipophilicity of CPE plays a crucial role in determining the effective permeation enhancement of the active molecule. They found that the more lipophilic O-aceylmenthol derivative significantly increased the flux of lipophilic model drugs, ketoprofen and indomethacin.

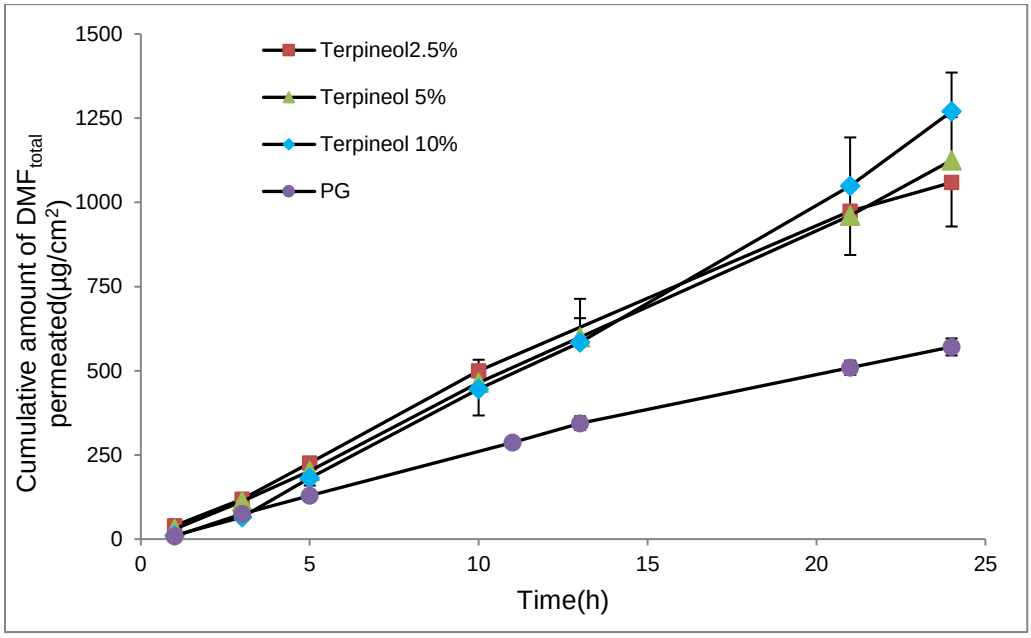

Figure 4.9. Effect of different concentrations of terpineol in propylene glycol (PG) on the permeation of DMF (µg/cm^2) against time (h) through human cadaver skin. (Each point represents the mean±S.D. of five experiments).

On the other hand, the more hydrophilic derivatives were more effective in enhancing the transdermal permeation of the hydrophilic model drugs, 5-fluorouracil and lidocaine (131). The same hypothesis can explain why Cin did not enhance the permeability of diclofenac (a highly lipophilic drug) as compared to a more lipophilic terpene, nerolidol(129). In this study, Cin was shown to be a better enhancer than Terp, this could be partly due to being more hydrophilic than Terp with calculated log p values of 2.84, and 3.28, respectively (132). Although Cin offers one H-bonding group (ether-O) in comparison to Terp, which has 2 groups available for H bonding, it was a more effective enhancer. An effect that can be attributed to the lower boiling point of Cin (137°C) than that of Terp (217°C), which suggest that Cin possesses weaker cohesive forces and hence less energy is required for its molecules to H-bond with the polar headgroups of ceramides (127). Furthermore, Cin is more miscible with PG than Terp, and PG can improve the permeation of Cin into the stratum corneum resulting in a synergistic effect (133).

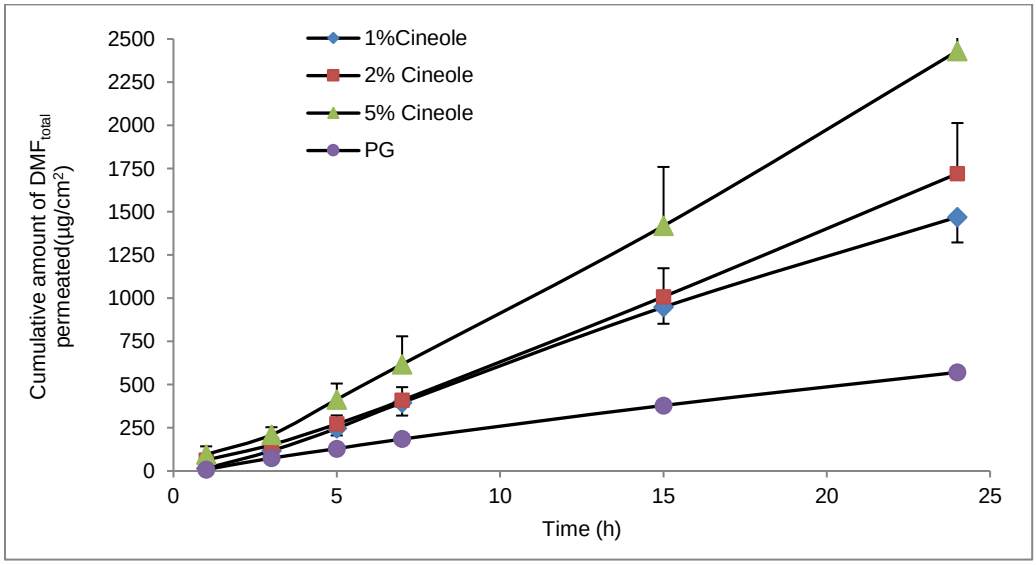

Figure 4.10. Effect of different concentrations of cineole propylene glycol (PG) on the permeation of DMF (µg/cm^2) against time (h) through human cadaver skin. (Each point represents the mean±S.D. of five experiments).

4.3.4.2. Effect of Tween 80

Tween 80 is a nonionic surfactant widely incorporated into topical preparations as a solubilizer and CPE (134). Surfactants can enhance the permeation of active molecules by several mechanisms, solubilization and fluidization of the stratum corneum lipids, and interaction with keratin causing the disruption of stratum corneum structure. This effect is attributed to their amphiphilic nature, where the surfactant hydrophilic groups interact with the keratin domains and their bound water effecting an aqueous filled spaces that ultimately affects the drug partitioning (135).

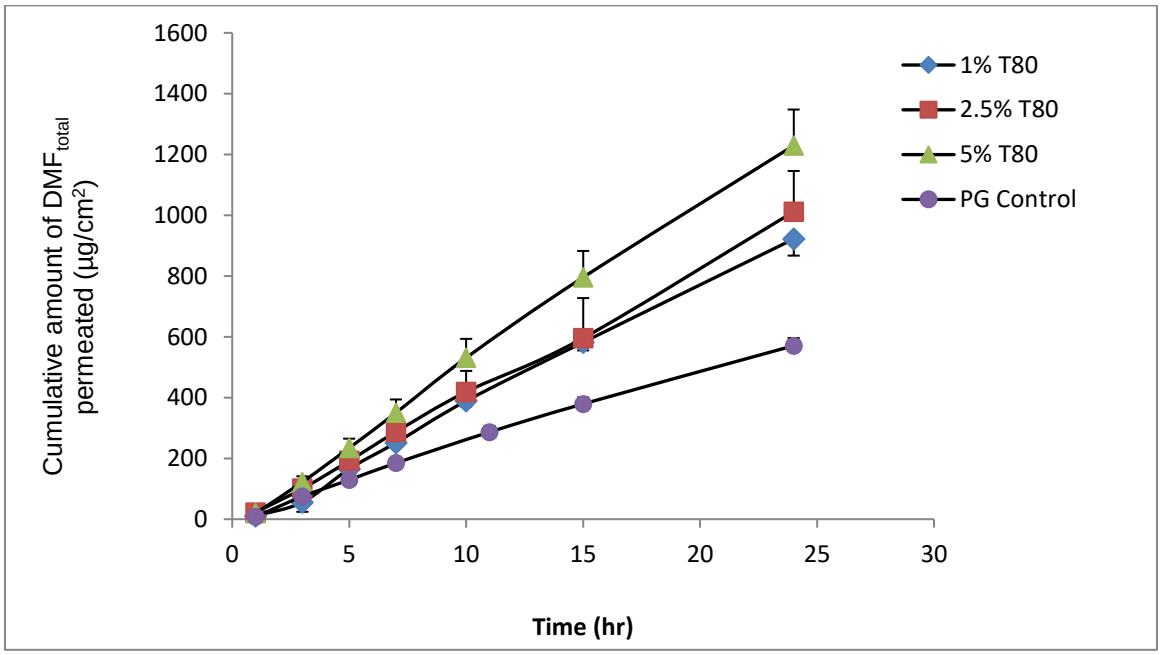

Figure 4.11. Effect of different concentrations of Tween 80 (T80) in propylene glycol (PG) on the permeation of DMF (µg/cm^2) against time (h) through human cadaver skin. (Each point represents the mean ± S.D. of five experiments).

The transdermal permeation profile of DMF from formulations containing different concentrations of T80 are depicted in Figure 4.14. Our results showed that the flux of DMF increased significantly upon the addition of T80, and there was a reduction of the lag time that was not present with other PEs were used. The enhancement effect of T80 may be due to a synergistic action of the combination of T80 and PG, the latter increasing the critical micelle concentration of T80 causing a greater number of free T80 monomers to be available for interaction with the stratum corneum (136, 137).

4.3.4.3. Effect of NMP

N-methyl pyrrolidone (NMP) is one of most commonly studied pyrrolidones for penetration enhancement. It acts as a solvent for stratum corneum lipids promoting the partitioning of the drug molecules (138). It may also create a depot within the skin that provides a prolonged or sustained delivery of drugs (37). Another mechanism of penetration enhancement proposed for NMP is through solvent drag effect(139). NMP has significantly increased the flux of DMF. However, the lag time was not decreased, and only P was increased with 20% NMP ($p < 0.05$). Such an effect may be attributable to the diffusion of NMP into the stratum corneum before exerting its penetration enhancement effects.

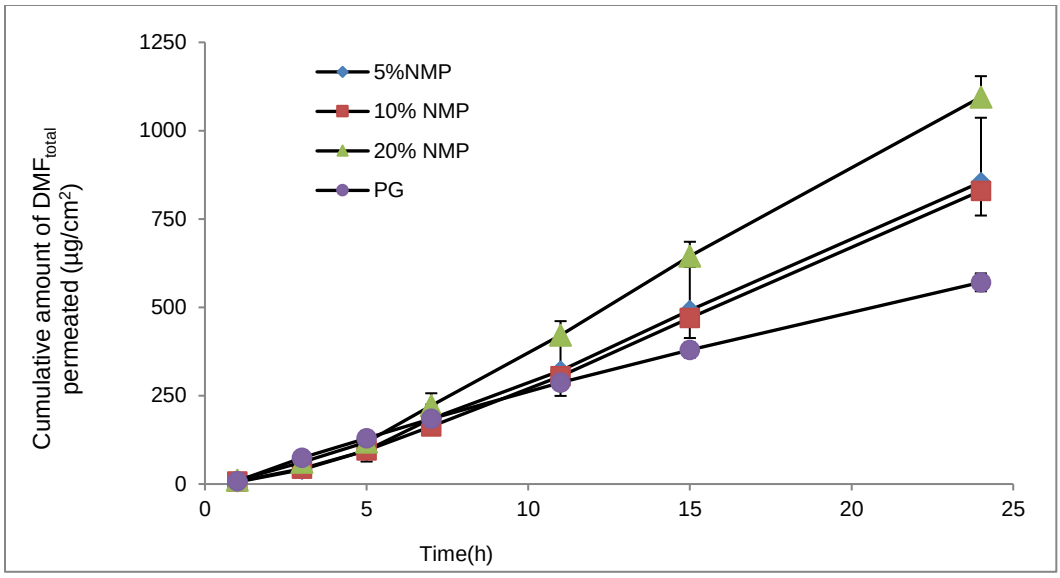

Figure 4.12. Effect of different concentrations of NMP in propylene glycol (PG) on the permeation of DMF (µg/cm^2) against time (h) through human cadaver skin. (Each point represents the mean ± S.D. of five experiments).

4.3.4.4. Effect of Azone

Azone is a highly lipophilic compound (log P = 6.2) (37). It exerts its penetration enhancement effect by squeezing into the lipid bilayer and changing /disrupting lipid packing resulting in increased stratum corneum lipid fluidity (130). Azone is not distributed evenly throughout the skin; it can either exist individually, or as domains within the lipid bilayers (140). The results showed that Az significantly increased the permeation of DMF compared to that of formulation without enhancer. Increasing the concentration of Azone resulted in higher flux and permeability coefficient ($p < 0.05$). However, the lag time was not reduced.

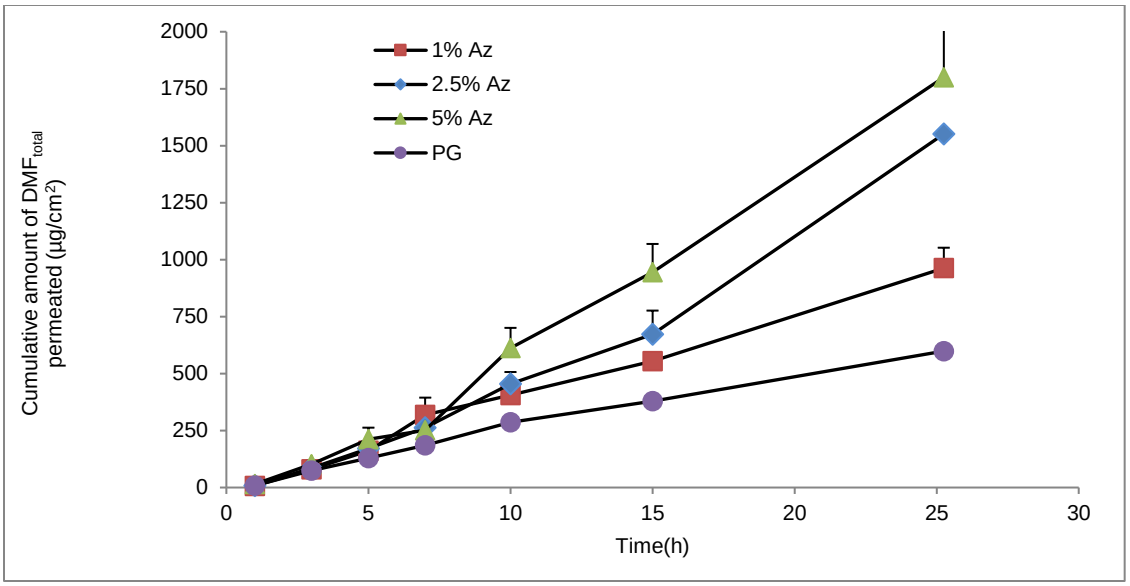

Figure 4.13. Effect of different concentrations of Azone (Az) in propylene glycol (PG) on the permeation of DMF (µg/cm^2) against time (h) through human cadaver skin. (Each point represents the mean ± S.D. of five experiments).

4.3.4.5. Effect of Transcutol P

Transcutol P (Tc) is a powerful solvent that has the advantage of being miscible with both hydrophilic and lipophilic solvents. It is widely used as a cosolvent in topical formulations. In addition, it increases the permeant concentration within the skin creating a depot effect (141). It is speculated that Tc effects the swelling of the lipids within the SC, while maintaining their bilayer structure. Drugs, especially the lipophilic ones, tend to dissolve into the swollen lipid creating a depot within the skin (142). It is difficult to describe Tc universally as being a penetration enhancer. Although it does modify the SC, Tc may limit the systemic absorption of the topically applied drugs (143). However, our results showed that the incorporation of Tc as a PE caused a significant increase in the flux of DMF compared to control formulation ($p < 0.05$).

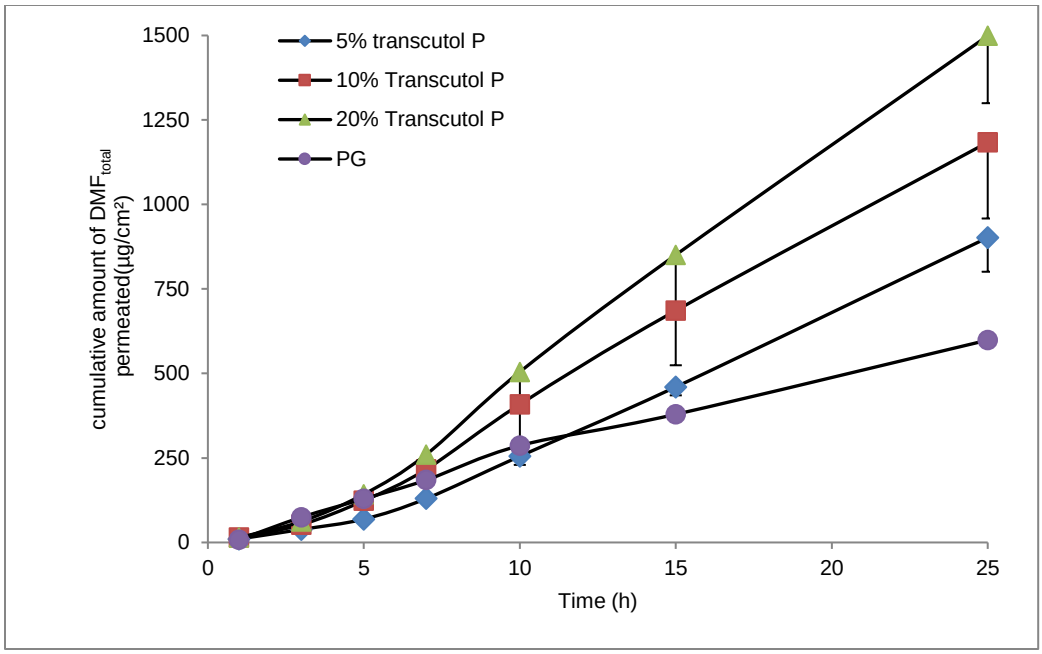

Figure 4.14. Effect of different concentrations of Transcutol P in propylene glycol (PG) on the permeation of DMF (µg/cm^2) against time (h) through human cadaver skin. (Each point represents the mean±S.D. of five experiments).

A study of the transdermal permeation of alfuzocin hydrochloride showed that 20% Tc produced a maximum solubility and flux of the drug (144). On the other hand, the lag time for DMF flux was markedly increased with Tc. Similarly, an increased diffusional lag time was observed when Tc was used to enhance the transdermal delivery of clonazepam, which was attributed to a higher drug solubility within the skin (145).

4.3.4.6. Effect of Concentration of PE

Furthermore, Figure 4.15 shows that increasing the concentration of Az, Tc, and Cin caused an increase in the flux with good linearity (R= 0.99, 0.93, 0.85, respectively). It was found that the concentration of Tc plays an important role in determining its enhancement activity. At a concentration lower than 40%, Tc enhanced the permeation of

clebopride. However, at a higher concentration, the permeation of the drug was retarded (146) A similar observation was reported when 50% Tc was incorporated with the UV filters 2-hydroxy-4-methoxybenzophenone and 2-octyl-4-methoxycinnamate (142). Apparently, the concentration of Tc used in our study was within the penetration enhancement range.

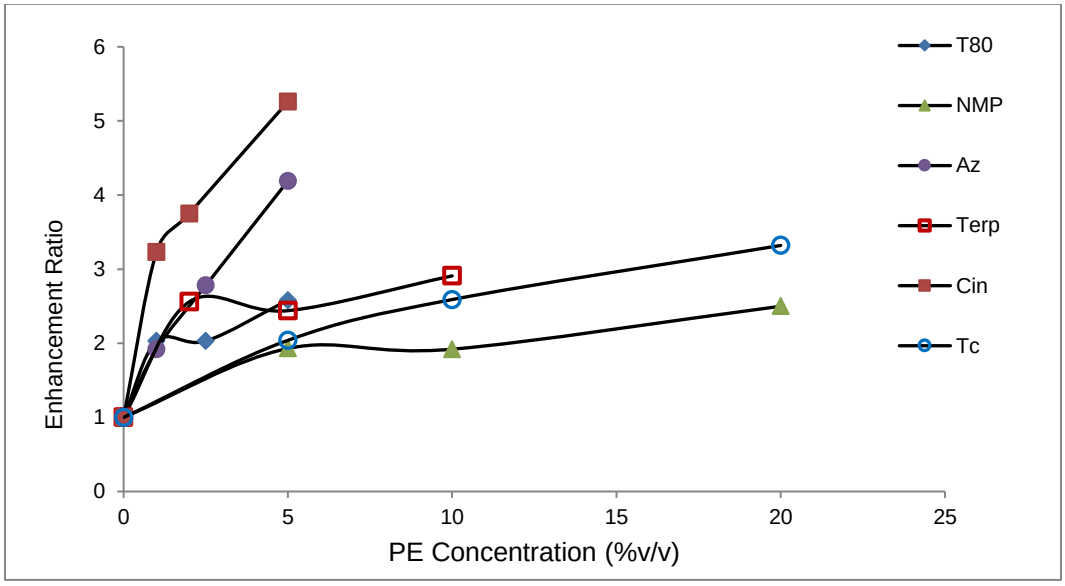

Figure 4.15. Effect of penetration enhancer concentration (PE) on the enhancement ratio (ER) of DMF. Data represents ER values at different concentration of the PE; Solid squares, Cineole; solid circles, Azone; solid diamond, Tween 80; solid triangle, NMP; open square, terpineol; open circle, Transcutol.

On the other hand, the other PEs did not show a similar behavior. For T80, no effect was observed on the rate of permeation when the concentration of T80 was increased from 1% to 2.5%. However, 5% T80 produced a larger flux and P (55.7±5.4, and 5.1±0.49, respectively) along with a reduced lag time. NMP showed a similar trend, where no

significant effect of increasing the concentration of NMP from 5% to 10%. On the contrary, 20% NMP brought about a marked increase in the flux ($p < 0.05$). A similar behavior, or even reduced flux was observed with surfactants and terpenes, and was attributed to either micelle formation, or limited solubility of terpenes in the vehicle, respectively (135, 147, 148). The partitioning of the PE into the stratum corneum and formation of a depot might be responsible for the temporary halt of further enhancement.

4.4. Conclusions

DMF was shown to permeate through human skin in vitro. The flux and the amount permeated were significantly increased with the incorporation of PEs. PEs were most effective at the highest concentration used and 5% (v/v) cineole in PG was the best vehicle to deliver DMF. Further *in vivo* studies are required to confirm that DMF can be delivered transdermally to achieve the required plasma therapeutic levels. Among the PEs tested, 5% cineole is a good candidate to be incorporated in the formulation of DMF transdermal delivery system for treatment of neurodegenerative diseases such as AD.

Chapter 5: Effects of pH and ionic form of nicotine on transdermal co-delivery with dimethyl fumarate across human skin in vitro.

5.1. Introduction

Alzheimer's disease (AD) is a progressive degenerative disorder affecting the central nervous system causing memory deterioration, reduced cognition, confusion, depression, hallucination and related psychoses. Eventually, patients will need institutional care (4, 149). To date, there are only 4 approved drugs for the treatment of AD. They fall into two classes: the acetylcholinesterase inhibitors (AChEI) and the N-methyl-D-aspartate receptors (NMDAR). These drugs are only palliative treatment with no real cure for AD so far (150). Other AD pathological targets were the focus of new drug development directions, such as amyloid-β (Aβ) and tau proteins (p-Tau) pathways. However, these agents were not successful in clinical trials (151). In theory, due to the complexity of AD pathophysiological pathways, it would be better to target more than one of these pathways through combination therapy (152). It is suggested that oxidative stress associated with elevated levels of reactive oxygen species (ROS) predisposes the accumulation of Aβ and p-Tau with the subsequent pathological manifestations of AD. Therefore, tackling the oxidative stress would be a potentially good approach for treating the disease (153). One way could be through activating the nuclear factor (erythroid-derived 2)-related factor 2 (Nrf2) pathway involved in cytoprotection by drugs such as dimethyl fumarate (DMF) (114). DMF, a small molecule that is approved for the treatment of multiple sclerosis, activates the Kelch-like ECH-associated protein (Keap1)-Nrf2 pathway inducing the expression of multiple cytoprotective genes. These genes encode for cytoprotective

antioxidant enzymes and proteins such as glutathione synthesizing enzymes, NADPH, etc. Also, it acts as anti-inflammatory and immunomodulatory through reducing pro-inflammatory cytokine production and activation of T-cells (120-122, 154). Based on the hypothetical involvement of the cholinergic system in the development and progression of AD, nicotine, the nicotinic acetylcholine receptor (nAChR) agonistic prototype, may potentially enhance cognition through binding to presynaptic nAChR facilitating the release of neurotransmitters involved in memory and learning (155). Additionally, nicotine has been suggested to activate the non-amyloidogenic pathway of Amyloid Precursor Protein (APP) processing, which not only attenuates Aβ toxicity, but also causes the release of a large soluble fragment with a range of trophic and protective functions (12). Further, chronic nicotine was shown to restores normal Aβ levels and prevents short-term memory, and improve memory recognition and reduce synaptic plasticity impairment in rat model of Alzheimer's disease (156, 157). Nicotine, the main tobacco addictive principle, is a tertiary alkaloid with a molecular weight of 162.23g/mol and log p of 1.17 (158, 159). Nicotine structure is depicted in Figure 5.1. It is already marketed in the form of transdermal patches for smoke cessation. Currently, all of the approved AD drugs except one are administered orally. Patients usually rely on caregivers to provide their medication and this by itself is a huge burden to the caregivers given the clinical symptoms of the patients. Consequently, non-compliance is considered a major challenge in the treatment of AD.

Indeed, transdermal delivery of drugs for AD offers exceptional advantages over oral route, not only by avoiding the GIT adverse effect but also by reducing the fluctuations of drug concentrations in the blood. The transdermal route is particularly advantageous in patients

with neurological disease, since they are often unable/unwilling to swallow tablets or are forgetful as in case of AD patients (160). Rivastigmine transdermal patches enhanced tolerability of the drug and allowed the administration of higher doses extending its indication to severe AD compared to oral dosage form, which is approved for mild to moderate cases only (161). However, transdermal delivery is limited by the ability of the drug molecule to penetrate the skin layers and reach the blood circulation at therapeutic concentrations. Several factors come into play with this regard, including the drug solubility, partition coefficient, molecular weight, ionization, etc. Good candidates for transdermal delivery are molecules with molecular weight of less than 500 Da, a log P of 1-3, and being non-ionized (162). According to the classical pH-partition theory, lipid soluble non-ionized molecules are the only ones available for absorption. However, this theory does not define well the transdermal permeation of ionizable molecules (163). Several studies have shown that both ionized and non-ionized species of drugs can penetrate the skin at different rates suggesting that there are some pathways or aqueous pores that allow the transport of charged species (164-166). However, little is known about the skin permeation of such ionizable molecules in the presence of other actives.

The objective of this study was to investigate the feasibility of the transdermal co-delivery of DMF and nicotine as a potential treatment for AD. The study also investigated the effect of pH and the ionic form on the transdermal permeation of both drugs using human cadaver skin as a preliminary step towards formulating both drugs as a potential therapy for the management of AD.

5.2. Materials and Methods

5.2.1. Materials

Dimethyl fumarate (DMF), (-)-Nicotine hydrogen tartrate salt (NHT), high-performance liquid chromatography (HPLC) grade water, phosphate buffer solution (1.0 M, pH 7.4), sodium phosphate monobasic, methanol and acetonitrile were purchased from Sigma-Aldrich Co. (St. Louis, MO, USA). Phosphate-buffered saline tablets (PBS, pH 7.4) was purchased from MP Biomedicals, LLC (Solon, OH, USA). O-Phosphoric Acid 85% was purchased from Fisher Scientific (Hampton, NH, USA). (S)-(-)-Nicotine (NB), 99% was purchased from Alfa Aesar (Haverhill, MA, USA). Dermatomed human cadaver skin from the posterior torso (female, aged 69) was obtained from New York Firefighter Skin Bank (NY, USA).

5.2.2. High-performance liquid chromatography (HPLC)

5.2.2.1. Equipment and mobile phase

The HPLC instrument was Agilent 1100 series HPLC instrumentation (Agilent Technologies, CA, USA) coupled with UV detection (Diode array detector- DAD) and HP Chemstation software V. 32. For the analysis of nicotine and DMF, a mobile phase of 65% 0.05M sodium Phosphate Buffer (adjusted to pH 3.2 with 85% orthophosphoric acid) and 35% Acetonitrile was pumped through a Phenomenex Luna® 5 µm C8 110 Å Column 250 X 4.6 mm with an injection volumes of 10uL and with a flow rate of 1.0mL/minute. The column temperature was set to 25°C with UV detection of 230 nm for DMF and 259 nm for Nicotine and with stop time of 10 minutes.

5.2.2.2. Standard solutions and calibration curves

A stock solution of nicotine base was prepared at concentrations of 0.5mg/ml. The stock solution was prepared by mixing accurately weighed amount of 99% nicotine base liquid equivalent to 50 mg of nicotine base with mobile phase buffer in 100ml volumetric flask. Standard solutions of nicotine were prepared by serial dilution of the stock solution with 0.05M monobasic sodium phosphate, pH 3.2. the standard solutions had a concentration range of 1.95-500µg/ml that covered the range of expected concentration in the skin permeation samples. Standard solutions for DMF and MMF were prepared as discussed in chapter 4.

5.2.2.3. Method validation

The HPLC method for nicotine was validated by testing the linearity and precision through inter- and intra-day variability and determining the limit of quantification and limit of detection as discussed previously in chapter 3.

5.2.3. Preparation of formulations

Saturated suspensions of DMF with either nicotine hydrogen tartrate salt (NHT) or nicotine base (NB) were prepared by adding excess amount of DMF with either excess amount of NHT or a fixed amount of NB in Propylene Glycol:0.2 M Phosphate Buffer Solution (50:50). The final apparent pH* was adjusted to 4.5, 5.5 and 6.5 using 85% Orthophosphoric Acid. Formulations without pH adjustment were prepared as negative controls. Furthermore, a similar set of formulations containing DMF alone without nicotine was prepared for comparison. Solubilities of DMF and NHT in the formulations incubated at 32° C for 48 hours were determined by filtering the formulations using 0.45µm syringe

filters. The filtered formulations were diluted appropriately and analyzed using a validated HPLC method.

5.2.4. In vitro skin permeation studies

Skin permeation was performed in vitro by using vertical glass Franz diffusion cells in a heat block (Logan Instruments, Somerset, NJ) with human cadaver skin of 0.64 cm^2 donor/diffusion area. Before using, the skin was slowly thawed, cut into appropriate pieces and then soaked in filtered PBS (pH 7.4) for 15 minutes. Dermatomed human cadaver skin with the dermal side in contact with receptor compartment was then mounted on Franz diffusion cells and the receptor compartment was filled with PBS (pH 7.4) and stirred at 600 rpm. The diffusion cells equilibrated at 37^oC for 15 minutes. Once reached equilibrium, at time zero 0.6 mL of each formulation was applied to each donor compartment and was covered with parafilm to prevent evaporation. At time points 1, 3, 5, 7, 11, 18, and 24 hours, 300µL aliquots were withdrawn from each receptor compartment and immediately replaced with an equal volume of PBS, pH 7.4. At the end of 24 hours, samples withdrawn were analyzed to determine DMF and Nicotine using a validated HPLC method described below.

5.2.5. Determination of Nicotine and DMF concentration in the skin

After commencement of the permeation study, formulation (DMF combined with nicotine) and the donor compartment were collected into 50 ml centrifuge tubes. The surface of the skin was wiped with Q-tips, which were collected along with the formulation in the same 50 ml centrifuge tubes. 5 ml Methanol was added into each tube for the

extraction of drugs. The tubes were sonicated for 1 hour then kept for 24 hours at 37° C before HPLC analysis. The skin was removed from the Franz diffusion cell and was cut around the diffusional area, air dried and accurately weighed. After weighing skin was then cut into small pieces and homogenized with 1 ml methanol in BeadBug™ microtube homogenizer for a total of 9 minutes (3 cycles of 3 minutes each). The skin samples were kept for 24 hours at 37° C and were centrifuged at 12000 rpm for 5 min and were filtered through a 0.45 µm polypropylene filter media with polypropylene housing before HPLC analysis. Nicotine and DMF concentrations were expressed as ng of Nicotine/DMF per skin weight in mg.

5.2.6. Data analysis

The cumulative amounts of DMF and Nicotine permeated per unit skin surface area (µg/cm^2) were plotted against time (hours). The steady state flux (*J*) was determined from the slope of the linear portion of the plot.

The permeability coefficient was calculated using equation (1)

$$p = \frac{J}{C_v} \quad \ldots\ldots(1)$$

where C_v is the total donor concentration of DMF and/or Nicotine.

5.2.7. Statistical analysis

Results are reported as mean ± SD (n=4-5). The cumulative amount of drug permeated per unit area (*Q24*) and (*J*) obtained for formulations was compared using the one-way analysis of variance (ANOVA), and Student-t test. Differences among the treatments were assumed to be significant at $p < 0.05$.

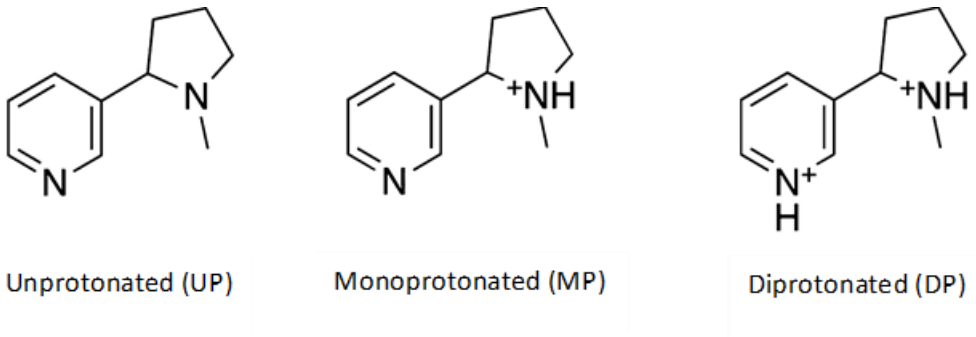

Figure 5.1. Chemical structure of nicotine free base and its ionization forms.

5.3. Results and Discussion

5.3.1. HPLC method validation

We have adapted the same HPLC method used to quantify DMF and MMF to determine the concentration of nicotine in the analyzed samples simultaneously, which resulted in an enormous reduction in equipment utilization time and HPLC solvents consumption. Nicotine had an absorption peak at 3.5 min at a wavelength of 259 nm. The calibration curve of nicotine was constructed by analyzing standard solutions in the concentration range of 1.95-500µg/ml using the HPLC method parameters for 3 injections and the average area under the peak was plotted against the concentration of the standard solution as shown in Figure 5.2.

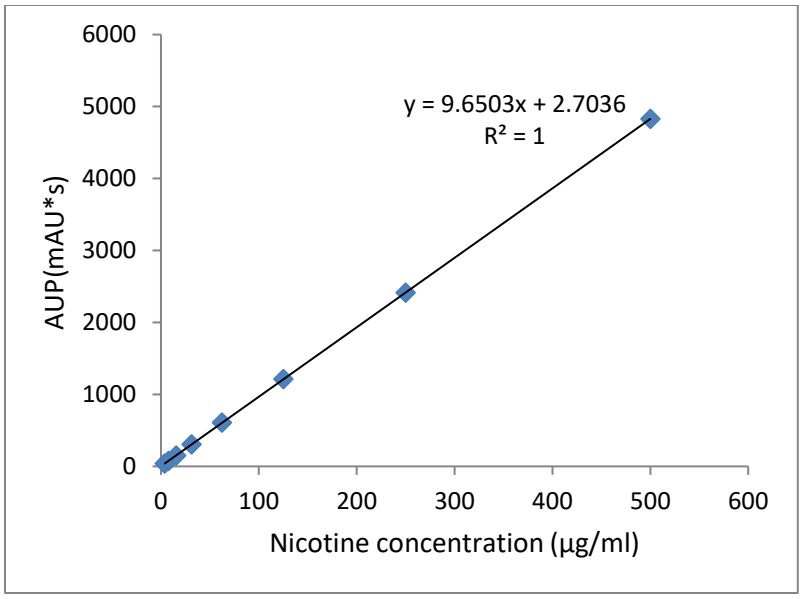

Figure 5.2. Nicotine standard calibration curve for HPLC assay method. Area under the peak (AUP) of the chromatogram against the concentration of nicotine. Values represent an average of 3 injections.

The method revealed a perfect linearity with R^2 of unity and LQ and LD of and µg/ml, respectively for nicotine assay. Table 3.1 shows the intra- and inter-day precision data for three different concentrations of nicotine from 3 runs at different times on the same day or different days. All of the %RSD values fell below 2%, which indicted the repeatability and precision of the method.

Table 5.1. Intra-Day and Inter-Day Precision Analyses of nicotine, n=3.

Nicotine Concentration (µg/ml)	**Intra-Day Analysis**		**Inter-Day Analysis**	
	AUP (mAU*s) ±SD	**%RSD**	**AUP (mAU*s) ±SD**	**%RSD**
15.6	76.2 0.4±	0.55	76.6±0.9	1.2
62.25	606.8±0.8	.13	607.2±1.3	0.19
125.0	112.9±3.7	0.3	1214.7±4.7	0.38

5.3.2. In vitro skin permeation studies

The effects of pH and the form of nicotine on the transdermal permeation of both of DMF and nicotine when combined together across human cadaver skin were investigated. Suspensions of DMF with either nicotine hydrogen tartrate (NHT) or nicotine base (NB) were prepared at pH* values of 4.5, 5.5, and 6.5 to maximize the thermodynamic activity of DMF for permeation (167). Achieving the same conditions was not possible for NB, since it is present as a miscible liquid (168). Hence, a fixed concentration of NB was used throughout the study based on the solubility of NHT in the vehicle. It is imperative to note that since the formulations used for the study contained 50% v/v propylene glycol in buffer, true pH is difficult to measure and that only apparent pH* values are recorded. The solubility study results of DMF listed in Table 5.2 showed that solubility was not affected by neither changing the pH nor adding NHT or NB with a mean of 3.5 ±0.3 mg/ml at 32º C in the vehicle at various pH*values. Individual solubilities of DMF are listed in Table 1 reflects non-significant difference amongst different formulations except for DMFUM-NB, which showed dramatically lower solubility in unadjusted formula ($p < 0.05$). Similarly, the solubility of NHT, as shown in Table 5.3, was not affected by the change in pH within the limits of studied range and had a mean solubility of 3.3±0.1 mg/ml at 32º C. Preliminary solubility results revealed extensive hydrolysis of DMF at pH values higher than 6.5, which is in agreement with already published literature (118, 169). Therefore, such pH values were excluded from further investigation.

The permeation parameters of DMF are listed in Table 5.2 and permeation profiles from DMF-NHT formulations are depicted in Figure 5.3 and show that DMF had the highest flux and amount permeated per unit area at pH* 6.5 ($p < 0.05$), and that reducing the pH*

resulted in observed reduction in both parameters. Where DMF flux as well as the amount of DMF permeated per unit area (Q_{24}) showed approximately a 2-fold increase at this pH* compared to lower pH* values. In addition, controlling the pH seemed to have a significant effect on the permeation of DMF as indicated by the lowest flux and amount permeated for the unadjusted pH*-formulation ($p < 0.05$). Further, DMF from DMF-NB formulations

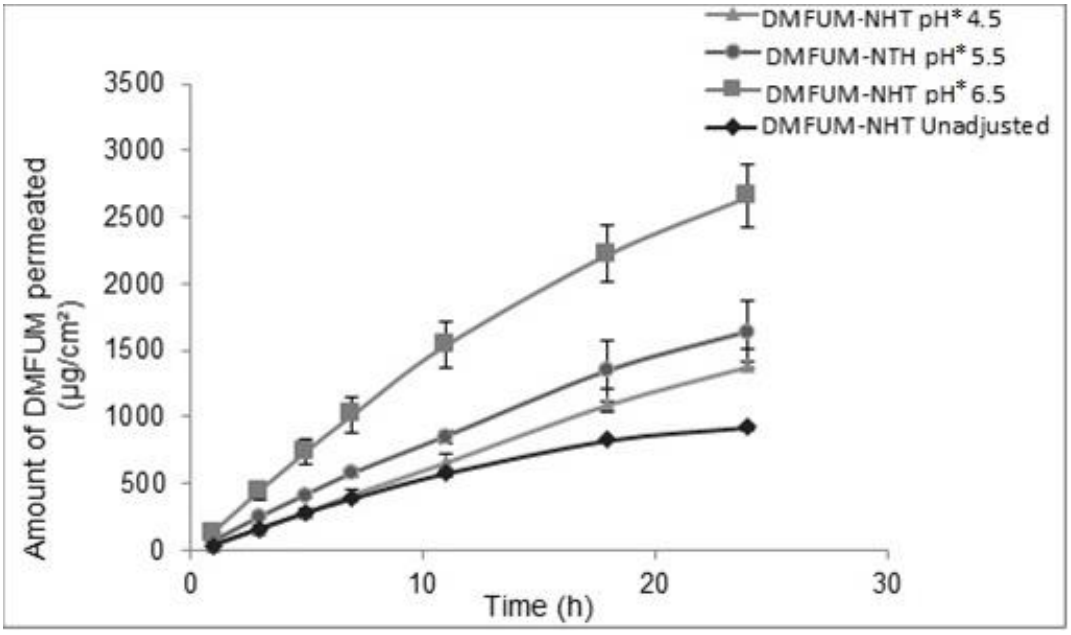

Figure 5.3. Skin permeation profile of dimethyl fumarate from DMF-NHT formulation at different pH* values through human cadaver skin. Each value represents the mean ±S.D. (n=4).

showed quite similar trend seen with DMF-NHT formulations, as depicted in Figure 5.4, where DMF had a highly significant increase in flux (J) value at pH* 6.5 ($p < 0.05$).The rank order of DMF flux from both formulation-sets with respect to pH* was found to be as follows: $flux_{pH6.5^*} > flux_{pH5.5^*} > flux_{pH4.5^*} > flux_{pH^*\ unadjusted}$. Overall, adjusting the pH* has a significant impact on the permeation of DMF when combined with nicotine regardless of its form.

Table 5.2. Permeation parameters of DMF from different formulations at different pH*.

Formulation	pH*	Solubility[a] (mg/ml)	Flux (µg/cm²/h)	P x10⁻² (cm/h)	Lag time (h)	Q_{24} (µg/cm²)
DMFUM-NHT	4.5	3.7±0.4	60.2±5.6	1.7±0.2	0.4±0.0	1384.7±120.7
	5.5	3.8±1.0	77.8±4.9	2.2±0.1	0.3±0.1	1572.4±83.8
	6.5	3.6±0.1	138.3±14.1	3.9±0.4	0.2±0.0	2657.0±232.4
	Unadjusted (7.6)	2.3±0.2	66.5±0.9	2.9±0.1	0.5±0.1	889.9±43.5
DMFUM-NB	4.5	3.2±0.2	65.0±8.6	1.9±0.2	0.5±0.2	1481.0±159.7
	5.5	3.4±0.6	77.1±4.3	2.2±0.1	0.3±0.1	1609.8±80.8
	6.5	3.7±0.8	114.7±10.7	3.3±0.3	0.2±0.0	2133.1±168.3
	Unadjusted (8.4)	0.3±0.1	26.9±3.8	2.6±0.4	1.0±0.1	234.8±46.6
DMFUM alone	4.5	3.1±0.1	84.9±7.7	2.4±0.2	0.5±0.1	1638.8±69.4
	5.5	2.9±0.2	74.7±6.0	2.1±0.1	0.3±0.2	1333.4±88.5
	6.5	3.7±0.4	83.4±6.0	2.4±0.2	0.4±0.2	1454.4±213.7
	Unadjusted	2.4±0.1	42.2±6.2	1.2±0.2	2.1±0.2	387.6±46.1

Data are presented as mean ± S.D. (n=4-5). DMFUM skin permeability coefficient (*P)* is determined by dividing the flux (*J*) by the DMFUM donor concentration, lag time is obtained from the x-intercept of the extrapolated linear line of the flux. Q_{24} is the cumulative amount of DMFUM permeated per cm^2 at the end of 24 hours.

[a] Solubility data represent mean ± S.D. (n=3).

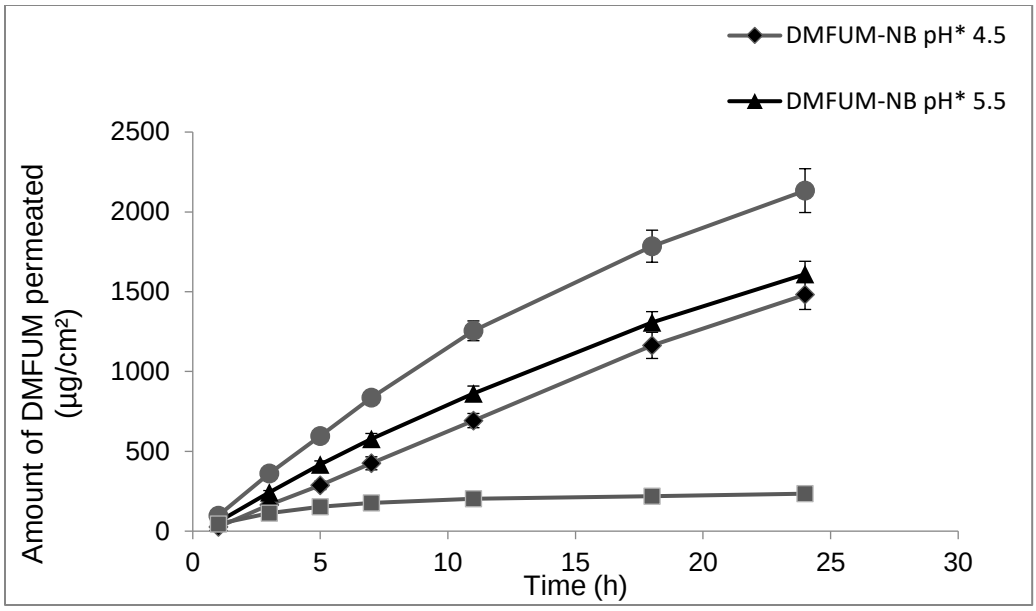

Figure 5.4. Skin permeation profile of dimethyl fumarate from DMF-NB formulation at different pH* values through human cadaver skin. Each value represents the mean ±S.D. (n=4).

Although non pH* -adjusted formulations were suspensions, they showed dramatically lower *J* and Q_{24} for DMF. Indeed, these formulations exhibited relatively high pH* values, 8.4 and 7.6 for DMF-NB and DMF-NHT, respectively. At such high values, DMF underwent extensive hydrolysis to its monomethyl ester as detected by HPLC. Monomethyl fumarate exhibited much lower permeability than DMF in preliminary testing. Although DMF is not an ionizable molecule, it seems to be affected by changing the pH* in the presence of nicotine.

To investigate whether combining nicotine as either form with DMF could affect the permeation of the latter as a function of pH*, similar formulations containing only DMF were prepared and tested for the permeation rate of the drug. Figure 5.5 shows the permeation profiles of DMF from formulations containing NB, NHT, or no nicotine at pH*

4.5. It seems that the presence of either NB or NHT has significantly reduced DMF flux ($p < 0.05$) (Table 5.2).

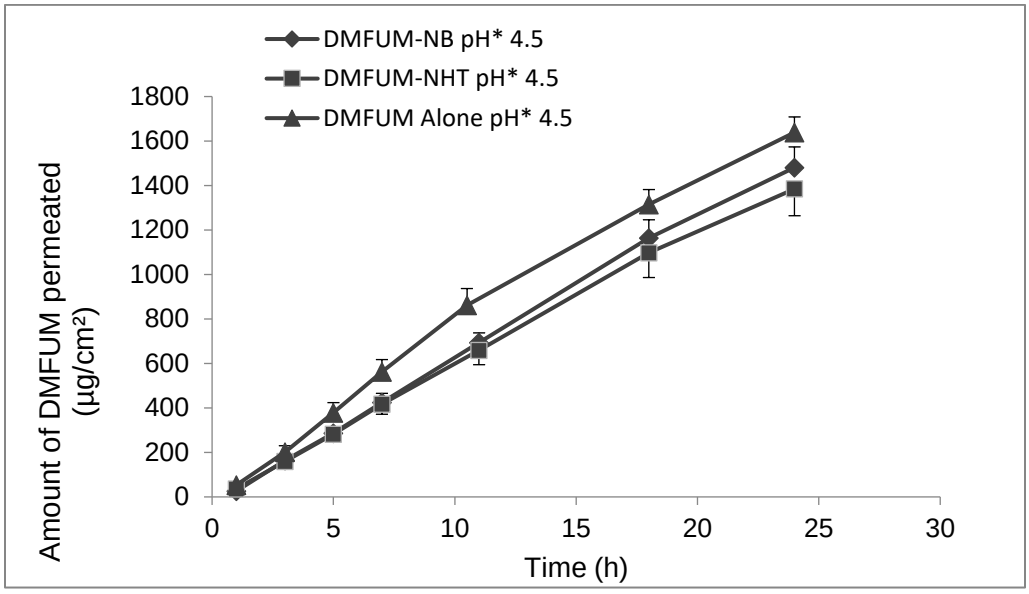

Figure 5.5. Skin permeation profile of dimethyl fumarate with or without nicotine at pH* 4.5 through human cadaver skin. Each value represents the mean ±S.D.(n=4).

In addition, NHT has significantly less (Q_{24}) compared to formulation containing DMF alone ($p < 0.05$). Surprisingly, upon increasing the pH* the effect of nicotine on DMF permeation exhibited some change, where DMF flux was slightly higher in the presence of nicotine than that for DMF alone formulations. Figure 5.6 depicts the permeation profiles of DMF from different formulations at pH 5.5* indicating that both NB and NHT DMF had significantly higher Q_{24} than when DMF alone was tested ($p < 0.05$). Furthermore, upon increasing the pH* to 6.5 both NB and NHT caused a dramatic increase in DMF J and Q_{24} ($p < 0.05$) with NHT having the greatest effect as shown in figure 5.6.

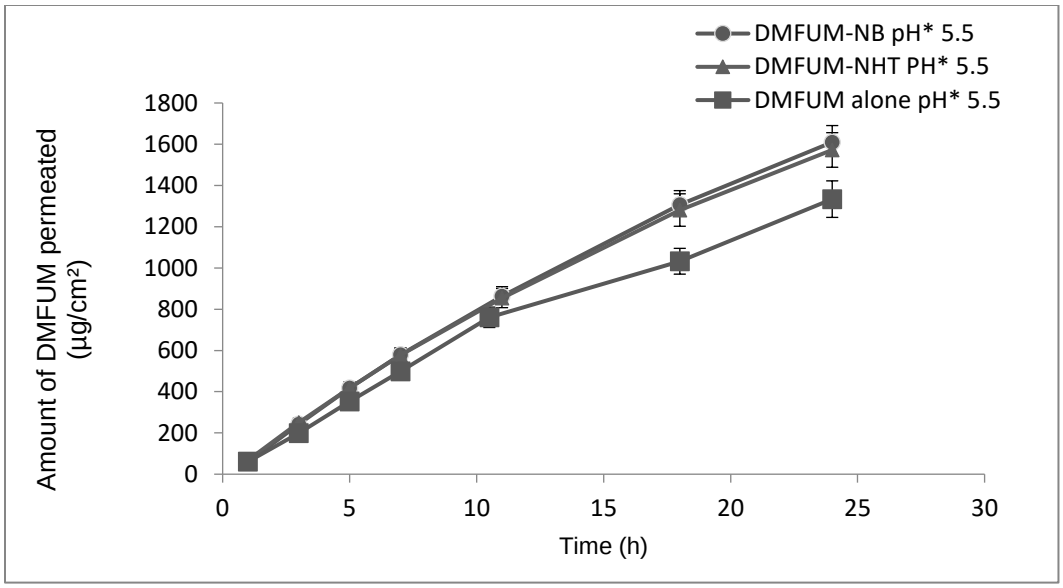

Figure 5.6. Skin permeation profile of dimethyl fumarate with or without nicotine at pH*5.5 through human cadaver skin. Each value represents the mean ±S.D.(n=4).

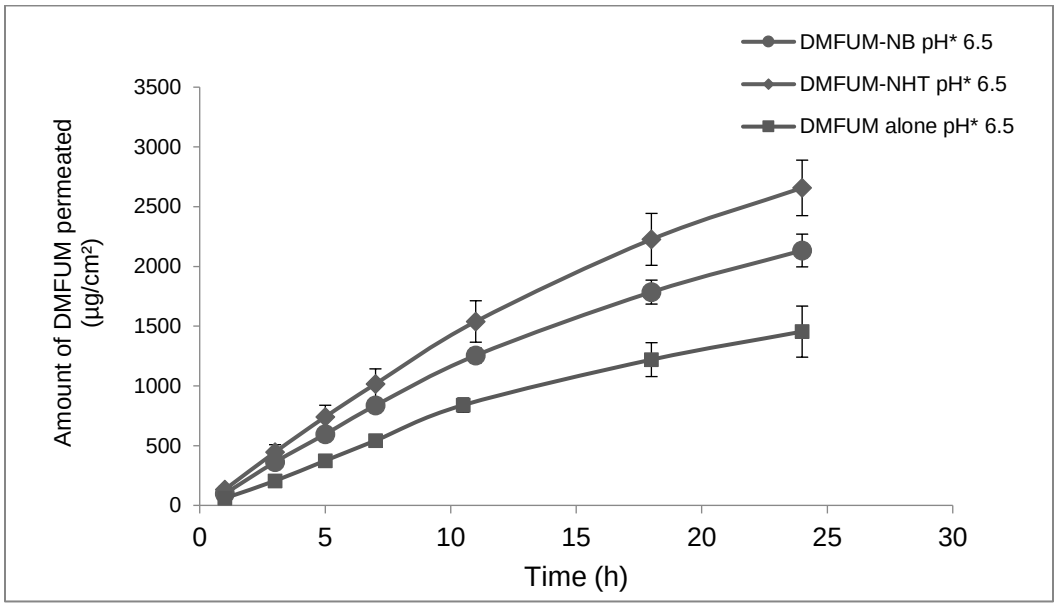

Figure 5.7. Skin permeation profile of dimethyl fumarate with or without nicotine at pH*6.5 through human cadaver skin. Each value represents the mean ±S.D.(n=4)

On the other hand, when the effect of pH* change upon DMF alone formulations was investigated, the results showed that increasing the pH* within the studied range did not

have any effect on neither DMFUM *J* nor Q_{24}. However, adjusting the pH* had a great impact on the aforementioned permeation parameters (Table 5.2). These results reflect a similar trend for DMF with nicotine regardless of the form used. It is noteworthy that the DMF alone formulation prepared without adjusting pH exhibited a high pH* value around 8.4, at which DMF undergoes extensive hydrolysis (118, 169). It seems that changing the pH* for DMF alone formulation did not have any effect of its permeability, such that there was no significant difference in the permeability coefficient (*P*) values of DMF. However, non-adjusted formulation exhibited a dramatically lower permeability ($1.2\pm0.2 \times 10^{-3}$ cm/h) and associated with a longer t_{lag}. On the other hand, upon combining with nicotine a different behavior was noticed, where a significant drop in DMF *P* value was noticed at pH* 4.5 with either of NB or NHT ($p < 0.05$). Then, the *P* showed increase with higher pH*, where at pH 6.5 it became significantly larger than when DMF permeated alone ($p < 0.05$). That pattern was consistent for both NB and NHT. Assuming the vehicle had no effect on the skin barrier function, and drug concentration and membrane thickness being consistent, no difference is expected in the permeation parameters of DMF by changing the pH*, which is in agreement with our finding for DMF alone formulation. Since all formulations were saturated suspension of DMF, hence equal thermodynamic activity, the observed difference in fluxes could be attributed to change in the barrier property. It seemed that nicotine at pH* 6.5, in particular, had an enhancing effect on the permeation of DMF exemplified by an observed increase in DMF flux of 1.4 and 1.7-fold with NB and NHT, respectively. Nicotine permeation, on the other hand showed a different pattern. Table 5.3 depicts the permeation parameters of nicotine across human cadaver skin from both DMF-NB and DMF-NHT at different pH* values.

Table 5.3. Permeation parameters of nicotine from different formulations at different pH*

Formulation	pH*	Solubility[a] (mg/ml)	Flux (µg/cm²/h)	P x10⁻³ (cm/h)	Q_{24} (µg/cm²)
DMFUM-NB	4.5	3.4±0.03[b]	7.8±2.4	2.5±0.8	187.3±59.7
	5.5	3.3±0.02[b]	6.2±0.8	1.9±0.2	131.6±23.5
	6.5	3.5±0.4[b]	4.8±0.3	1.5±0.1	130.2±18.2
	Unadjusted (8.4)	3.3±0.2[b]	10.2±1.9	3.2±0.6	294.4±56.2
DMFUM-NHT	4.5	3.4±0.1	4.5±0.7	1.4±0.2	138.8±35.0
	5.5	3.4±0.3	4.3±1.3	1.4±0.4	129.4±14.0
	6.5	3.3±0.5	4.6±0.2	1.4±0.1	132.7±27.6
	Unadjusted (7.6)	3.1±0.5	11.4±0.7	3.6±0.2	213.5±11.7

Data are presented as mean ± S.D. (n=4-5). Nicotine skin permeability coefficient (*P)* is determined by dividing the flux (*J*) by the nicotine donor concentration. Q_{24} is the cumulative amount of nicotine permeated per cm^2 at the end of 24 hours.
[a] Solubility data represent mean ± S.D. (n=3).
[b] This value represents the concentration of NB in the formula.

The permeation profiles of formulations prepared with NB and NHT shown in Figures 5.8 and 5.9, respectively revealed a similar trend, where all pH*adjusted formulations had less nicotine permeation than the non-adjusted one. . Nicotine is a dibasic alkaloid that can exist as an unprotonated (UP) (free base), monoprotonated (MP), or deprotonated (DP) species depending on the pH of the medium, as shown in Figure 5.1. It has 2 pka constants: pK_{a1} 3.1, and pK_{a2} 8.02 at 25ºC according to Barlow and Hamilton (170). However, at 37º C they are determined to be 2.77 and 7.65, respectively (171). In aqueous solutions and depending on the pH of the solution the ionization of nicotine base takes place as follows:

$NicH^{2+} \rightleftharpoons H^{+} + NicH^{+}$ (2) with pK_{a1} as the dissociation equilibrium constant.

$NicH^+ \rightleftharpoons H^+ + Nic$ (3) with pK_{a2} as the dissociation equilibrium constant.

And the fraction of UP (f_{UP}) is determined according to eq.4:

$$f_{UP} = \frac{[Nic]}{[Nic]+[NicH^+]+[NicH^{2+}]} \qquad (4)$$

By substituting the equilibrium constants expressions for eq.s 2 and 3 into eq 4 with rearrangement results in eq. 5:

$$f_{UP} = \frac{1}{1+\frac{[H^+]}{K_{a2}}+\frac{[H^+]^2}{K_{a1}K_{a2}}} \qquad (5)$$

At pH above 4, $[NicH^{2+}]$ becomes negligible and eq.5 can be simplified into eq.6

$$f_{UP} = \frac{1}{1+\frac{[H^+]}{K_{a2}}} = \frac{1}{1+10^{pK_{a2}-pH}} \qquad (6)$$

Similarly, the fraction of MP species can be calculated according to eq. 7

$$f_{MP} = \frac{1}{1+\frac{K_{a2}}{[H^+]}} = \frac{1}{1+10^{pH-pK_{a2}}} \qquad (7)$$

Table 5.4 summarizes the % MP species of nicotine at theoretical pH tested, which hold true only in aqueous solutions. On the other hand, mixed organic and water solutions , such as the one we used in this study don't necessarily follow these assumptions due to two reasons, 1) the measured pH is only apparent value and does not correlate to the concentration of hydrogen ions, 2) pK_a value is expected to be affected by the added solvent. In a study of the effect of different cosolvents on the pK_a values of oxytetracycline, it was that 40% v/v PG in water caused an increase in apparent pK_a values of the drug by

about 0.03-0.36 log order (172). Additionally, several difficulties are associated with accurate pH measurement for such solutions. The inconsistency and reduced precision of such measurements could be due to the dehydration of the outer gel layer of the glass electrode, immiscibility of the electrode aqueous fill solution with the tested sample leading to the development of junction potential, incompatibility of the electrode body and the tested sample. Therefore assuming that the pH and pK_a in aqueous solutions are the same as in mixed organis:aquoes liquids is fairly problematic, unless in special situations where an acid added to the solvent mixture sufficiently strong to react with nicotine free base such that the concentration of the acid/concentration of nicotine $\gg 1$ (173).

Table 5.4 The theoretical % of monoprotonated nicotine species at each pH value in aqueous medium.

pH	% Ionized nicotine (MP)
4.5	99.9
5.5	99.3
6.5	93.4
7.6	52.9
8.4	15.1

NB containing formula at pH*4.5 showed an unexpected significantly higher nicotine flux and Q_{24} than the respective values at higher pH* ($p < 0.05$). Both DMFUM-NB and DMFUM-NHT non adjusted pH*formulations had higher pH*. This apparent pH may be associated with decreased ionization of nicotine and subsequently may have increased its permeation from both formulations. Nair *et al.*, have reported an increase in nicotine flux across porcine skin at higher pH (174). Similarly, Santi *et al*. also showed that the partition

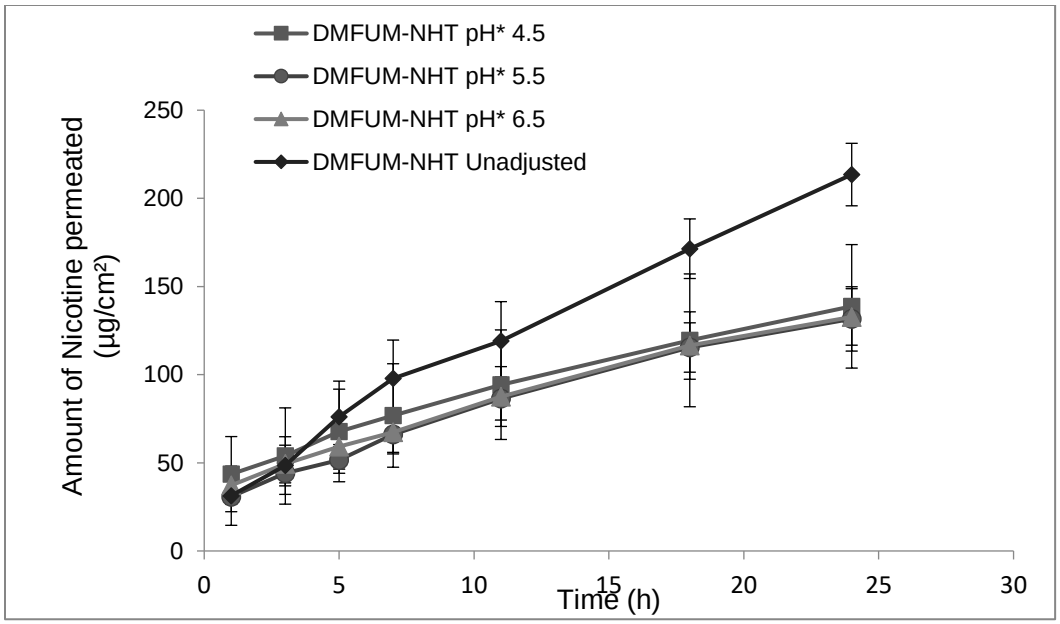

Figure 5.8. Skin permeation profile of nicotine from DMF-NHT formulation at different pH* values through human cadaver skin. Each value represents the mean ±S.D.(n=4).

coefficient of nicotine bitartrate along with its permeability and flux across polypropylene membranes have increased with increase in pH. The enhanced flux was attributed to increased partition coefficient despite the unchanged solubility of nicotine in the vehicles tested (175). However, nicotine was shown to deviate from pH-partition theory, which indicated a significant ion pair formation. Oakley and Swarbrick found that at pH 4.5 nicotine partitioned into n-butanol primarily as an ion pair and exhibited a considerable partitioning in the stratum corneum at pH values where almost exclusively present as ionized form. They suggested that ionized species can still permeate the skin as ion pairs through aqueous channels into the intracellular spaces of the keratinocytes (176). Ion pair formation was also suggested by Aungst in explaining the quite high skin penetration of nicotine salts at pH values where it is mostly present as ionized form the ionized species

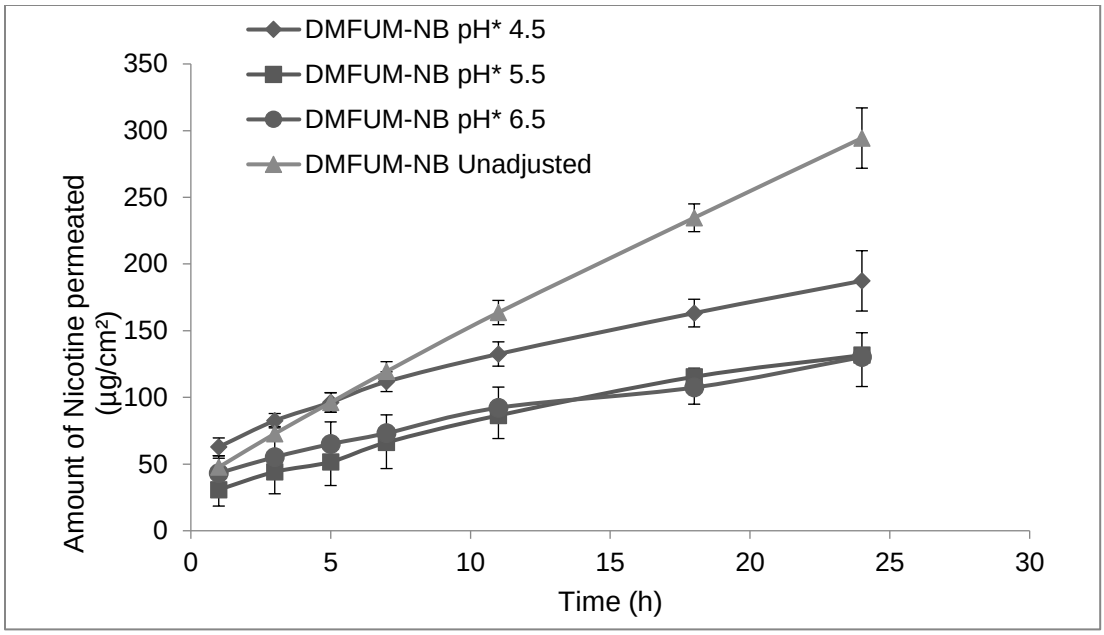

Figure 5.9. Skin permeation profile of nicotine from DMF-NB formulation at different pH* values through human cadaver skin. Each value represents the mean ±S.D.(n=4).

of nicotine and tartrate, which may have counteracted the effect of lower pH, hence increased ionization, on nicotine flux from NHT formulations. Interestingly, fluxes from NB at pH* 4.5, and 5.5 were significantly higher than those corresponding NHT fluxes at the same pH* values. More phosphoric acid was added to NB formulations than NHT formulations to bring down the pH* to the required value. With the solubility of NHT being unaffected by pH increase, more phosphoric acid added to NB formulations, potentially increased the concentration of ion pairs facilitating nicotine permeation. According to Fini et al., who studied the formation of diclofenac salts ion pairs, the higher counter ion concentration the more ion pairs formed that were then available for partitioning into the organic phase (n-octanol) (177). This observation could be the result of the interplay between phosphate ions and the tartrate counterion affecting the ion pair formation. Peck

et al. postulated that human epidermal membranes could have a pore size range of 15-20 Aº (178). An ion pair formed with tartrate is supposedly lager in size than one formed with phosphate, which might explain the lower flux and permeability of nicotine from NHT formulations.

Upon examining DMF skin content in Figure 5.10 that shows the amount of DMF per unit weight of skin, it can be realized that changing the pH* did not affect the skin DMF content for formulations without nicotine. However, this is not the case when NB or NHT were present. At pH* 4.5, the skin had a significantly lower DMF content when combined with nicotine than when it is formulated alone ($p < 0.05$). At pH* 5.5, there was no significant difference in the amount of DMF detected in the skin among formulations with or without nicotine. Finally, at pH* 6.5, NHT containing formulation had a dramatically higher DMF skin content than the rest of the tested formulations ($p < 0.05$).

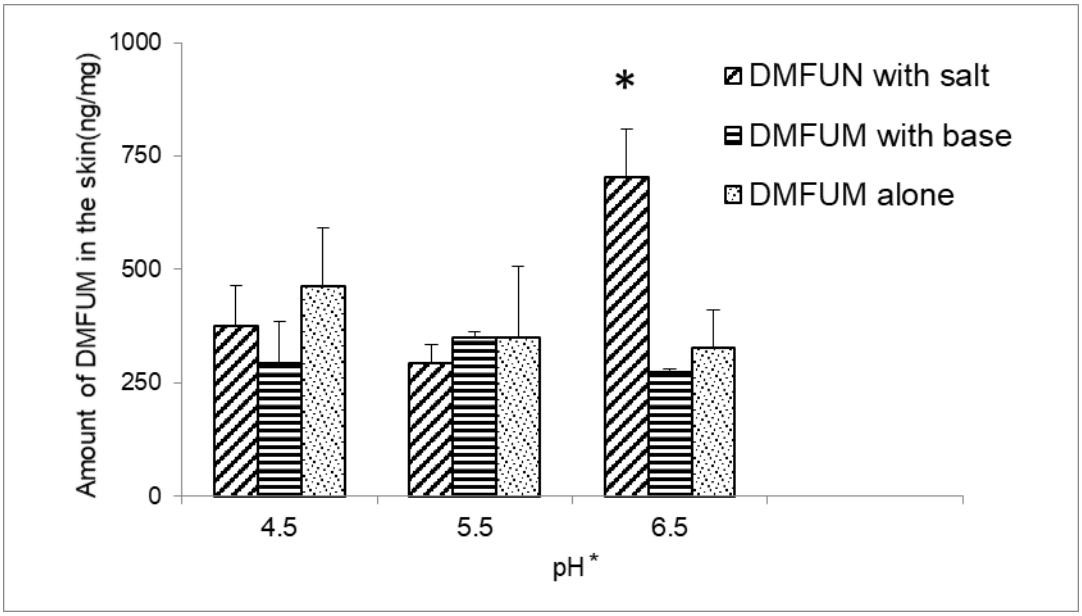

Figure 5.10. Dimethyl fumarate skin content from different formulation at different pH* values. Each value represents the mean ±S.D.(n=4).

Nicotine skin content shown in Figure 5.11, on the other hand, followed a pattern that can be correlated to its permeation profiles. Nicotine skin content was shown to decrease with increase in pH*. An interesting observation was that at pH* 4.5, nicotine has the highest skin content coupled with the lowest DMF flux.

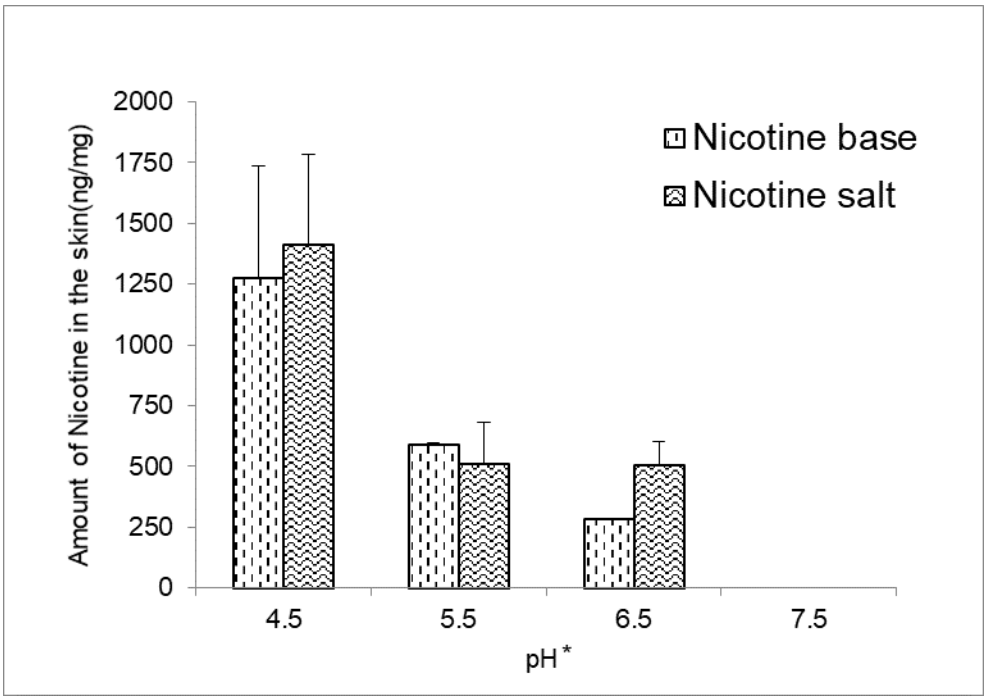

Figure 5.11. Nicotine skin content from different formulation at different pH* values. Each value represents the mean ±S.D.(n=4).

5.4. Conclusions

The present study investigated the skin permeation of DMF and nicotine as a function of pH* of the formulation (pH* 4.5, 5.5, and 6.5) and the form of nicotine (free base vs. salt). Results showed that combining DMF and nicotine together had a mutual effect on their permeability through human cadaver skin with respect to pH*. Although, nicotine is known to deviate from pH-partition theory, combination with DMF and pH* resulted in an unpredictable permeation pattern of NB that was not seen with NHT. DMF showed increase in flux with increase in pH* in the presence of either forms of nicotine, which at a at a pH* of 6.5 appeared to have enhancement of permeation reflected by an increased flux and permeability coefficient that were hard to explain. More work needs to be done to investigate the interaction of DMF and nicotine with the stratum corneum lipids at the molecular level to verify any enhancement activity. Additionally, more studies need to be conducted to correlate the apparent pH with the ionization of nicotine. Overall, our results show the feasibility of transdermal permeation of DMF combined with nicotine with factors as pH* and ionic form of nicotine play a significant role in formulating a potential transdermal delivery system containing both drugs.

Chapter 6: Development of nanostructured lipid carriers for the transdermal drug delivery system for dimethyl fumarate

6.1. Introduction

Neurodegenerative diseases are a group of chronic diseases affecting the nervous system, and examples are Alzheimer's disease (AD), multiple sclerosis (MS), Parkinson's disease (PD), among others. Despite their specific characteristics, they share some common features including protein deposition, oxidative stress, inflammation, and neuronal loss, etc.(24). The treatment of these diseases represents a huge challenge as they are increasing in prevalence due to the increase in elderly population (specific to AD), and the lack of a cure for any of them with the exception of some disease-modifying drugs that have been developed to tackle some of the diseases' hypothesized etiological factors (1, 179). Since inflammation is a common pathogenic feature to almost all neurodegenerative diseases, drugs with immunomodulative actions may be a promising choice in managing such illnesses. Dimethyl fumarate (DMF), a good example in this category, has immunomodulating actions through activating the (erythroid-derived 2)-like 2 (Nrf2) pathway, which plays a crucial role in cellular defense mechanisms against reactive oxygen species (ROS). In addition to its cytoprotective action, it was also shown to reduce inflammatory cytokines and activation of T-cells. Furthermore, it has a great potential for the treatment of AD through tackling the underlying pathogenetic factors predisposing the disease (122, 180). DMF oral tablets were approved for the treatment of relapsing remitting MS in 2013. However, their use is associated with gastrointestinal side effects which in some cases cause patients to abandon their treatment. An alternative route for delivering

the drug would be an optimum approach to avoid the drug side effects and improve patient compliance. Indeed, the transdermal route offers several advantaged over oral route, such as reducing side effect not only through avoiding the gastrointestinal tract but also by eliminating the inevitable drug level fluctuations associated with oral dosing (181). In addition, it may enhance the bioavailability of the drugs through avoiding hepatic first pass effect, offer a non-invasive alternative to patient population who cannot take or experience difficulty taking oral medication (9), as well as serving as a visual reminder of the medication being taken, which is extremely advantageous for AD patients (182). However, there are two major drawbacks associated with transdermal route; the fact that skin is one of the toughest barriers against drug absorption, and skin irritation and/or sensitization that may be associated with topically applied dedication. There have been several successful approaches to enhance the permeability of drugs through the skin including optimization of the drug delivery system using nanocarriers (183-185). Lipid based nanoparticles are of particular interest in transdermal and topical drug delivery applications as they are biocompatible, non-irritant, and have penetration enhancement capabilities (186). Lipid nano-carriers having a solid matrix (solid lipid nanoparticles (SLN) and nanostructure lipid carriers (NLC)) have gained wide popularity (187). They have been shown to markedly reduce skin irritation associated with the drug and/or vehicle(188-191). Additionally, they also enhance the stability of the active pharmaceutical ingredients (192). NLCs are considered as the second generation of the solid matrix lipid nano-carrier and were developed to overcome some of the shortcomings associated with SLN, specifically the potential expulsion of drug content upon lipid recrystallization (49). Although, lipid nano-carriers represent a perfect platform for formulating lipophilic drugs, successful

encapsulation of hydrophilic compounds was also reported (193, 194). In this chapter we explore the feasibility of developing NLCs for the transdermal delivery of DMF. Several methods of preparation were investigated with the aim of fabricating a stable NLC formulation that maintain the stability of the drug and help mitigate its irritation potential. The selected formulation was characterized for particle size, morphology, drug entrapment, release and skin deposition and permeation. Rhodamine B was used as a model compound mimicking the permeation profile and skin deposition of DMF, where Rhodamine B loaded NLCs were used to visualize the skin deposition of the probe using confocal microscopy. Finally, skin irritation potential was tested using 3D in vitro model, and stability of DMF NLCs was assessed at both RT and 4ºC for 60 days.

6.2. Material and Methods

6.2.1. Materials

Dimethyl fumarate (DMF), monomethyl fumarate (MMF), olive oil, castor oil, cotton seed oil, Rhodamine B, and tetraglycol (TG) were purchased from Sigma Chemical Co. (St. Louis, MO, USA). Tween 80 (T80), and phosphate-buffered saline tablets (PBS, pH 7.4) was purchased from Thermo Fisher Scientific Co. (Pittsburgh, PA, USA). Precirol AOT 5 (Glyceryl palmitostearate) (P-ATO 5), Transcutol P (Diethylene glycol monoethyl ether) (TC), Labrafac lipophile (Caprylic/Capric Triglyceride) (Lab), Lauroglycol™ FCC (Propylene glycol monolaurate (type I)) (FCC), caproyl 90 (propylene glycol monocaprylate) (Cap) were generous gifts from Gattefossé (Paramus, NJ). Kolliwax® GMS II (glyceryl monostearate) (GMS), Kollicream® 3C (cocoyl caprylocaprate), Kollicream® CP 15 (cetyl palmitate) (CP), Kolliwax® S Fine (stearic acid) (SA),

Cremophore EL (Polyoxyl castor oil) (CrEL) were generous gifts from BASF (Florham Park, NJ, USA). Oleic acid (OA) was a gift from Croda (Edison, NJ, USA). High-performance liquid chromatography (HPLC) grade water, methanol, ethyl acetate, chloroform, acetone, ethanol and acetonitrile were purchased from BDH VWR Analytical (Radnor, PA, USA). Dermatomed human cadaver skin was obtained from New York Firefighter Skin Bank (NY, USA). EpiDerm™ skin kit, EpiDerm™ culture medium, and MTT assay kit were purchased from MatTek Corporation (Ashland, MA).

6.2.2. Solubility screening

The solubility of DMF in different solid lipids, oils, and surfactants was investigated to determine the excipients that DMF has the maximum solubility in. Solid lipids included in the prescreening were glyceryl monostearate (GMS) (MP=54–64 °C), stearic acid (SA)(MP=57–65 °C), Precirol ATO 5 (P-ATO 5) (MP=50–60 °C), cetyl palmitate (CP) (MP=54 °C). Solubility testing in solid lipid was performed by weighing 2 g of each lipid in glass vials. The lipids were melted using a magnetic stirrer hot plate at 70 ºC, then pre-weighed amounts of DMF were added into each vial incrementally until no longer drug crystals disappeared. The vials were kept at room temperature to solidify and to observe visually any recrystallization of DMF. On the other hand, the solubility of DMF in some oils, solvents, and liquid surfactants were evaluated by adding excess of DMF into glass vials containing 5 ml of each of oleic acid (OA), Transcutol P (TC), Labrafac lipophile (Lab), Lauroglycol™ FCC (FCC), caproyl 90 (Cap), Kollicream® 3C (3C), tetraglycol (TG), isopropyl myristate, olive oil, cotton seed oil, Tween 20 and Tween 80 and stirred magnetically at 40º C for 48 hours. The samples were filtered using 0.45µm

PTFE syringe filters, diluted appropriately and analyzed using HPLC to determine the solubility of DMF.

6.2.3. Method of preparation of NLCs

Three different methods for the preparation of DMF NLCs were explored, high pressure homogenization (HPH), solvent-diffusion emulsification method (SDE), and microemulsion method.

6.2.3.1. High pressure homogenization

The first batch of DMF NLCs was prepared using HPH technique (54), where the molten lipid phase containing the solid lipid, oil, and the dissolved DMF at 70º C was added to the aqueous phase composed of aqueous solution of the surfactant at the same temperature. The phases were homogenized using IKA T25 Ultra-Turrax homogenizer (IKA, Staufen, Germany) operated at 16000 RPM for 5 minutes. The hot pre-emulsion was passed through an Avestin Emulsiflex C3 High Pressure Homogenizer (Avestin Inc., Ottawa, Canada) using the following parameters: Cycles 1 and 2 at a homogenization pressure of 1000 bars, cycles 3-5 at a homogenization pressure of 1500 bars and cycles 6-20 at a homogenization pressure of 2000 bars. At the end of the homogenization cycles, the sample was divided into two portions, one kept at room temperature and the other was refrigerated immediately.

6.2.3.2. Solvent -diffusion emulsification method

The solvent-diffusion method (195) involved the mutual saturation of the organic solvent, ethyl acetate, and water for HPLC in a separatory funnel for 15 minutes for

preparing the lipid and aqueous phases, respectively. The solid lipid, oil and DMF were dissolved in water saturated ethyl acetate. Water saturated with ethyl acetate was used to dissolve the surfactant. The organic and the aqueous phases were mixed at a ratio of 1:2 respectively and homogenized at 12000 rpm using IKA T25 Ultra-Turrax homogenizer (IKA, Staufen, Germany) for 10 minutes. 75 ml of water for HPLC was added to the emulsion to induce the diffusion of the organic solvent and precipitation of the lipid nanoparticles. The suspension then is passed through a High-Pressure Homogenizer to reduce the particle size of the NLCs. A blank and DMF loaded formulations were prepared.

6.2.3.3. Microemulsion method

6.2.3.3.1. The construction of pseudoternary phase diagram

The pseudoternary diagrams were constructed using water titration method to determine the microemulsion (ME) area (196). The selected solid lipids (P-ATO 5 or GMS) and oils (TC or TG) at 7:3 mixing ratio, respectively, were mixed with surfactant-cosurfactant mixture (S-Co mix) comprised of the surfactant and cosurfactant at either 1:1, or 2:1 mixing ratios. The lipid phase and S-Co mix were heated to 65-70 º C, about 5 degrees above the melting point of the solid lipid, and then mixed at ratios of 9:1 to 1:9. The mixtures were stirred magnetically and titrated dropwise with water at the same temperature until it became permanently turbid. The pseudoternary phase diagrams were plotted using the percentages of the three components of each tested mixture.

6.2.3.3.2. Preparation of DMF NLCs by microemulsion method

DMF NLCs were prepared using hot ME method (197), where the solid lipid, oil, surfactant mixture, and DMF were heated to 65º C and stirred magnetically until all DMF

dissolved. Then, water heated at the same temperature was added dropwise with stirring until the formation of the clear ME. The NLCs are obtained upon solidification of lipid through cooling the ME with continuous stirring. Blank NLCs and Rhodamine B loaded NLCs were prepared by the same method with the exclusion of DMF for the former and replacing it with the dye for the latter.

6.2.4. Particle size and morphology of NLCs

The particle size of the NLCs and polydispersity index PDI were measured for the developed NLCs by dynamic light scattering (DLS) using Delsa Nano™ C particle size analyzer (Beckman Coulter, CA, USA) at 25º C. The samples were diluted appropriately with deionized water. Measurements were obtained as an average of 50 readings and done at n=4 for each sample. The surface morphology of the selected NLCs formulation was examined using transmission electron microscopy JEM 100 CX TEM (JEOL Ltd, Japan). The selected formulation, diluted 10 times with water for HPLC, was dropped onto carbon coated copper grid and allowed to dry. Then, a drop of 2% phosphotungstic acid was applied and excess was removed carefully by blotting.

6.2.5. Entrapment efficiency and drug loading efficiency

The amount of drug encapsulated was calculated indirectly by measuring the amount of free drug and subtracting it from the total amount of drug used initially. The free DMF was determined using ultrafiltration-centrifugation method with Vivaspin 500 MWCO 10K Da (GE Healthcare, USA). An accurately weighed amount of the NLCs suspension was added into the centrifuge tubes and spun at 14k rpm for 30 min. The free drug in the filtrate was determined using HPLC. The total DMF loaded was determined by

lysing an accurately weighed samples of NLC dispersion using a solvent mixture of chloroform: methanol 1:1, the resulting solution was diluted appropriately with methanol and analyzed for DMF using HPLC. The entrapment efficiency (%EE) was calculated using the following equation:

$$\%EE = \frac{W_t - W_f}{W_t} \times 100$$

The drug loading efficiency (DL) was calculated using the following equation:

$$\%DL = \frac{W_t - W_f}{(W_t - W_f) + W_{Lipid}} \times 100$$

The drug recovery (DR) was calculated according to the following equation:

$$\%DR = \frac{W_t}{W_i} \times 100$$

Where, W_t, W_f, W_{lipid}, and W_i are the total weight of the drug in the formulation, weight of free drug, weight of the lipid in the formulation, and the initial amount of the drug added to the formulation, respectively.

6.2.6. Dimethyl fumarate quantification using HPLC

The HPLC system consisted of an Agilent 1100 Series Hewlett-Packard liquid chromatograph and the Agilent Chemstation software. The HPLC instrument was equipped with a UV detector (Agilent Dual Absorbance Detector G1315A), a pump (Agilent Quaternary pump G1311A), and an automatic injector (Agilent ALS G1313A Auto-samplers). A reversed-phase column (Luna C18, Phenomenex, 5 µm 250 x 4.6mm) was used as the stationary phase at ambient temperature. The mobile phase, 0.05M monobasic

sodium phosphate at pH 3.2: acetonitrile (65:35, v/v), was pumped at a flow rate of 1.0 mL/min, and the UV detector was set at a wavelength of 230nm.

6.2.7. In vitro drug release study

The release of DMF from selected formulations was studied using vertical Franz diffusion cells (Logan Instruments, Somerset, NJ) mounted with a semipermeable membrane with MWCO of 2K Da (Thermo Fisher Scientific Co. (Pittsburgh, PA, USA). 0.2 ml of NLC dispersions were applied into the donor chamber of the diffusion cell and the receptor medium was 5.0 mL phosphate buffer saline PBS (pH 7.4, 20 mM) maintained at 37°C using a heating block and stirred continuously at 600 rpm. At 2, 4, 6, 8, 10, 18, 20, and 24 hours, 0.3 ml samples were withdrawn and replenished by an equal volume of fresh receptor medium. The samples were analyzed using HPLC to determine the amount of DMF released. The experiment was performed as triplicates. The cumulative percent of DMF released per unit of surface area was plotted against time and fitted to several models including, Higuchi equation, first order, and zero order equations to obtain the best fit model (198) and regression analysis was performed.

6.2.8. In vitro skin permeation study

The in vitro skin permeation study was conducted using vertical Franz diffusion cells (Logan Instruments, Somerset, NJ) mounted with dermatomed human cadaver skin harvested from the posterior torso of a 64 years male donor (New York Firefighter Skin Bank, NY, USA). The skin was kept at -80º C until the time of the study, when it was cut into square pieces of about 2 cm and thawed by soaking in PBS at room temperature for 20 min. Each skin piece was clamped between the donor and receptor compartments, with

the stratum corneum facing upward toward the donor that had a diffusion area of 0.64 cm^2. The donor compartment was filled with 0.2 mL of the selected NLCs formulation, which has been cleared of free drug immediately prior to the permeation study by packing in a Slide-A-Lyzer™ Dialysis Cassettes 2K MWCO (Thermo Scientific Pierce Protein Biology, Rockford, lL, USA) immersed in 200 ml DI for 2 hours (199). In addition, the permeation of saturated suspension of DMF in PBS was run a control. The receptor compartments were filled with 5.0 mL PBS (pH 7.4, 20mM), as the receptor medium, which was maintained at 37°C using a heating block and stirred continuously at 600 rpm. Samples of 0.3 ml were withdrawn from the receptor compartment at predetermined time points (2, 4, 6, 8, 10, 18, 20, and 24 h) and replaced immediately with an equal volume of PBS (pH 7.4, 20mM). Samples withdrawn were analyzed using HPLC to determine the normalized DMF concentration. All experiments were performed with five replicates.

At the end of the permeation study, the donor compartment along with the formulation were removed. The surface of the skin was carefully cleaned off any formulation traces by washing with a known volume of the extracting solution and then carefully wiping off the surface with 3-4 Q-tips soaked with the same solvent. The skin was removed off the receptor compartment, cut around the diffusional area, air dried and accurately weighed. The dry skin was then cut into small pieces and homogenized with 1 ml methanol in BeadBug™ (Benchmark Scientific, Edison, NJ) microtube homogenizer for a total of 9 minutes (3 cycles of 3 minutes each). The skin samples were kept for 24 hours at 37° C to ensure complete drug extraction and were centrifuged at 12000 rpm for 5 min and were filtered through a 0.45 µm polypropylene syringeless filters before HPLC

analysis. The DMF skin content was expressed as the average weight of DMF in ng per skin weight in mg of five replicates.

6.2.9. Confocal microscopy

The biodistribution of Rhodamine B dye encapsulated in NLC was used to visualize the penetration of the dye in an effort to simulate DMF permeation. Dermatomed cadaver human skin samples of a 59 years Caucasian male donor posterior torso were obtained from New York Firefighters Skin Bank (New York, NY). Vertical Franz diffusion cells with application surface area of 0.64 cm^2 (Logan Instruments, Somerset, NJ) were used for this study. 0.2 ml Rhodamine B loaded NLCs suspension was applied on the skin for 1, and 24 h. At the end of the permeation study, excess formulation was removed from the skin, the surface was rinsed with deionized water and dried with a cotton swab, cut into smaller pieces frozen with liquid nitrogen and were stored at -80°C until use. The cut pieces were embedded in Optimal Cutting Temperature (OCT) medium filled molds and frozen with the aid of dry ice. Vertical cross-sections (20 μm) of the skin were prepared with a cryostat (Leica CM1850 Cryostat, Buffalo Grove, IL), which were collected on glass slides. The samples were then subjected to fluorescent and phase-contrast microscopy (Zeiss LSM 780, Jena, Germany) to visualize the disposition of the dye.

6.2.10. In vitro skin irritation test

The skin irritation potential of DMF NLCs was tested using the EpiDerm Skin Irritation test (EpiDerm SIT), which utilizes a three-dimensional (3D) *in vitro* reconstructed human epidermal (RHE) model. The test was conducted as per the manufacturer validated protocol

corresponding to a 4-day procedure started by conditioning the tissue received (Day 0) and incubation in a 6-well plate with 0.9 ml assay medium (EPI-100-ASY, MatTek) at 37 ± 1° C, 5 ± 1% CO_2, 95 % RH. On Day 1, the tissues were exposed to the test (DMF NLCs) and blank NLCs, negative control (Dulbecco's Phosphate-Buffered Saline [DPBS]), and positive control (5% sodium dodecyl sulfate [SDS]) all in triplicates for 60 min, rinsed thoroughly according to protocol and incubated for 24 hr. The media were collected on Day 2 and stored at -20° C for cytokine analysis, and the tissues were incubated in fresh media for another 18 h for MTT (3-(4,5-Dimethylthiazol-2-yl)-2,5-diphenyltetrazolium bromide) test. Skin irritation is evaluated through measuring the cells viability and inflammatory cytokine, IL-1α, released into the media. Cells viability was tested using the MTT assay. Tissue inserts were placed in 24-well plate prefilled with 0.3ml of MTT solution provided with the EpiDerm kit and incubated for 3 h at 37 ± 1° C, 5 ± 1% CO_2, 95 % RH. Then, the inserts were washed and transferred into another 24-well plate prefilled with 2 ml of extracting solvent, isopropyl alcohol, per well, sealed and shaken on a plate shaker for 2 hours at room temperature. The optical density (OD) of the extract was measured at 570 nm and the percent tissue viability was calculated using the following equation:

$$\%Viability = \frac{OD_{sample}}{OD_{negative\ control}} \times 100$$

IL-1α released into the medium due to tissue irritation was quantified using ELISA kit Quantikine® ELISA human IL-1α/IL-1F1 from Bio-techne (Minneapolis, MN). The manufacturer protocol was followed to perform the test and the OD of samples were measured at 450 nm using a microplate reader (TECAN, Morrisville, NC). The

concentration of IL-1α was determined against a standard calibration curve and any concentration above the cut-off point of 50 pg/ml was considered to be associated with skin cell irritation.

6.2.11. Stability

The stability of the selected DMF NLCs dispersion was monitored for 60 days at room temperature (RT) and 4°C. The stability testing included the determination of total DMF content at specified time intervals and visual inspection appearance of crystals, separation, and precipitation. All reported data were the mean of three separate measurements.

6.2.12. Data analysis

The individual permeation profile of each formulation was obtained by plotting the cumulative amounts of DMF permeated per skin unit area versus time. The flux (*J*) represents the slope of the linear portion of the plot. The lag time is equal to the x-axis intercept of the extrapolated linear portion of the permeation profile. All data are expressed as mean± standard deviation of four replicates. ANOVA and Student's t-test were used to test the level of significance. Results were considered statistically significant at p-value < 0.05.

6.3. Results and discussion

6.3.1. Solubility screening

There is a wide range of lipid selections for the formulation of NLCs, such as mono, di or triglycerides, waxes, fatty acids, etc. (54). However, there are some general and some

specific requirements that must be considered when choosing the right excipients. Generally, the lipid blends must be non-toxic, non-irritant and/or skin sensitizing and approved by the FDA a generally recognized as safe (GRAS) material. In addition, the drug solubility in the lipid plays a very crucial role in the selection, as it influences the drug loading, and encapsulation pattern (drug concentrated core, drug concentrated shell, or homogenous drug matrix) ultimately affecting the release profile of the drug (196, 200). In our study, solid lipids were chosen for prescreening based on their lower melting points to avoid high temperatures that can affect the stability of DMF. DMF solubility in SA and CP was about 1.5% w/w and more than 2% w/w in GMS and P-ATO5. Upon cooling and solidification, DMF crystals were observed from SA and CP solid solutions implicating low drug solubility. Therefore they were not selected for further formulation, as drug low solubility in the lipid matrix can adversely affect the drug loading (201). Since P-ATO 5 and GSM solid solutions with DMF did not show any visual crystallization of DMF and had higher DMF solubility, they were selected for formulating the NLCs. The solubility of DMF in different oils, surfactants, and cosolvents was also investigated. Based on the results of the solubility study shown in Figure 6.1, Lab, TC, TG, CH-LE, Tween 80 were selected for preliminary formulation of DMF NLCs using different methods of preparation.

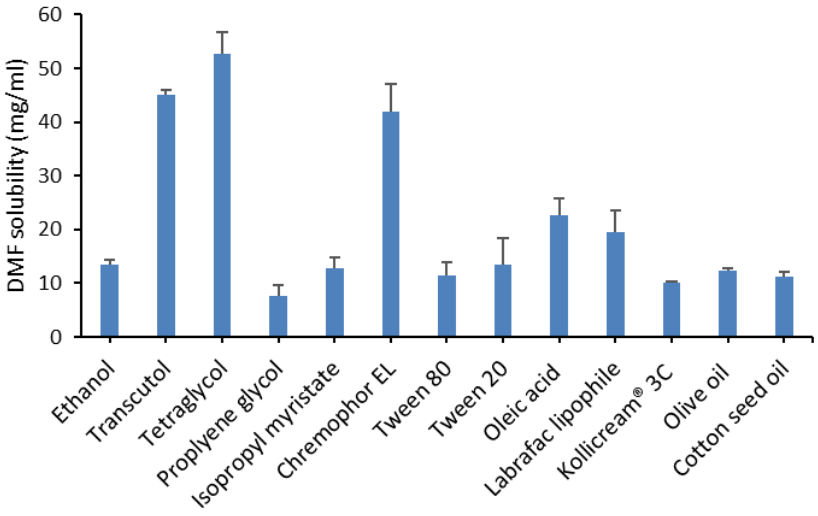

Figure 6.1. Solubility of dimethyl fumarate in various solvents, oils, and surfactants at 40º C (n=2-3).

6.3.2. Preparation and characterization of NLCs

There are several methods reported in the literature for the preparation of NLC, such as high pressure homogenization (HPH) method, high shear homogenization-ultrasonification method, solvent emulsification-evaporation method, microemulsion method, emulsification-solvent diffusion, etc. (202). First, we investigated the suitability of hot HPH to produce DMF NLC, as it is the most widely used method, and easily scalable (203). DMF NLCs were prepared with GSM as solid lipid, oleic acid as the oil at a ratio of 7:3 and the percentage of total lipid used at 5%w/w and 10%w/w, Tween 80 was used as an emulsifier at 2%w/w and 4% w/w. First, four different blank NLC were prepared, then NLC formulation loaded with DMF at 1%w/w of total lipid was produced. The characteristics of preliminary NLCs prepared by HPH are listed in Table 6.1.

Table 6.1: Particle size, polydispersity index and drug content blank and DMF loaded NLC prepared by HPH and kept at room temperature.

Formula	Total lipid %w/w	SL:LL[a]	Tween 80 %w/w	Particle size (nm)		PDI		%Drug recovery
				Day1	Week1	Day1	Week1	
#1 blank	5	7:3	2	185	475.2	0.304	0.215	_
#2 blank	5	7:3	4	431*	672.4	0.316	0.296	_
#3 blank	10	7:3	2	279	437	0.327	0.206	_
# 4 blank	10	7:3	4	447*	698.3	0.31	0.288	_
#1 loaded	5	7:3	2	411	312	0.327	0.239	50%

[a] SL, solid lipid; LL, liquid lipid; PDI, polydispersity index.
* Processed in HPH as 10 cycles, 5 cycles at 500 bar and 5 cycles at 1000 bar.

The results showed that formulation #1 with 5%w/w total lipid and 2% Tween 80 had the smallest particle size, therefore we chose it to investigate the feasibility of loading with DMF. Formula #1 loaded DMF NLC had significantly larger particle size than the #1 blank counterpart at day one. However, loaded NLC showed reduced particle size and a lower PDI after a week unlike blank NLCs, which grew larger. The reduction in particle size may be due to the release of surface bound drug (204). When NLCs were assayed for DMF content, only 50% of the initial loading amount was recovered. To further investigate the possible causes, we tested the pre-emulsion prior to processing through HPH and total DMF recovered was 96%±4. DMF tends to sublime (205) and might have escaped from the formulation during processing through the hot HPH due to excessive heat required to prevent the molten lipid from solidifying and clogging the instrument tubing. Hence, hot HPH would not be a suitable method for producing DMF NLC. Since, HPH can also be

used to reduce the particle size of suspension R, we anticipated that if we prepared a course nano-micro-suspension of the lipid particles in a way that avoids the use of excessive heat, we might be able to reduce the particle size by passing through HPH. So, we used another method, solvent diffusion method (SDM) to prepare DMF NLC. This method involves emulsifying the drug using a partially water miscible no toxic solvent, which then diffuses into the external water phase leaving the lipid containing the dissolved/dispersed drug molecules droplets to solidify (206). First, we investigated the feasibility of SD by preparing blank formulation. Formula #1 blank as shown in Table 6.1 was replicated using SDM and was tested for particle size before and after processing through HPH. Processing the #1 blank suspension produced by SDM through HPH resulted in particle size reduction from 580.0±95.1nm to 133.1±4.9 nm and 108.5±4.8 nm after 10 and 15 cycles, respectively. Next, the same formula loaded with DMF was prepared using SDM and passed through HPH to reduce the particle size. Similarly, The DMF loaded formulation prepared with SDM had less than 50% drug recovery. To verify the cause of low drug content, the formulation was assayed for DMF before processing through HPH, and the results showed that after 24 hours, DMF total content recovered dropped from 99.7% to 63%, which indicated that DMF was not loaded and majorly present in the aqueous external phase, where it can easily escape. Similarly, Hu et al. reported a very low clobetasol propionate drug recovery and loading in solid lipid nanoparticles (SLN) prepared by SDM (207). Therefore, SDM was not suitable to encapsulate DMF. Since, both hot HPH and SDM were not successful no further studies were performed on their products and were not included in further results and discussions. Finally, we explored hot microemulsion method to produce NLC. First, pseudoternary phase diagrams were constructed to

determine the concentrations of the components comprising the microemulsion boundaries. Phase diagrams with various components mixing ratios were depicted in Figures. 6.2-6.4, which represent the following systems: a lipid phase (P-ATO5: Lab 7:3) and S-mix (CrEL:TC 1:1), a lipid phase (GMS: Lab 7:3) and S-mix (CrEL: TC 2:1), and a lipid phase (P-ATO5: OA 7:3) and S-mix (CrEL: TG 2:1), respectively. The clear ME regions were represented in the ternary diagrams as shaded areas. The phase diagram study showed that the first system investigated had a limited ME region Figure 6.2, and that increasing the ratio of the surfactant to co-surfactant to 2:1 caused a dramatic increase in ME area. Therefore, the two systems made with S-mix ratio of 2:1 were further investigated by selecting a prototype formulation of each system and preliminary testing for drug recovery to confirm the suitability of the formulation before further investigation.

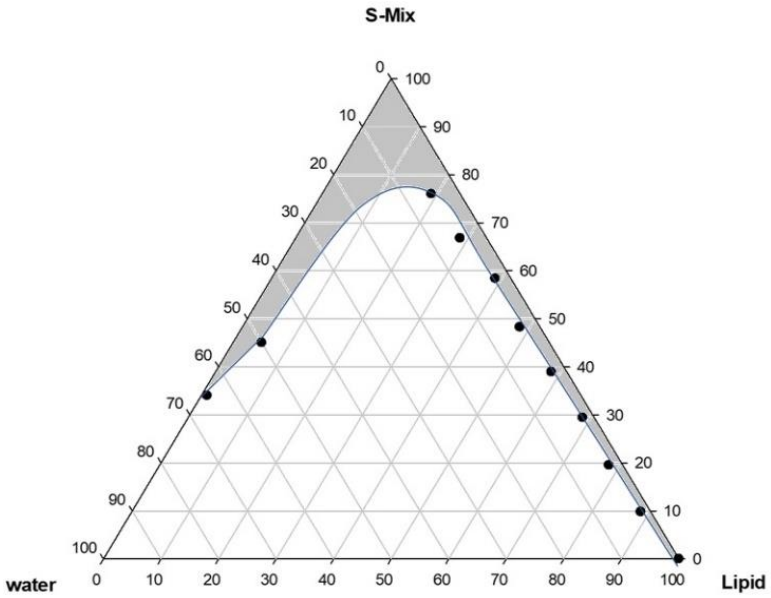

Figure 6.2. Pseudoternary phase diagram showing the microemulsion (shaded area) of Precirole ATO 5: Labrafac (Lipid), Surfactant: cosurfactant (Cremophor EL:Transcutol 1:1).

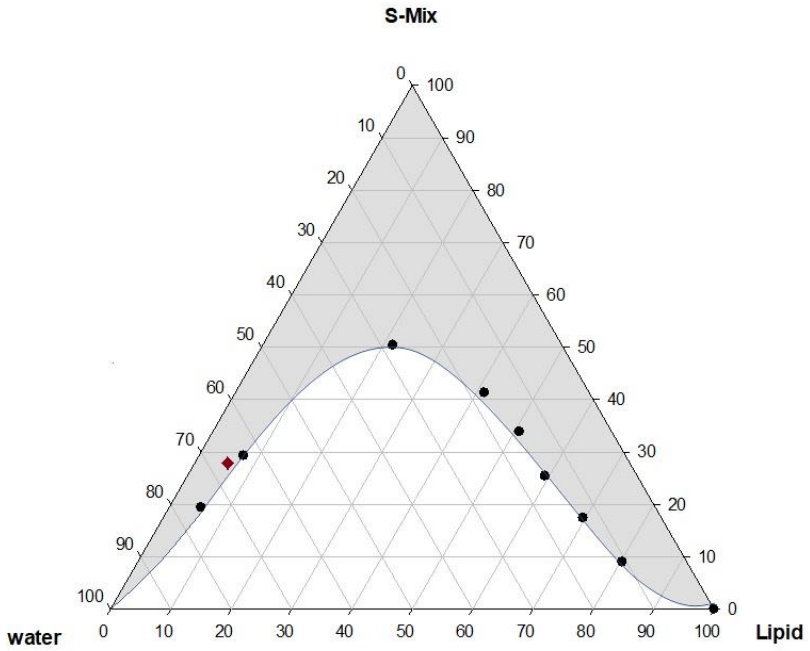

Figure 6.3. Pseudoternary phase diagram showing the microemulsion (shaded area) of GMS: Labrafac (Lipid), Surfactant: cosurfactant (Cremophor EL:Transcutol 2:1). The diamond represents the concentrations of the components of the tested formulation.

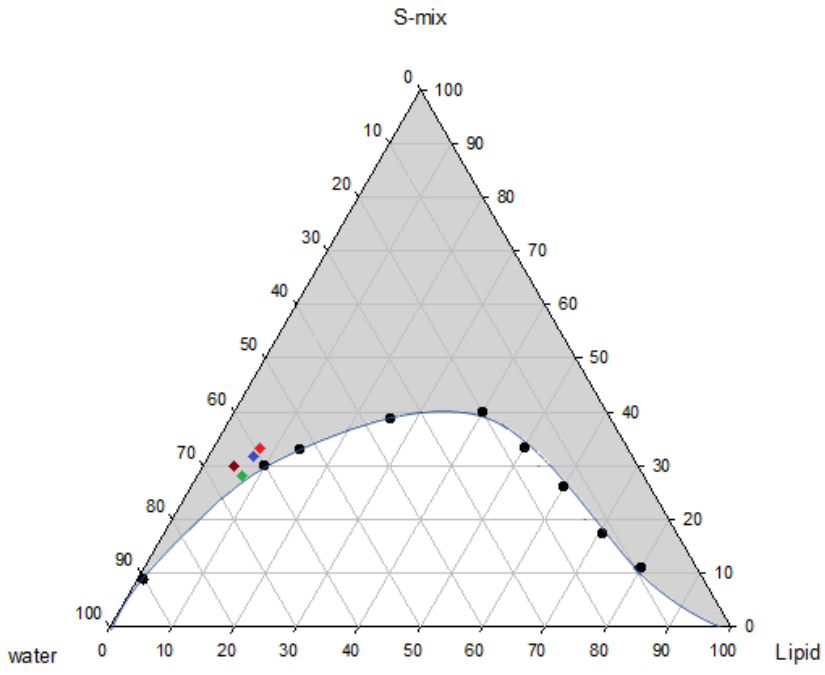

Figure 6.4: Pseudoternary phase diagram showing the microemulsion (shaded area) of Precirole ATO 5: Oleic acid (Lipid), Surfactant: cosurfactant (Cremophor EL:Tetraglycol 2:1). The diamonds represent the concentrations of the components of the tested formulations.

Table 6.2. Composition, particle size, polydispersity index, drug recovery and %EE of DMF NLC prepared by hot microemulsion method.

Formula	Total lipid Composition and %w/w	S-mix Composition and %w/w	Particle size (nm) ±SD*	PDI ±SD*	Drug recovery ±SD*	%EE ±SD*
NLC-G 5%	GMS/Lab 5%	CrEL/ TC 27%	110.2±2.0	0.33±0.01	43.2±1.3	12.2±0.8
NLC-P 5%	P-ATO5/ OA 5%	CrEL/ TG 30%	141.3±2.3	0.15±0.01	96.1±4.6	90.5±8.3
NLC-P 5.2%	P-ATO 5/ OA 5.2%	CrEL/ TG 31.2%	93.5±3.5	0.29±0.01	70.1±3.5	65.4±2.1
NLC-P 6.7%	P-ATO 5/ OA 6.7%	CrEL/ TG 26.6%	174.3±4.9	0.30±0.01	95.5±6.4	63.2±4.5
NLC-P 7.5%	P-ATO 5/ OA 7.5%	CrEL/ TG 33.3%	146.5±2.3	0.30±0.00	65.2±2.3	81.8±1.2

*Standard deviation of the means, n=3-4.

The NLC formulations prepared by microemulsion method were screened for particle size, PDI, DMF recovery, and %EE to narrow down to the best performing formulation, and the results were shown in table 6.2. The main focus was on formulations t56hat exhibited high DMF recovery. All formulations were tested for % DMF recovery. Formula NLC-G 5% was made with GMS as solid lipid had the lowest DMF recovery. On the other hand, NLC-P5% made with P-ATO5 showed very promising results, therefore we tested 3 more different combinations of that system. Although lower than that of NLC-P5%, the rest of the tested formulations had better DMF recovery percentage than NLC-G 5%. The process of ME involved heating the lipids 5 degrees above their melting point. Since GMS

meting point is 58-61ºC and P-ATO 5 melting point is 53-56º C, ME produced with GMS was heated more than the ones prepared with P-ATO 5. Exposing DMF to a higher temperature may have increased the instability of the drug and ultimately resulted in a lower recovery. Further, it seems that P-ATO 5 may play a role in providing stability to DMF formulations manifested by higher recovery of DMF and better % EE. In addition, NLC-G 5% had a very low %EE of 12%. Therefore, GMS containing formulations were excluded from further investigation due to both low DMF recovery and entrapment efficiency. For NLC-P formulations, it seemed that there was no correlation between the amounts of total lipid and surfactant/co-surfactant and the nanoparticles characteristics. NLC-P 5.2% had a significantly lower particle size ($p < 0.05$). On the other hand, NLC-P 6.7% had a significantly larger particle size ($p < 0.05$). Formula NLC-P 5.2% had about 70% drug recovery at the day of preparation. However, upon further determination of total DMF within the first week, it was shown that the DMF % recovered decreased to 67% on day 2 and 60% on day 5. The reduction of total DMF content for NLC-P 5.2% could be explained by possible expulsion of the drug from the NLC into the aqueous dispersion medium in which the nano-carriers were suspended and subsequent volatilization. Formula NLC-P 6.7%, on the other hand showed a very low % EE compared with the other formulation. Finally, formula NLC-P 5% exhibited maximum drug recovery and % EE among the investigated formulas and a calculated % DL of 16.2%±0.3 and was further investigate. TEM imaging showed the morphology of the NLCs to be mostly spherical to oval with a particle size dramatically smaller than the values obtained with the DLS. These results were expected and could be attributed to the fact that for TEM the particles were being measured in their solid state whereas in DLS, the hydrodynamic diameter of the

NLCs is being measured (208) and these results are in agreement with published literature (209, 210).

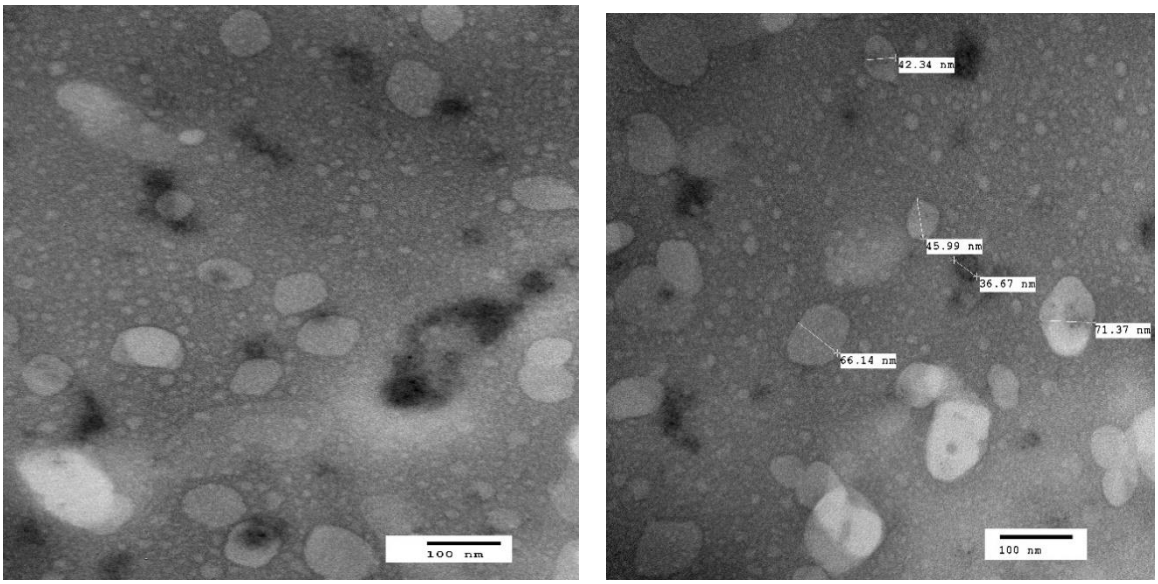

Figure 6.5. Transmission electron micrographs of dimethyl fumarate loaded NLC (formula NLC-P 5%)

6.3.3. In vitro drug release study

In vitro release profile of DMF from NLC-P 5% and NLC-P 7.5% is shown in Figure 6.6. Both formulations had a biphasic release profile. A faster initial phase (burst) due to the release of surface entrapped DMF, then followed by a slower sustained release phase due to the diffusion of core entrapped drug molecules. This release profile has been previously reported with lipid nanoparticles (211-213). DMF exhibited a faster release from formulations containing 5% total lipid than 7.5%, where 50% of DMF was released at 6 and 8 hours, respectively. However, later part of release profiles from both formulations were superimposed. The slower release could be attributed to the lower DMF

loading in NLC-P 7.5%. Also, higher lipid content would result in slower diffusion due to increased matrix viscosity according to Stokes–Einstein law (214).

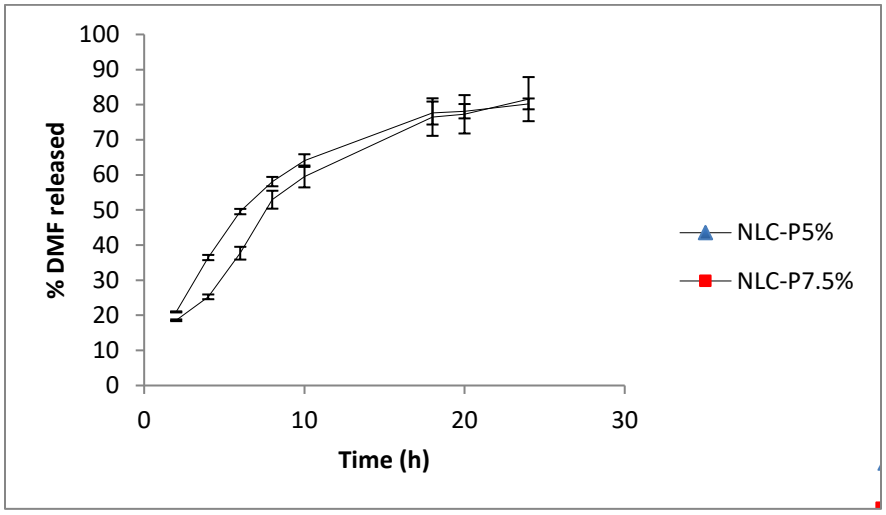

Figure 6.6. In vitro dimethyl fumarate release profile from NLC-P 5% and NLC-P 7.5% total lipid. Data points represent means ±S.D. (n=3).

The release data of DMF from NLC-P 5% were fitted to different kinetic models and linear regression coefficient R^2 values were used to determine the goodness of fit of the respective models. The release parameters listed in Table. 6.3, showed that Fickian diffusion model (Higuchi) was the best to describe the kinetics of DMF release from the NLC formulation.

Table 6.3. Different release kinetic models which describe release s of dimethyl fumarate from NLC-P 5% (n=3).

Model	Equation [a]	K	R^{2} [b]
Zero order	$Q_t = Q_0 + Kt$	6.2 µg/cm²/h	0.984
First order	$logQ_t = logQ_0 + \frac{Kt}{2.303}$	0.073 h^{-1}	0.935

Higuchi	$Q_t = K_H\sqrt{t}$	26.6 µg/cm²/h½	0.998

[a] Q_t, amount released at time t; Q_0, amount at time 0; K, release rate constant; t, time.
[b] R^2, linearity coefficient.

6.3.5. In vitro skin permeation study

The permeation profiles of DMF from NLC-P 5% and control formulation shown in figure 6.7 reveals a dramatically higher amount of DMF permeated through human cadaver skin from the NLC-P 5% dispersion compared to control. The permeation parameters of DMF through human cadaver skin are listed in Table 6.4. These results denote an extremely statistically significant difference between the tested formulation and control ($p < 0.05$). NLC-P5% formulation provided a 2.6-fold increase in flux over control. Formulating DMF as NLC has significantly improved the drug permeability through human cadaver skin and reduced the lag time ($p < 0.05$).

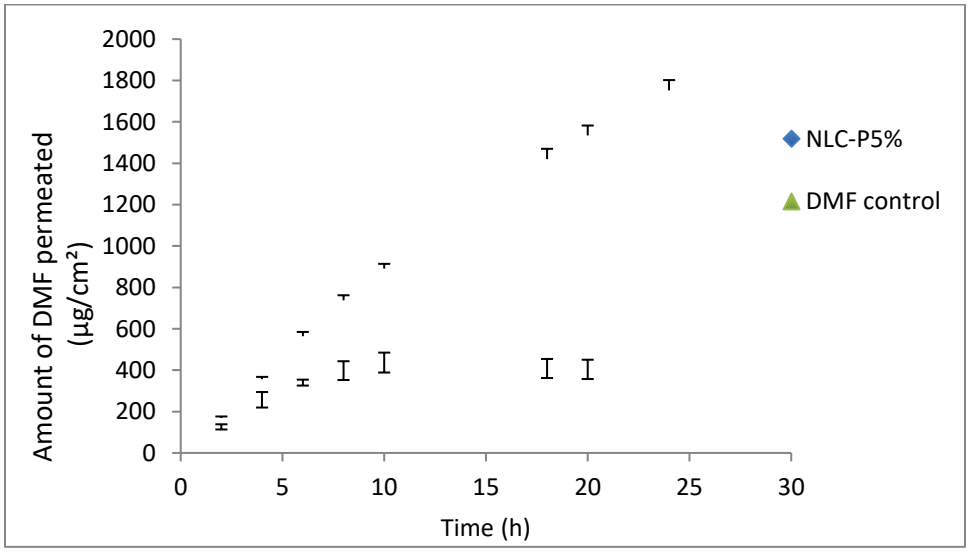

Figure 6.7. In vitro skin permeation profile of dimethyl fumarate (DMF) from the selected DMF loaded nanostructured lipid carriers in comparison with a suspension of DMF through human cadaver skin. Data represent means ±S.D. (n=4-5).

Lipid nanoparticle have an established record of skin penetration enhancement (51). Lombardi Borgia et al. found that NLCs loaded with Red Nile dye were able to enhance its penetration through pig skin by 3-fold compared with a cream formulation (215). Elmowafy et al. also found that NLCs loaded dapsone have enhanced the permeation of the drug compared with dapsone hydroalcoholic solution. They attributed the results to the possibility of repulsion occurring between the negatively charged NLCs and the SC proteins creating channels that facilitate the permeation of the particle (213).

Table 6.4. Permeation parameters of DMF from selected nanostructured lipid carrier formulation and control.

Formulation	Flux (µg/cm²/h)	Permeability coefficient x10⁻² (cm/h)	Lag time (h)	Q_{24} (µg/cm²)[a]
NLC-P5%	92.4±1.6*	4.1±0.1*	0.1±0.0*	1752.3±49.7*
Control	35.25±3.3	1.2±0.2	2.1±0.2	401.1±29.6

[a] Q_{24}, the amount permeated per unit area.
* Statistically significant from control ($p < 0.05$).

There are several proposed mechanisms that could explain the penetration enhancement action of NLCs, due to their small particle size they have a large exposed surface area available to interact with skin surface forming weal bods such as Van der Waals forces. Eventually forming a thin film on top of the skin, which can also act as an occlusive layer preventing water loss and increasing the SC hydration level favoring the penetration enhancement of the API (52). In addition, NLCs lipid could potentially interact with the skin lipids altering its packing and affecting the drug deposition within the skin layers

(216). The significant enhancement of DMF permeation from NLCs could be due to a combined effect of several mechanism. They carried a negative charge, although very low, with zeta potential of -5.5mv. This may affect the protein structures of the skin. Furthermore, NLCs may erode releasing its matrix contents including oleic acid, which is a well-known and widely used penetration enhancer(217). Oleic acid acts by sequestering in between the lipid layers disrupting the packing of the molecules (44).

In our results, we presume the possibility of oleic acid release from the NLC fluidizing the lipids of the SC and subsequently enhancing the diffusivity of DMF, which may explain the high DMF skin content compared to control as shown in Figure 6.8.

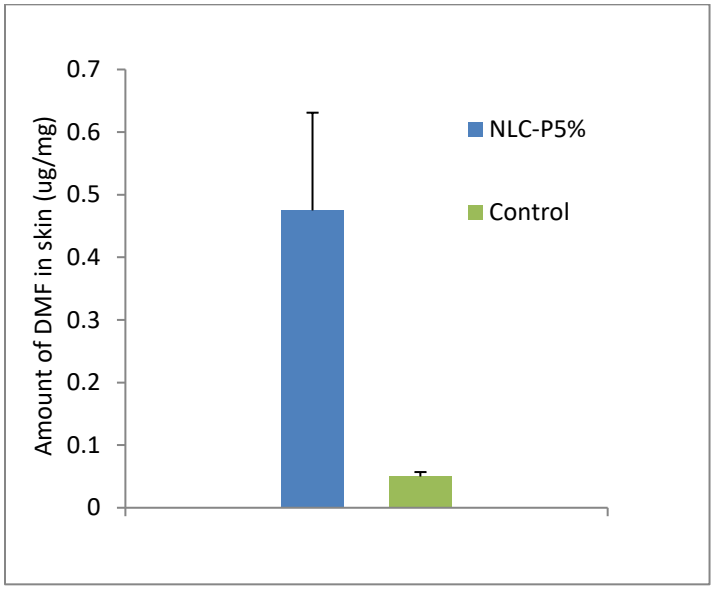

Figure 6.8. Dimethyl fumarate skin content from NLC-P 5% and DMF control after 24 hours. Each value represents the mean ±S.D. (n=4-5).

6.3.6. Confocal microscopy

Confocal microscopy was utilized to visualize the skin deposition of Rhodamine B -NLC through dermatomed human cadaver skin. The results are illustrated in Figure 6.9.

Rhodamine was selected as a probe to simulate DMF based on published data (218). The images were analyzed using Fiji (version 1.52, NIH, Bethesda, MD, USA) an open source software for biological image analysis (219), which enabled us to assess the permeation of the probe semi-quantitatively. Figure 6.9 shows the intensity of the dye permeated at 1 hour and 24 hours appearing as a very dark shade (black color). A rectangular portion of 300 µm depth along the skin image starting at the epidermis edge was selected and analyzed for pixel color intensity. The data is plotted as a X, Y scatter image, where x-axis representing the horizontal distance across the selected area that is equivalent to the

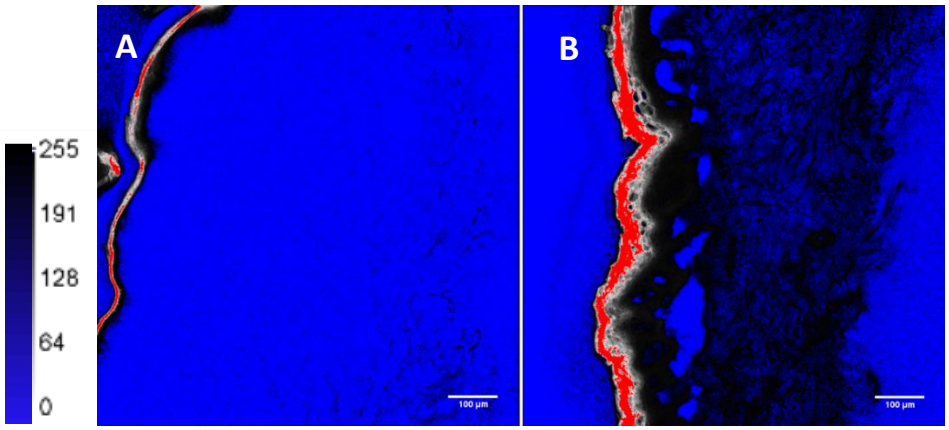

Figure 6.9. Confocal microscope images showing the penetration of Rhodamine B from NLCs and its deposition within dermatomed human cadaver skin 1 h (A) and 24 h (B) after application of the formulation

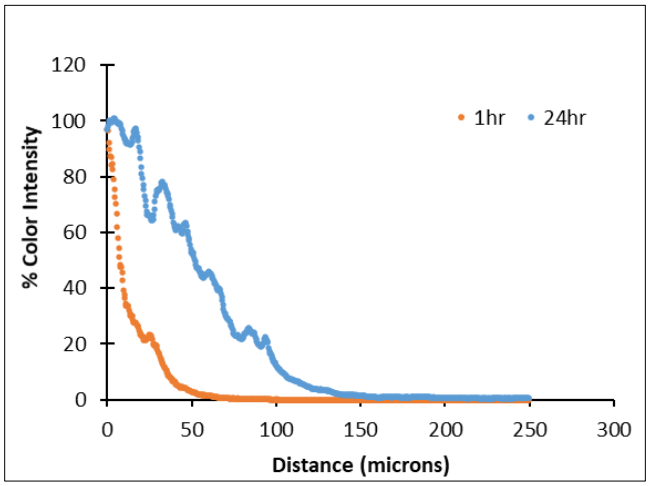

Figure 6.10. Percent color intensity vs. distance of NLC loaded Rhodamine after 1, and 24 hours permeation through human cadaver skin.

thickness of the skin, and the y-axis representing the average percent of the vertical pixel intensity as depicted in Figure 6.10. This figure clearly shows that the relative percent intensity of color has increased over the course of permeation, and with depth of the skin. The results of the confocal microscopic imaging support the effectiveness of NLC for the potential transdermal delivery of actives. However, due to difference in log p and molecular weight between DMF and Rhodamine B, the probe may not provide an accurate prediction of DMF permeation behavior.

6.3.7. In vitro skin irritation test

The skin irritation potential of the developed DMF NLCs (NLC-P 5%) was tested using Epiderm™ Skin Irritation Test (SIT), which is considered to be an acceptable replacement to in vivo rabbit skin irritation test (220, 221). The results of MTT assay performed on Epiderm™ treated with dispersions of DMF loaded and blank NLC to detect cell viability shown in Figure 6.11. indicate that DMF-NLC are considered to be non-irritant according

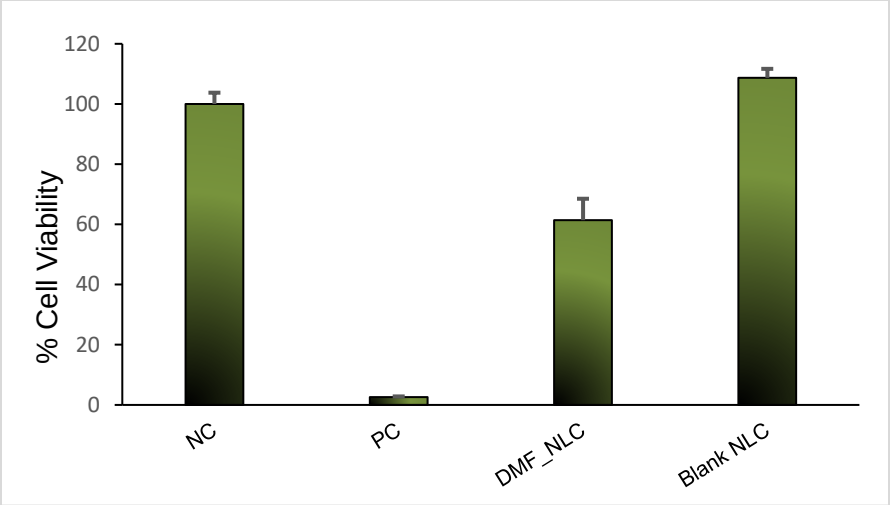

Figure 6.11. Percentage tissue viability of EpiDerm™, treated with DMF loaded NLC and blank NLC, positive control; PC, and negative control; NC obtained from MTT assay. Data are shown as means ± S.D.

to Epiderm™ protocol's result interpretation, which states that a reduction in cell viability of more than 50% is an indication of skin irritation (222). The property of nanoparticles to provide controlled release of encapsulated active molecule may be responsible for reducing the skin irritation. Researchers have reported that retinoic acid, which skin irritation is well documented, loaded in solid lipid nanoparticles was significantly less irritant than commercially available gels and creams (190, 191). Figure 6.12 Shows the average IL-1α from EpiDerm™ tissue insets treated with DMF loaded NLC and blank NLC, positive control, and negative control obtained from ELISA assay. The average amount of IL-1α released by the tissue inserts treated with DMF NLC was 61.4±16.8 pg/ml was significantly lower than that of the positive control ($p < 0.05$). However, it was higher than the cut off value of 50 pg/ml. Values greater than 50 pg/ml may be associated with some skin irritation reactions in sensitive patients (16).

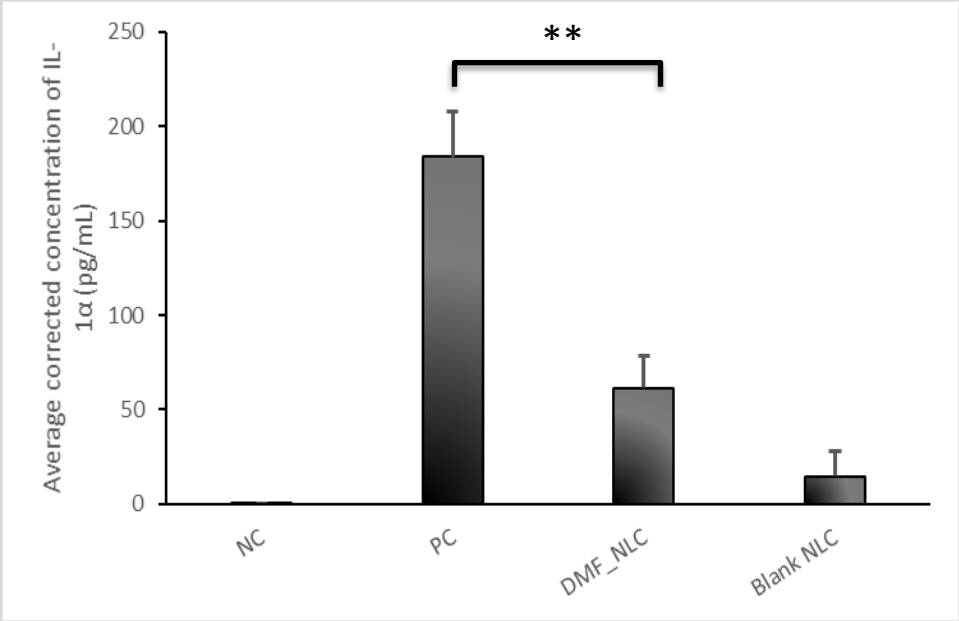

Figure 6.12. Release of IL-1α from EpiDerm™ treated with DMF loaded NLC and blank NLC, positive control; PC, and negative control; NC obtained from ELISA assay. Data are shown as means ± S.D. ($p < 0.05$).

5.3.8. Stability

The encapsulation of DMF aimed to stabilize the drug against sublimation and reduce its skin irritation potential. We observed during the earlier formulation development stages of DMF NLCs that free DMF would be escaping from the NLCs aqueous dispersion at a very fast rate. This observation was confirmed by the close monitoring of drug recovery of the prepared formulations, where formulations that had low %EE would exhibit a fast decrease in total DMF content within few days. So, we anticipate that a stable formula would continue to have a constantly high total DMF content. Following the 60 days storage of DMF NLC-P5% at 4º C and RT, it was found that DMF recovery was at 96.8%±7.4 and 72.4%±2.0 for formulations stored at 4º C and RT, respectively. The short-term stability results indicate that formulating DMF as NLC was a successful approach to maintain the stability of DMF and drug load. Further, storing the NLC dispersion at RT showed a

significant reduction in total DMF remaining compared to storing at 4º C ($p < 0.05$) signifying that storage temperature is a crucial factor in the formulation stability. These results could be attributed to the reduction in %EE associated with higher temperature, where free DMF may easily escape the dispersion. Das et al also reported a decrease in %EE and %DL of clotrimazole loaded NLCs at elevated temperatures (186). RT samples did not show any change to their appearance over the course of the study. Samples stored at 4º C, on the other hand, started to show some separation and appearance of clearer supernatant. However, upon shaking the sample turned back into a homogenous translucent dispersion without any visible particles or crystals.

6.4. Conclusions

The transdermal route represents a promising alternative to deliver drugs for treating neurodegenerative diseases. In the present study we were able to develop nanostructure lipid carriers loaded with DMF using microemulsion method. The developed NLCs were found to have a good %EE of 90.5% and %DL of 16.2%, and good stability. Our results emphasized that the choice of the components of the NLCs plays a governing role in determining the characteristics of the resultant nanoparticles. Furthermore, the selection of the method of preparation greatly depends on the drug stability profile. The NLCs permeation results showed their potential to deliver DMF transdermally with reduced irritation potential. Next step will be incorporating DMF into a polymeric film to produce transdermal patches through a full factorial design of experiment, which takes into account the effect of using different polymers, the concertation of the polymer, plasticizer,

incorporation of penetration enhancers, and NLCs load on the characteristics of the film and DMF flux.

References

1. Gitler AD, Dhillon P, Shorter J. Neurodegenerative disease: models, mechanisms, and a new hope. Dis Model Mech. 2017;10(5):499-502.
2. Liu Z, Zhou T, Ziegler AC, Dimitrion P, Zuo L. Oxidative Stress in Neurodegenerative Diseases: From Molecular Mechanisms to Clinical Applications. Oxidative medicine and cellular longevity. 2017;2017:2525967-.
3. Dugger BN, Dickson DW. Pathology of Neurodegenerative Diseases. Cold Spring Harb Perspect Biol. 2017;9(7):a028035.
4. Zahodne LB, Ornstein K, Cosentino S, Devanand DP, Stern Y. Longitudinal Relationships Between Alzheimer Disease Progression and Psychosis, Depressed Mood, and Agitation/Aggression. The American Journal of Geriatric Psychiatry. 2015;23(2):130-40.
5. Meraz-Ríos MA, Franco-Bocanegra D, Toral Rios D, Campos-Peña V. Early onset Alzheimer's disease and oxidative stress. Oxidative medicine and cellular longevity. 2014;2014.
6. Ghasemi N, Razavi S, Nikzad E. Multiple Sclerosis: Pathogenesis, Symptoms, Diagnoses and Cell-Based Therapy. Cell J. 2017;19(1):1-10.
7. Pappalardo JL, Hafler DA. Multiple sclerosis enters a grey area. Nature Publishing Group; 2019.
8. Goldenberg MM. Multiple sclerosis review. P T. 2012;37(3):175-84.
9. Ita K. Recent trends in the transdermal delivery of therapeutic agents used for the management of neurodegenerative diseases. J Drug Target. 2017;25(5):406-19.
10. Prausnitz MR, Langer R. Transdermal drug delivery. Nature biotechnology. 2008;26(11):1261-8.

11. Kumar L, Verma S, Singh M, Chalotra T, Utreja P. Advanced Drug Delivery Systems for Transdermal Delivery of Non-Steroidal Anti-Inflammatory Drugs: A Review. Curr Drug Deliv. 2018;15(8):1087-99.
12. Brown D, Ramlochansingh C, Manaye KF, Tizabi Y. Nicotine promotes survival of cells expressing amyloid precursor protein and presenilin: implication for Alzheimer's disease. Neurosci Lett. 2013;535:57-61.
13. Newhouse P, Kellar K, Aisen P, White H, Wesnes K, Coderre E, et al. Nicotine treatment of mild cognitive impairment: a 6-month double-blind pilot clinical trial. Neurology. 2012;78(2):91-101.
14. Danysz W, Parsons CG. Alzheimer's disease, β-amyloid, glutamate, NMDA receptors and memantine – searching for the connections. Br J Pharmacol. 2012;167(2):324-52.
15. 2020 Alzheimer's disease facts and figures. Alzheimer's & Dementia. 2020;16(3):391-460.
16. Kandarova H, Willoughby JA, De Jong WH, Letasiova S, Milasova T, Bachelor MA, et al. Pre-validation of an in vitro skin irritation test for medical devices using the reconstructed human tissue model EpiDerm™. Toxicology in Vitro. 2018;50:407-17.
17. Du X, Wang X, Geng M. Alzheimer's disease hypothesis and related therapies. Translational Neurodegeneration. 2018;7(1):2.
18. Saxena A, Saini R. The Structural Hybrids of Acetylcholines-terase Inhibitors in the Treatment of Alzheimer's Disease: A Review. J Alzhei-mers Neurodegener. 2018;4:015.
19. Hamulakova S, Imrich J, Janovec L, Kristian P, Danihel I, Holas O, et al. Novel tacrine/acridine anticholinesterase inhibitors with piperazine and thiourea linkers. International journal of biological macromolecules. 2014;70:435-9.
20. Ulep MG, Saraon SK, McLea S. Alzheimer Disease. The Journal for Nurse Practitioners. 2018;14(3):129-35.
21. Nguyen TT, Giau VV, Vo TK. Current advances in transdermal delivery of drugs for Alzheimer's disease. Indian Journal of Pharmacology. 2017;49(2):145-54.
22. Lee DH, Gold R, Linker RA. Mechanisms of oxidative damage in multiple sclerosis and neurodegenerative diseases: therapeutic modulation via fumaric acid esters. Int J Mol Sci. 2012;13(9):11783-803.
23. Chaudhuri A. Multiple sclerosis is primarily a neurodegenerative disease. J Neural Transm (Vienna). 2013;120(10):1463-6.
24. Gironi M, Arnò C, Comi G, Penton-Rol G, Furlan R. Chapter 4 - Multiple Sclerosis and Neurodegenerative Diseases. In: Boraschi D, Penton-Rol G, editors. Immune Rebalancing: Academic Press; 2016. p. 63-84.
25. Agache P, Lihoreau T, Mac-Mary S, Fanian F, Humbert P. The Human Skin: An Overview. In: Humbert P, Fanian F, Maibach HI, Agache P, editors. Agache's Measuring the Skin: Non-invasive Investigations, Physiology, Normal Constants. Cham: Springer International Publishing; 2017. p. 1-4.
26. Someya T, Amagai M. Toward a new generation of smart skins. Nature Biotechnology. 2019;37(4):382-8.
27. Wong R, Geyer S, Weninger W, Guimberteau JC, Wong JK. The dynamic anatomy and patterning of skin. Exp Dermatol. 2016;25(2):92-8.
28. Prausnitz MR, Elias PM, Franz TJ, Schmuth M, Tsai J-C, Menon GK, et al. Skin barrier and transdermal drug delivery. Dermatology. 2012;3:2065-73.
29. Arda O, Göksügür N, Tüzün Y. Basic histological structure and functions of facial skin. Clinics in Dermatology. 2014;32(1):3-13.
30. Ng KW, Lau WM. Skin Deep: The Basics of Human Skin Structure and Drug Penetration. In: Dragicevic N, Maibach HI, editors. Percutaneous Penetration Enhancers Chemical Methods in Penetration Enhancement: Drug Manipulation Strategies and Vehicle Effects. Berlin, Heidelberg: Springer Berlin Heidelberg; 2015. p. 3-11.

31. Wiedersberg S, Guy RH. Transdermal drug delivery: 30+ years of war and still fighting! Journal of Controlled Release. 2014;190:150-6.
32. Oertel W, Ross JS, Eggert K, Adler G. Rationale for transdermal drug administration in Alzheimer disease. Neurology. 2007;69(4 Suppl 1):S4-9.
33. Small G, Dubois B. A review of compliance to treatment in Alzheimer's disease: potential benefits of a transdermal patch. Current medical research and opinion. 2007;23(11):2705-13.
34. Szunerits S, Boukherroub R. Heat: A Highly Efficient Skin Enhancer for Transdermal Drug Delivery. Frontiers in Bioengineering and Biotechnology. 2018;6(15).
35. Iqbal B, Ali J, Baboota S. Recent advances and development in epidermal and dermal drug deposition enhancement technology. International Journal of Dermatology. 2018;57(6):646-60.
36. Williams AC, Barry BW. Penetration enhancers. Adv Drug Deliv Rev. 2004;56(5):603-18.
37. Williams AC, Barry BW. Penetration enhancers. Advanced Drug Delivery Reviews. 2012;64, Supplement:128-37.
38. Asbill CS, Michniak BB. Percutaneous penetration enhancers: local versus transdermal activity. Pharm Sci Technolo Today. 2000;3(1):36-41.
39. Barry BW. Lipid-Protein-Partitioning theory of skin penetration enhancement. Journal of Controlled Release. 1991;15(3):237-48.
40. Dragicevic N, Maibach HI. Percutaneous penetration enhancers chemical methods in penetration enhancement: nanocarriers: Springer; 2016.
41. Dragicevic N, Atkinson JP, Maibach HI. Chemical Penetration Enhancers: Classification and Mode of Action. In: Dragicevic N, Maibach HI, editors. Percutaneous Penetration Enhancers Chemical Methods in Penetration Enhancement: Modification of the Stratum Corneum. Berlin, Heidelberg: Springer Berlin Heidelberg; 2015. p. 11-27.
42. Barry BW. Breaching the skin's barrier to drugs. Nature Biotechnology. 2004;22(2):165-7.
43. Schroeter A, Eichner A, Mueller J, Neubert RHH. Penetration Enhancers and Their Mechanism Studied on a Molecular Level. In: Dragicevic N, Maibach HI, editors. Percutaneous Penetration Enhancers Chemical Methods in Penetration Enhancement: Modification of the Stratum Corneum. Berlin, Heidelberg: Springer Berlin Heidelberg; 2015. p. 29-37.
44. Lane ME. Skin penetration enhancers. International Journal of Pharmaceutics. 2013;447(1):12-21.
45. Benson HA. Transdermal drug delivery: penetration enhancement techniques. Curr Drug Deliv. 2005;2(1):23-33.
46. Karande P, Mitragotri S. Enhancement of transdermal drug delivery via synergistic action of chemicals. Biochimica et Biophysica Acta (BBA) - Biomembranes. 2009;1788(11):2362-73.
47. Escobar-Chávez JJ, Díaz-Torres R, Rodriguez-Cruz I, Dominguez-Delgado C, Morales R, Ángeles-Anguiano E, et al. Nanocarriers for transdermal drug delivery. skin. 2012;19:22.
48. Escobar-Chávez JJ, Rodríguez-Cruz IM, Domínguez-Delgado CL, Díaz-Torres R, Revilla-Vázquez AL, Aléncaster NC. Nanocarrier systems for transdermal drug delivery. Recent Advances in Novel Drug Carrier Systems. 2012:201-40.
49. Pardeike J, Hommoss A, Muller RH. Lipid nanoparticles (SLN, NLC) in cosmetic and pharmaceutical dermal products. Int J Pharm. 2009;366(1-2):170-84.
50. Muchow M, Maincent P, Müller RH. Lipid nanoparticles with a solid matrix (SLN®, NLC®, LDC®) for oral drug delivery. Drug development and industrial pharmacy. 2008;34(12):1394-405.
51. Jaiswal P, Gidwani B, Vyas A. Nanostructured lipid carriers and their current application in targeted drug delivery. Artificial Cells, Nanomedicine, and Biotechnology. 2016;44(1):27-40.
52. Müller RH, Alexiev U, Sinambela P, Keck CM. Nanostructured Lipid Carriers (NLC): The Second Generation of Solid Lipid Nanoparticles. In: Dragicevic N, Maibach HI, editors. Percutaneous Penetration Enhancers Chemical Methods in Penetration Enhancement: Nanocarriers. Berlin, Heidelberg: Springer Berlin Heidelberg; 2016. p. 161-85.

53. Schäfer-Korting M, Mehnert W, Korting H-C. Lipid nanoparticles for improved topical application of drugs for skin diseases. Advanced drug delivery reviews. 2007;59(6):427-43.
54. Tamjidi F, Shahedi M, Varshosaz J, Nasirpour A. Nanostructured lipid carriers (NLC): A potential delivery system for bioactive food molecules. Innovative Food Science & Emerging Technologies. 2013;19:29-43.
55. Gordillo-Galeano A, Mora-Huertas CE. Solid lipid nanoparticles and nanostructured lipid carriers: A review emphasizing on particle structure and drug release. European Journal of Pharmaceutics and Biopharmaceutics. 2018;133:285-308.
56. (CHMP) CfMPfHU. Guideline on quality of transdermal patches. In: (CHMP) CfMPfHU, editor.: European Medicine Agency

2014.
57. Pastore MN, Kalia YN, Horstmann M, Roberts MS. Transdermal patches: history, development and pharmacology. Br J Pharmacol. 2015;172(9):2179-209.
58. Administration USFaD. Approved Drug Products with Therapeutic Equivalence Evaluations. 40th ed. Rockville, MD, USA 2020 2020.
59. Isaac M, Holvey C. Transdermal patches: the emerging mode of drug delivery system in psychiatry. Ther Adv Psychopharmacol. 2012;2(6):255-63.
60. Citrome L, Zeni CM, Correll CU. Patches: Established and Emerging Transdermal Treatments in Psychiatry. The Journal of clinical psychiatry. 2019;80(4).
61. Adler G, Mueller B, Articus K. The transdermal formulation of rivastigmine improves caregiver burden and treatment adherence of patients with Alzheimer's disease under daily practice conditions. International journal of clinical practice. 2014;68(4):465-70.
62. Winblad B, Kawata AK, Beusterien KM, Thomas SK, Wimo A, Lane R, et al. Caregiver preference for rivastigmine patch relative to capsules for treatment of probable Alzheimer's disease. Int J Geriatr Psychiatry. 2007;22(5):485-91.
63. Al Hanbali OA, Khan HMS, Sarfraz M, Arafat M, Ijaz S, Hameed A. Transdermal patches: Design and current approaches to painless drug delivery. Acta Pharmaceutica. 2019;69(2):197-215.
64. Kandavilli S, Nair V, Panchagnula R. Polymers in transdermal drug delivery systems. Pharmaceutical technology. 2002;26(5):62-81.
65. Padula C, Nicoli S, Aversa V, Colombo P, Falson F, Pirot F, et al. Bioadhesive film for dermal and transdermal drug delivery. European Journal of Dermatology. 2007;17(4):309-12.
66. Zhong H, Chan G, Hu Y, Hu H, Ouyang D. A Comprehensive Map of FDA-Approved Pharmaceutical Products. Pharmaceutics. 2018;10(4):263.
67. Hwang I, Kim HN, Seong M, Lee SH, Kang M, Yi H, et al. Multifunctional smart skin adhesive patches for advanced health care. Advanced healthcare materials. 2018;7(15):1800275.
68. Santos LF, Correia IJ, Silva AS, Mano JF. Biomaterials for drug delivery patches. European Journal of Pharmaceutical Sciences. 2018;118:49-66.
69. Venkatraman S, Gale R. Skin adhesives and skin adhesion: 1. Transdermal drug delivery systems. Biomaterials. 1998;19(13):1119-36.
70. Minghetti P, Cilurzo F, Casiraghi A. Measuring adhesive performance in transdermal delivery systems. 2004.
71. Cilurzo F, Gennari CG, Minghetti P. Adhesive properties: a critical issue in transdermal patch development. Expert opinion on drug delivery. 2012;9(1):33-45.
72. Zhao C, Quan P, Liu C, Li Q, Fang L. Effect of isopropyl myristate on the viscoelasticity and drug release of a drug-in-adhesive transdermal patch containing blonanserin. Acta pharmaceutica sinica B. 2016;6(6):623-8.
73. Lobo S, Sachdeva S, Goswami T. Role of pressure-sensitive adhesives in transdermal drug delivery systems. Ther Deliv. 2016;7(1):33-48.

74. Watkinson AC, Kearney M-C, Quinn HL, Courtenay AJ, Donnelly RF. Future of the transdermal drug delivery market – have we barely touched the surface? Expert Opinion on Drug Delivery. 2016;13(4):523-32.
75. Alkilani ZA, McCrudden CMT, Donnelly FR. Transdermal Drug Delivery: Innovative Pharmaceutical Developments Based on Disruption of the Barrier Properties of the Stratum Corneum. Pharmaceutics. 2015;7(4).
76. Cilurzo F, Gennari CGM, Minghetti P. Adhesive properties: a critical issue in transdermal patch development. Expert Opinion on Drug Delivery. 2012;9(1):33-45.
77. Hung S-Y, Fu W-M. Drug candidates in clinical trials for Alzheimer's disease. Journal of Biomedical Science. 2017;24:47.
78. Gaudig M, Richarz U, Han J, Van Baelen B, Schauble B. Effects of galantamine in Alzheimer's disease: double-blind withdrawal studies evaluating sustained versus interrupted treatment. Current Alzheimer Research. 2011;8(7):771-80.
79. Riepe M, Weinman J, Osae-Larbi J, Mulick Cassidy A, Knox S, Chaves R, et al. Factors Associated with Greater Adherence to and Satisfaction with Transdermal Rivastigmine in Patients with Alzheimer's Disease and Their Caregivers. Dement Geriatr Cogn Disord. 2015;40(1-2):107-19.
80. Chan AL, Chien YW, Jin Lin S. Transdermal delivery of treatment for Alzheimer's disease: development, clinical performance and future prospects. Drugs Aging. 2008;25(9):761-75.
81. Pai MC, Aref H, Bassil N, Kandiah N, Lee JH, Srinivasan AV, et al. Real-world evaluation of compliance and preference in Alzheimer's disease treatment. Clin Interv Aging. 2015;10:1779-87.
82. Scott LJ, Goa KL. Galantamine. Drugs. 2000;60(5):1095-122.
83. Lilienfeld S. Galantamine—a novel cholinergic drug with a unique dual mode of action for the treatment of patients with Alzheimer's disease. CNS drug reviews. 2002;8(2):159-76.
84. Corey-Bloom J. Galantamine: a review of its use in Alzheimer's disease and vascular dementia. Int J Clin Pract. 2003;57(3):219-23.
85. Shrivastava A, Gupta V. Methods for the determination of limit of detection and limit of quantitation of the analytical methods. Chronicles of Young Scientists. 2011;2(1):21-5.
86. I. HW. Analysis of data on the medicament release from ointments. Journal of Pharmaceutical Sciences. 1962;51(8):802-4.
87. Soler LI, Boix A, Lauroba J, Colom H, Domenech J. Transdermal delivery of alprazolam from a monolithic patch: formulation based on in vitro characterization. Drug Dev Ind Pharm. 2012;38(10):1171-8.
88. Jung E, Lee EY, Choi HK, Ban SJ, Choi SH, Kim JS, et al. Development of drug-in-adhesive patch formulations for transdermal delivery of fluoxetine: In vitro and in vivo evaluations. Int J Pharm. 2015;487(1-2):49-55.
89. Zhang C, Luo H, Lin G, Zhu Z, Zhang F, Zhang J, et al. Transdermal patches for D-threo-methylphenidate (free base): Formulation aspects and in vivo pharmacokinetics. Journal of Drug Delivery Science and Technology. 2016;35:50-7.
90. Liu C, Hui M, Quan P, Fang L. Drug in adhesive patch of palonosetron: Effect of pressure sensitive adhesive on drug skin permeation and in vitro-in vivo correlation. Int J Pharm. 2016;511(2):1088-97.
91. Weng W, Quan P, Liu C, Zhao H, Fang L. Design of a Drug-in-Adhesive Transdermal Patch for Risperidone: Effect of Drug-Additive Interactions on the Crystallization Inhibition and In Vitro/In Vivo Correlation Study. J Pharm Sci. 2016;105(10):3153-61.
92. Furuishi T, Io T, Fukami T, Suzuki T, Tomono K. Formulation and in vitro evaluation of pentazocine transdermal delivery system. Biol Pharm Bull. 2008;31(7):1439-43.
93. Amnuaikit T, Songkram C, Pinsuwan S. Enhancement of Mycophenolate Mofetil Permeation for Topical Use by Eucalyptol and N-Methyl-2-pyrrolidone. Scientifica (Cairo). 2016;2016:9672718.

94. Ameen D, Michniak-Kohn B. Transdermal delivery of dimethyl fumarate for Alzheimer's disease: Effect of penetration enhancers. International Journal of Pharmaceutics. 2017;529(1):465-73.
95. Diez I, Peraire C, Obach R, Domenech J. Influence of d-limonene on the transdermal penetration of felodipine. Eur J Drug Metab Pharmacokinet. 1998;23(1):7-12.
96. Lee PJ, Ahmad N, Langer R, Mitragotri S, Prasad Shastri V. Evaluation of chemical enhancers in the transdermal delivery of lidocaine. International Journal of Pharmaceutics. 2006;308(1):33-9.
97. Gwak HS, Chun IK. Effect of vehicles and penetration enhancers on the in vitro percutaneous absorption of tenoxicam through hairless mouse skin. International Journal of Pharmaceutics. 2002;236(1):57-64.
98. Agyralides GG, Dallas PP, Rekkas DM. Development and in vitro evaluation of furosemide transdermal formulations using experimental design techniques. International Journal of Pharmaceutics. 2004;281(1):35-43.
99. Kakubari I, Sasaki H, Takayasu T, Yamauchi H, Takayama S, Takayama K. Effects of Ethylcellulose and 2-Octyldodecanol Additives on Skin Permeation and Irritation with Ethylene–Vinyl Acetate Copolymer Matrix Patches Containing Formoterol Fumarate. Biological and Pharmaceutical Bulletin. 2006;29(8):1717-22.
100. Ravula R, Herwadkar AK, Abla MJ, Little J, Banga AK. Formulation optimization of a drug in adhesive transdermal analgesic patch. Drug Dev Ind Pharm. 2016;42(6):862-70.
101. Michaelis M, Leopold CS. Mixture design approach for early stage formulation development of a transdermal delivery system. Drug Development and Industrial Pharmacy. 2015;41(9):1532-40.
102. Sachdeva V, Bai Y, Kydonieus A, Banga AK. Formulation and optimization of desogestrel transdermal contraceptive patch using crystallization studies. Int J Pharm. 2013;441(1-2):9-18.
103. Jain P, Banga AK. Induction and inhibition of crystallization in drug-in-adhesive-type transdermal patches. Pharm Res. 2013;30(2):562-71.
104. Thomas NS, Panchagnula R. Combination strategies to enhance transdermal permeation of zidovudine (AZT). Pharmazie. 2003;58(12):895-8.
105. Yao C, Raoufinia A, Gold M, Nye JS, Ramael S, Padmanabhan M, et al. Steady-state pharmacokinetics of galantamine are not affected by addition of memantine in healthy subjects. J Clin Pharmacol. 2005;45(5):519-28.
106. Huang X, Brazel CS. On the importance and mechanisms of burst release in matrix-controlled drug delivery systems. Journal of Controlled Release. 2001;73(2):121-36.
107. Mufamadi MS, Choonara YE, Kumar P, Modi G, Naidoo D, van Vuuren S, et al. Ligand-functionalized nanoliposomes for targeted delivery of galantamine. International Journal of Pharmaceutics. 2013;448(1):267-81.
108. Ho KY, Dodou K. Rheological studies on pressure-sensitive silicone adhesives and drug-in-adhesive layers as a means to characterise adhesive performance. Int J Pharm. 2007;333(1-2):24-33.
109. Venkatraman S, Gale R. Skin adhesives and skin adhesion. 1. Transdermal drug delivery systems. Biomaterials. 1998;19(13):1119-36.
110. Li N, Quan P, Wan X, Liu C, Liu X, Fang L. Mechanistic insights of the enhancement effect of sorbitan monooleate on olanzapine transdermal patch both in release and percutaneous absorption processes. European Journal of Pharmaceutical Sciences. 2017;107:138-47.
111. Liu C, Quan P, Li S, Zhao Y, Fang L. A systemic evaluation of drug in acrylic pressure sensitive adhesive patch in vitro and in vivo: The roles of intermolecular interaction and adhesive mobility variation in drug controlled release. Journal of Controlled Release. 2017;252:83-94.
112. Dumont M, Beal MF. Neuroprotective strategies involving ROS in Alzheimer disease. Free Radical Biology and Medicine. 2011;51(5):1014-26.

113. Chen X, Guo C, Kong J. Oxidative stress in neurodegenerative diseases. Neural Regen Res. 2012;7(5):376-85.
114. Linker RA, Lee DH, Ryan S, van Dam AM, Conrad R, Bista P, et al. Fumaric acid esters exert neuroprotective effects in neuroinflammation via activation of the Nrf2 antioxidant pathway. Brain. 2011;134(Pt 3):678-92.
115. Bovenschen HJ, Langewouters AM, van de Kerkhof PC. Dimethylfumarate for psoriasis: Pronounced effects on lesional T-cell subsets, epidermal proliferation and differentiation, but not on natural killer T cells in immunohistochemical study. Am J Clin Dermatol. 2010;11(5):343-50.
116. Mrowietz U, Asadullah K. Dimethylfumarate for psoriasis: more than a dietary curiosity. Trends in Molecular Medicine. 2005;11(1):43-8.
117. Bomprezzi R. Dimethyl fumarate in the treatment of relapsing–remitting multiple sclerosis: an overview. Therapeutic Advances in Neurological Disorders. 2015;8(1):20-30.
118. Litjens NHR, van Strijen E, van Gulpen C, Mattie H, van Dissel JT, Thio HB, et al. In vitro pharmacokinetics of anti-psoriatic fumaric acid esters. BMC Pharmacology. 2004;4:22-.
119. Scannevin RH, Chollate S, Jung M-y, Shackett M, Patel H, Bista P, et al. Fumarates promote cytoprotection of central nervous system cells against oxidative stress via the nuclear factor (erythroid-derived 2)-like 2 pathway. Journal of Pharmacology and Experimental Therapeutics. 2012;341(1):274-84.
120. di Nuzzo L, Orlando R, Nasca C, Nicoletti F. Molecular pharmacodynamics of new oral drugs used in the treatment of multiple sclerosis. Drug Design, Development and Therapy. 2014;8:555-68.
121. Yamazaki H, Tanji K, Wakabayashi K, Matsuura S, Itoh K. Role of the Keap1/Nrf2 pathway in neurodegenerative diseases. Pathology international. 2015;65(5):210-9.
122. Zheng H, Fridkin M, Youdim M. New Approaches to Treating Alzheimer's Disease. Perspectives in Medicinal Chemistry. 2015;7:1-8.
123. Barrett DA, Rutter N, Davis SS. An in Vitro Study of Diamorphine Permeation Through Premature Human Neonatal Skin. Pharmaceutical Research.10(4):583-7.
124. Roy SD, Manoukian E. Permeability of Ketorolac Acid and Its Ester Analogs (Prodrug) through Human Cadaver Skin. Journal of Pharmaceutical Sciences. 1994;83(11):1548-53.
125. Thomas NS, Panchagnula R. Transdermal delivery of zidovudine: effect of vehicles on permeation across rat skin and their mechanism of action. Eur J Pharm Sci. 2003;18(1):71-9.
126. Herkenne C, Naik A, Kalia YN, Hadgraft J, Guy RH. Effect of propylene glycol on ibuprofen absorption into human skin in vivo. J Pharm Sci. 2008;97(1):185-97.
127. Jain AK, Thomas NS, Panchagnula R. Transdermal drug delivery of imipramine hydrochloride. I. Effect of terpenes. J Control Release. 2002;79(1-3):93-101.
128. Narishetty ST, Panchagnula R. Transdermal delivery of zidovudine: effect of terpenes and their mechanism of action. J Control Release. 2004;95(3):367-79.
129. Arellano A, Santoyo S, Martin C, Ygartua P. Enhancing effect of terpenes on the in vitro percutaneous absorption of diclofenac sodium. International Journal of Pharmaceutics. 1996;130(1):141-5.
130. del Rio-Sancho S, Serna-Jimenez CE, Calatayud-Pascual MA, Balaguer-Fernandez C, Femenia-Font A, Merino V, et al. Transdermal absorption of memantin--effect of chemical enhancers, iontophoresis, and role of enhancer lipophilicity. Eur J Pharm Biopharm. 2012;82(1):164-70.
131. Zhao L, Fang L, Xu Y, Zhao Y, He Z. Effect of O-acylmenthol on transdermal delivery of drugs with different lipophilicity. Int J Pharm. 2008;352(1-2):92-103.
132. Griffin S, Wyllie SG, Markham J. Determination of octanol–water partition coefficient for terpenoids using reversed-phase high-performance liquid chromatography. Journal of Chromatography A. 1999;864(2):221-8.

133. Yamane MA, Williams AC, Barry BW. Terpene Penetration Enhancers in Propylene Glycol/water Co-solvent Systems: Effectiveness and Mechanism of Action. Journal of Pharmacy and Pharmacology. 1995;47(12A):978-89.
134. Otto A, du Plessis J, Wiechers JW. Formulation effects of topical emulsions on transdermal and dermal delivery. Int J Cosmet Sci. 2009;31(1):1-19.
135. Shokri J, Nokhodchi A, Dashbolaghi A, Hassan-Zadeh D, Ghafourian T, Barzegar Jalali M. The effect of surfactants on the skin penetration of diazepam. Int J Pharm. 2001;228(1-2):99-107.
136. Nokhodchi A, Shokri J, Dashbolaghi A, Hassan-Zadeh D, Ghafourian T, Barzegar-Jalali M. The enhancement effect of surfactants on the penetration of lorazepam through rat skin. Int J Pharm. 2003;250(2):359-69.
137. Sarpotdar PP, Zatz JL. Evaluation of penetration enhancement of lidocaine by nonionic surfactants through hairless mouse skin in vitro. Journal of Pharmaceutical Sciences. 1986;75(2):176-81.
138. Babu RJ, Pandit JK. Effect of penetration enhancers on the transdermal delivery of bupranolol through rat skin. Drug Deliv. 2005;12(3):165-9.
139. Cilurzo F, Vistoli G, Selmin F, Gennari CGM, Musazzi UM, Franzé S, et al. An Insight into the Skin Penetration Enhancement Mechanism of N-Methylpyrrolidone. Molecular Pharmaceutics. 2014;11(3):1014-21.
140. Jampilek J, Brychtova K. Azone analogues: classification, design, and transdermal penetration principles. Med Res Rev. 2012;32(5):907-47.
141. Trommer H, Neubert RH. Overcoming the stratum corneum: the modulation of skin penetration. A review. Skin Pharmacol Physiol. 2006;19(2):106-21.
142. Godwin DA, Kim N-H, Felton LA. Influence of Transcutol® CG on the skin accumulation and transdermal permeation of ultraviolet absorbers. European Journal of Pharmaceutics and Biopharmaceutics. 2002;53(1):23-7.
143. Osborne DW. Diethylene glycol monoethyl ether: an emerging solvent in topical dermatology products. J Cosmet Dermatol. 2011;10(4):324-9.
144. Prasanthi D, Lakshmi PK. Effect of Chemical Enhancers in Transdermal Permeation of Alfuzosin Hydrochloride. ISRN Pharmaceutics. 2012;2012:8.
145. Mura P, Faucci MT, Bramanti G, Corti P. Evaluation of transcutol as a clonazepam transdermal permeation enhancer from hydrophilic gel formulations. European Journal of Pharmaceutical Sciences. 2000;9(4):365-72.
146. Rhee YS, Huh JY, Park CW, Nam TY, Yoon KR, Chi SC, et al. Effects of vehicles and enhancers on transdermal delivery of clebopride. Arch Pharm Res. 2007;30(9):1155-61.
147. Kunta JR, Goskonda VR, Brotherton HO, Khan MA, Reddy IK. Effect of menthol and related terpenes on the percutaneous absorption of propranolol across excised hairless mouse skin. J Pharm Sci. 1997;86(12):1369-73.
148. Nokhodchi A, Sharabiani K, Rashidi MR, Ghafourian T. The effect of terpene concentrations on the skin penetration of diclofenac sodium. Int J Pharm. 2007;335(1-2):97-105.
149. Meraz-Ríos MA, Franco-Bocanegra D, Toral Rios D, Campos-Peña V. Early Onset Alzheimer's Disease and Oxidative Stress. Oxidative Medicine and Cellular Longevity. 2014;2014:14.
150. Folch J, Ettcheto M, Petrov D, Abad S, Pedrós I, Marin M, et al. Review of the advances in treatment for Alzheimer disease: strategies for combating β-amyloid protein. Neurología (English Edition). 2018;33(1):47-58.
151. Jobke B, McBride T, Nevin L, Peiperl L, Ross A, Stone C, et al. Setbacks in Alzheimer research demand new strategies, not surrender. PLOS Medicine. 2018;15(2):e1002518.
152. Gauthier S, Alam J, Fillit H, Iwatsubo T, Liu-Seifert H, Sabbagh M, et al. Combination Therapy for Alzheimer's Disease: Perspectives of the EU/US CTAD Task Force. The journal of prevention of Alzheimer's disease. 2019;6(3):164-8.

153. Bahn G, Jo D-G. Therapeutic approaches to Alzheimer's disease through modulation of NRF2. Neuromolecular medicine. 2019;21(1):1-11.
154. Campolo M, Casili G, Lanza M, Filippone A, Paterniti I, Cuzzocrea S, et al. Multiple mechanisms of dimethyl fumarate in amyloid β-induced neurotoxicity in human neuronal cells. Journal of Cellular and Molecular Medicine. 2018;22(2):1081-94.
155. Rezvani AH, Levin ED. Cognitive effects of nicotine. Biological Psychiatry. 2001;49(3):258-67.
156. Srivareerat M, Tran TT, Salim S, Aleisa AM, Alkadhi KA. Chronic nicotine restores normal Abeta levels and prevents short-term memory and E-LTP impairment in Abeta rat model of Alzheimer's disease. Neurobiol Aging. 2011;32(5):834-44.
157. Esteves I, Lopes-Aguiar C, Rossignoli M, Ruggiero R, Broggini A, Bueno-Junior L, et al. Chronic nicotine attenuates behavioral and synaptic plasticity impairments in a streptozotocin model of Alzheimer's disease. Neuroscience. 2017;353:87-97.
158. Benowitz NL, Hukkanen J, Jacob P. Nicotine Chemistry, Metabolism, Kinetics and Biomarkers. In: Henningfield JE, London ED, Pogun S, editors. Nicotine Psychopharmacology. Berlin, Heidelberg: Springer Berlin Heidelberg; 2009. p. 29-60.
159. Information. NCfB. Nicotine, CID=89594 [Available from: https://pubchem.ncbi.nlm.nih.gov/compound/Nicotine.
160. Sozio P, Cerasa LS, Marinelli L, Di Stefano A. Transdermal donepezil on the treatment of Alzheimer's disease. Neuropsychiatr Dis Treat. 2012;8:361-8.
161. Khoury R, Rajamanickam J, Grossberg GT. An update on the safety of current therapies for Alzheimer's disease: focus on rivastigmine. Ther Adv Drug Saf. 2018;9(3):171-8.
162. Marwah H, Garg T, Goyal AK, Rath G. Permeation enhancer strategies in transdermal drug delivery. Drug Delivery. 2016;23(2):564-78.
163. Hadgraft J, Valenta C. pH, pKa and dermal delivery. International Journal of Pharmaceutics. 2000;200(2):243-7.
164. Vavrova K, Lorencova K, Klimentova J, Novotny J, Holy AN, Hrabalek A. Transdermal and dermal delivery of adefovir: effects of pH and permeation enhancers. European journal of pharmaceutics and biopharmaceutics : official journal of Arbeitsgemeinschaft fur Pharmazeutische Verfahrenstechnik eV. 2008;69(2):597-604.
165. Swarbrick J, Lee G, Brom J, Gensmantel NP. Drug permeation through human skin II: Permeability of ionizable compounds. 1984;73(10):1352-5.
166. Østergaard Knudsen N, Pommergaard Pedersen G. pH and Drug Delivery. (eds): pH of the Skin: Issues and Challenges. Curr Probl Dermatol. Basel K, 2018, vol 54, pp 143-151. doi: 10.1159/000489528, editor: Basel, Karger; 2018.
167. Ishii H, Todo H, Sugibayashi K. Effect of thermodynamic activity on skin permeation and skin concentration of triamcinolone acetonide. Chem Pharm Bull (Tokyo). 2010;58(4):556-61.
168. Kuswahyuning R, Roberts MS. Concentration dependency in nicotine skin penetration flux from aqueous solutions reflects vehicle induced changes in nicotine stratum corneum retention. Pharm Res. 2014;31(6):1501-11.
169. Ameen D, Michniak-Kohn B. Transdermal delivery of dimethyl fumarate for Alzheimer's disease: Effect of penetration enhancers. Int J Pharm. 2017;529(1-2):465-73.
170. Barlow RB, Hamilton JT. Effects of ph on the activity of nicotine and nicotine monomethiodide on the rat diaphragm preparation. Br J Pharmacol Chemother. 1962;18(3):543-9.
171. Clayton PM, Vas CA, Bui TTT, Drake AF, McAdam K. Spectroscopic Studies on Nicotine and Nornicotine in the UV Region. Chirality. 2013;25(5):288-93.
172. Tongaree S, Flanagan DR, Poust RI. The Effects of pH and Mixed Solvent Systems on the Solubility of Oxytetracycline. Pharmaceutical Development and Technology. 1999;4(4):571-80.
173. Pankow JF, Duell AK, Peyton DH. Free-Base Nicotine Fraction αfb in Non-Aqueous versus Aqueous Solutions: Electronic Cigarette Fluids Without versus With Dilution with Water. Chemical Research in Toxicology. 2020;33(7):1729-35.

174. Nair MK, Chetty DJ, Ho H, Chien YW. Biomembrane permeation of nicotine: mechanistic studies with porcine mucosae and skin. Journal of pharmaceutical sciences. 1997;86(2):257-62.
175. Santi P, Catellani PL, Colombo P, Ringard-Lefebvre C, Barthélémy C, Guyot-Hermann A-M. Partition and transport of verapamil and nicotine through artificial membranes. International Journal of Pharmaceutics. 1991;68(1):43-9.
176. Oakley DM, Swarbrick J. Effects of ionization on the percutaneous absorption of drugs: partitioning of nicotine into organic liquids and hydrated stratum corneum. Journal of pharmaceutical sciences. 1987;76(12):866-71.
177. Fini A, Fazio G, Gonzalez-Rodriguez M, Cavallari C, Passerini N, Rodriguez L. Formation of ion-pairs in aqueous solutions of diclofenac salts. Int J Pharm. 1999;187(2):163-73.
178. Peck KD, Ghanem AH, Higuchi WI. Hindered diffusion of polar molecules through and effective pore radii estimates of intact and ethanol treated human epidermal membrane. Pharm Res. 1994;11(9):1306-14.
179. Badhe RV, Chejara DR, Kumar P, Choonara YE, Pillay V. Neurodegenerative Disease Conditions and Genomic Treatment for Better Health. Genomics-Driven Healthcare: Springer; 2018. p. 281-310.
180. Carlström KE, Ewing E, Granqvist M, Gyllenberg A, Aeinehband S, Enoksson SL, et al. Therapeutic efficacy of dimethyl fumarate in relapsing-remitting multiple sclerosis associates with ROS pathway in monocytes. Nature communications. 2019;10(1):1-13.
181. Boada M, Arranz FJ. Transdermal is better than oral: observational research of the satisfaction of caregivers of patients with Alzheimer's disease treated with rivastigmine. Dementia and geriatric cognitive disorders. 2013;35(1-2):23-33.
182. Molinuevo JL, Arranz FJ. Impact of transdermal drug delivery on treatment adherence in patients with Alzheimer's disease. Expert Rev Neurother. 2012;12(1):31-7.
183. Kuchler S, Radowski MR, Blaschke T, Dathe M, Plendl J, Haag R, et al. Nanoparticles for skin penetration enhancement--a comparison of a dendritic core-multishell-nanotransporter and solid lipid nanoparticles. Eur J Pharm Biopharm. 2009;71(2):243-50.
184. Aziz K, Ahmad N, Kohli K. Enhanced Anti Arthritic Potential of Tacrolimus by Transdermal Nanocarrier System. Journal of Nanoscience and Nanotechnology. 2017;17(7):4573-83.
185. Kurmi BD, Tekchandani P, Paliwal R, Paliwal SR. Transdermal Drug Delivery: Opportunities and Challenges for Controlled Delivery of Therapeutic Agents Using Nanocarriers. Curr Drug Metab. 2017;18(5):481-95.
186. Das S, Ng WK, Tan RBH. Are nanostructured lipid carriers (NLCs) better than solid lipid nanoparticles (SLNs): Development, characterizations and comparative evaluations of clotrimazole-loaded SLNs and NLCs? European Journal of Pharmaceutical Sciences. 2012;47(1):139-51.
187. Schwarz JC, Weixelbaum A, Pagitsch E, Löw M, Resch GP, Valenta C. Nanocarriers for dermal drug delivery: Influence of preparation method, carrier type and rheological properties. International Journal of Pharmaceutics. 2012;437(1):83-8.
188. Zhao J, Piao X, Shi X, Si A, Zhang Y, Feng N. Podophyllotoxin-Loaded Nanostructured Lipid Carriers for Skin Targeting: In Vitro and In Vivo Studies. Molecules. 2016;21(11).
189. Pople PV, Singh KK. Development and evaluation of topical formulation containing solid lipid nanoparticles of vitamin A. AAPS PharmSciTech. 2006;7(4):91.
190. Castro GA, Coelho AL, Oliveira CA, Mahecha GA, Orefice RL, Ferreira LA. Formation of ion pairing as an alternative to improve encapsulation and stability and to reduce skin irritation of retinoic acid loaded in solid lipid nanoparticles. Int J Pharm. 2009;381(1):77-83.
191. Castro GA, Oliveira CA, Mahecha GA, Ferreira LA. Comedolytic effect and reduced skin irritation of a new formulation of all-trans retinoic acid-loaded solid lipid nanoparticles for topical treatment of acne. Arch Dermatol Res. 2011;303(7):513-20.

192. Souza LG, Silva EJ, Martins ALL, Mota MF, Braga RC, Lima EM, et al. Development of topotecan loaded lipid nanoparticles for chemical stabilization and prolonged release. European Journal of Pharmaceutics and Biopharmaceutics. 2011;79(1):189-96.
193. Yuan H, Jiang SP, Du YZ, Miao J, Zhang XG, Hu FQ. Strategic approaches for improving entrapment of hydrophilic peptide drugs by lipid nanoparticles. Colloids Surf B Biointerfaces. 2009;70(2):248-53.
194. Liu J, Gong T, Wang C, Zhong Z, Zhang Z. Solid lipid nanoparticles loaded with insulin by sodium cholate-phosphatidylcholine-based mixed micelles: preparation and characterization. Int J Pharm. 2007;340(1-2):153-62.
195. Trotta M, Debernardi F, Caputo O. Preparation of solid lipid nanoparticles by a solvent emulsification-diffusion technique. Int J Pharm. 2003;257(1-2):153-60.
196. Chudasama A, Patel V, Nivsarkar M, Vasu K, Shishoo C. Investigation of microemulsion system for transdermal delivery of itraconazole. Journal of advanced pharmaceutical technology & research. 2011;2(1):30.
197. Mehnert W, Mäder K. Solid lipid nanoparticles: Production, characterization and applications. Advanced Drug Delivery Reviews. 2012;64:83-101.
198. Garg NK, Tyagi RK, Singh B, Sharma G, Nirbhavane P, Kushwah V, et al. Nanostructured lipid carrier mediates effective delivery of methotrexate to induce apoptosis of rheumatoid arthritis via NF-κB and FOXO1. International journal of pharmaceutics. 2016;499(1-2):301-20.
199. Kumar P, Sharma G, Kumar R, Malik R, Singh B, Katare OP, et al. Enhanced Brain Delivery of Dimethyl Fumarate Employing Tocopherol-Acetate-Based Nanolipidic Carriers: Evidence from Pharmacokinetic, Biodistribution, and Cellular Uptake Studies. ACS Chemical Neuroscience. 2017;8(4):860-5.
200. Sütő B, Weber S, Zimmer A, Farkas G, Kelemen A, Budai-Szűcs M, et al. Optimization and design of an ibuprofen-loaded nanostructured lipid carrier with a 23 full factorial design. Chemical Engineering Research and Design. 2015;104:488-96.
201. Kasongo W, Pardeike J, Müller RH, Walker RB. Selection and characterization of suitable lipid excipients for use in the manufacture of didanosine-loaded solid lipid nanoparticles and nanostructured lipid carriers. Journal of pharmaceutical sciences. 2011;100(12):5185-96.
202. Muller RH, Radtke M, Wissing SA. Solid lipid nanoparticles (SLN) and nanostructured lipid carriers (NLC) in cosmetic and dermatological preparations. Adv Drug Deliv Rev. 2002;54 Suppl 1:S131-55.
203. Souto E, Almeida A, Müller R. Lipid nanoparticles (SLN®, NLC®) for cutaneous drug delivery: structure, protection and skin effects. Journal of Biomedical Nanotechnology. 2007;3(4):317-31.
204. Khosa A, Reddi S, Saha RN. Nanostructured lipid carriers for site-specific drug delivery. Biomedicine & Pharmacotherapy. 2018;103:598-613.
205. Spencer RP. Tecfidera®: an approach for repurposing. Pharmaceutical Patent Analyst. 2014;3(2):183-98.
206. Souto EB, Baldim I, Oliveira WP, Rao R, Yadav N, Gama FM, et al. SLN and NLC for topical, dermal, and transdermal drug delivery. Expert Opinion on Drug Delivery. 2020;17(3):357-77.
207. Hu FQ, Yuan H, Zhang HH, Fang M. Preparation of solid lipid nanoparticles with clobetasol propionate by a novel solvent diffusion method in aqueous system and physicochemical characterization. Int J Pharm. 2002;239(1-2):121-8.
208. Eaton P, Quaresma P, Soares C, Neves C, de Almeida MP, Pereira E, et al. A direct comparison of experimental methods to measure dimensions of synthetic nanoparticles. Ultramicroscopy. 2017;182:179-90.
209. Wei H, Wu D-Q, Li Q, Chang C, Zhou J-P, Zhang X-Z, et al. Preparation of Shell Cross-Linked Thermoresponsive Micelles as well as Hollow Spheres Based on P(NIPAAm-co-HMAAm-co-MPMA)-b-PCL. The Journal of Physical Chemistry C. 2008;112(39):15329-34.

210. Xu F, Yan T-T, Luo Y-L. Synthesis and micellization of thermosensitive PNIPAAm-b-PLA amphiphilic block copolymers based on a bifunctional initiator. Macromolecular research. 2011;19(12):1287-95.
211. Khan N, Shah FA, Rana I, Ansari MM, Din FU, Rizvi SZH, et al. Nanostructured lipid carriers-mediated brain delivery of carbamazepine for improved in vivo anticonvulsant and anxiolytic activity. Int J Pharm. 2020;577:119033.
212. Üner M, Yener G, Ergüven M. Design of colloidal drug carriers of celecoxib for use in treatment of breast cancer and leukemia. Materials Science and Engineering: C. 2019;103:109874.
213. Elmowafy M, Shalaby K, Ali HM, Alruwaili NK, Salama A, Ibrahim MF, et al. Impact of nanostructured lipid carriers on dapsone delivery to the skin: in vitro and in vivo studies. International Journal of Pharmaceutics. 2019;572:118781.
214. Teeranachaideekul V, Souto EB, Junyaprasert VB, Müller RH. Cetyl palmitate-based NLC for topical delivery of Coenzyme Q10 – Development, physicochemical characterization and in vitro release studies. European Journal of Pharmaceutics and Biopharmaceutics. 2007;67(1):141-8.
215. Lombardi Borgia S, Regehly M, Sivaramakrishnan R, Mehnert W, Korting HC, Danker K, et al. Lipid nanoparticles for skin penetration enhancement-correlation to drug localization within the particle matrix as determined by fluorescence and parelectric spectroscopy. J Control Release. 2005;110(1):151-63.
216. Santos Maia C, Mehnert W, Schaller M, Korting HC, Gysler A, Haberland A, et al. Drug targeting by solid lipid nanoparticles for dermal use. J Drug Target. 2002;10(6):489-95.
217. Baek JS, Pham CV, Myung CS, Cho CW. Tadalafil-loaded nanostructured lipid carriers using permeation enhancers. Int J Pharm. 2015;495(2):701-9.
218. Esposito E, Cortesi R, Drechsler M, Fan J, Fu BM, Calderan L, et al. Nanoformulations for dimethyl fumarate: Physicochemical characterization and in vitro/in vivo behavior. European Journal of Pharmaceutics and Biopharmaceutics. 2017;115:285-96.
219. Schindelin J, Arganda-Carreras I, Frise E, Kaynig V, Longair M, Pietzsch T, et al. Fiji: an open-source platform for biological-image analysis. Nat Methods. 2012;9(7):676-82.
220. Kandárová H, Hayden P, Klausner M, Kubilus J, Sheasgreen J. An in vitro skin irritation test (SIT) using the EpiDerm reconstructed human epidermal (RHE) model. J Vis Exp. 2009(29):1366.
221. Kandárová H, Hayden P, Klausner M, Kubilus J, Kearney P, Sheasgreen J. In Vitro Skin Irritation Testing: Improving the Sensitivity of the EpiDerm Skin Irritation Test Protocol. Alternatives to Laboratory Animals. 2009;37(6):671-89.
222. Casas JW, Lewerenz GM, Rankin EA, Willoughby JA, Sr., Blakeman LC, McKim JM, Jr., et al. In vitro human skin irritation test for evaluation of medical device extracts. Toxicol In Vitro. 2013;27(8):2175-83.